# Real-time monitoring of cement sheath integrity under high-angle HPHT wellbore conditions.

WILCOX, L.B.

2023

# Real-Time Monitoring of Cement Sheath Integrity Under High Angle HPHT Wellbore Conditions.

**Lawrence B. Wilcox**

A Thesis presented for the degree of
Doctor of Philosophy.


School of Engineering
Robert Gordon University

March 2023

# Real-Time Monitoring of Cement Sheath Integrity Under High Angle HPHT Wellbore Conditions.

**Lawrence B. Wilcox**

A thesis submitted in partial fulfilment of the requirements of Robert Gordon University for the degree of Doctor of Philosophy.

March 2023

# Abstract

The lengthy time span over which the cemented well needs to retain its integrity is a massive challenge today. The cement plugs in abandoned wells, in conjunction with the annular cement sheath, need to prevent leakages well beyond the life of the wellbore. The results of a recent engineering study of $15,500$ wellbores in the Gulf of Mexico show that as a wellbore turns fifteen years of age, it develops a fifty percent chance of being adversely affected by sustained casing pressure. Even though a high percentage of the results are for wells in the Gulf of Mexico, similar numbers have been reported for the North Sea.

This research project investigated the mechanical behaviour of the cement sheath over the entire life cycle of the wellbore by applying analytical and numerical methods. Analytical and numerical models were developed and applied to explain wellbore phenomena such as cement failure and sand production by ascertaining the eligibility of elastic and non-elastic approaches. In addition, a three-dimensional geomechanical model was developed to predict the effect of a ductile formation on stress loading in the wellbore.

The results of the numerical and analytical models provided definitive results for casing-cement-formation deformation as a function of time under downhole operating conditions. The results show that wellbore pressure, wellbore temperature variation, and the Young's modulus of cement have a stronger influence on shear failure than other parameters.

**Keywords**: geomechanics; offshore; well; integrity; real-time; monitoring; cement; production; failure.

# Declaration

The work in this thesis is based on research carried out at the School of Engineering, Robert Gordon University, Aberdeen, UK. No part of this thesis has been submitted elsewhere for any other degree or qualification, and it is all my own work unless referenced to the contrary in the thesis.

# Acknowledgements

The author would like to express his gratitude to his supervising professor, Prof. Babs Oyeneyin, and his technical supervisor, Dr. Sheikh Islam, for their guidance and mentorship.

# Contents

# List of Figures

# List of Tables

# Chapter 1

# Background

Maintaining the integrity of an oil-well throughout its life cycle is vital for economic production of petroleum and more importantly, ensuring safety. The life cycle of an oil-well spans from the drilling and construction phase to the plugging and abandonment phase. Since oil-well materials (especially the oilwell cement sheath as it is the primary well barrier) are prone to degradation with increasing time and variations in pressure and temperature, the number of well integrity related problems normally tend to increase as the wells get older. An investigative study of about $15,500$ oil wells in the North Sea and the Gulf of Mexico showed that as a well becomes about fifteen years old, it has a 50% probability of being affected by sustained casing pressure, and about 35% of wells in these regions suffer from this problem [26, 46, 94].

Even though there have been some technological improvements in monitoring well integrity over time, the limitations of these techniques abound in the industry and have necessitated the need for better monitoring and predictive systems. This research project predicts the real-time mechanical behaviour of the oilwell cement sheath under various downhole operating conditions.

## 1.1 Motivation

Enumerated below are the problem statements that form the motivation for this research thesis;

1. After solidification, the oil-well cement should ideally form a leakage-tight seal in the annular space between the casing and rock formation. However, these annular seals are not always perfect and leakages sometimes occur along the wellbore. If left untreated, these leakages could compromise the integrity of the wellbore and in the worst case scenario, cause massive damage.

2. Unlike cement used in the construction industry, oilwell cement is placed in the annulus of the wellbore and has limited accessibility. Due to limited accessibility, monitoring the integrity of the wellbore is limited to tools and instruments that can be placed around the depth of interest which is typically thousands of feet. Developing an effective solution for predicting and monitoring the behaviour of the cement sheath within these limitations is challenging.

3. The Cement Bond Log (CBL), which is used in the industry to evaluate and ascertain the integrity of the oilwell cement, has been proven to have inaccuracies which makes it unreliable for determining the integrity of the cement sheath. The log uses changes in acoustic signal amplitude to determine the quality of cement bond on the outer casing wall and the measurement is largely qualitative, showing no clear indication of channelling and the formation of a microannulus.

4. The loads associated with harsh, downhole operating wellbore conditions are typically modelled in integrity monitoring softwares. However, the softwares do not incorporate the input mechanical properties in terms of stresses in the oilwell cement sheath. This is a shortcoming as industry softwares do not include necessary zonal isolation calculations. Even though complementary softwares are available, they are not always included as standard industry practice.

### 1.1.1 Aim and Objectives

The aim of this research project is to develop an innovative geomechanical monitoring system that can predict the mechanical behaviour of the oil-well cement under downhole operating wellbore conditions. The predictive model uses data such

as wellbore pressure, wellbore temperature, formation stress and temperature, and the mechanical properties of the rock formation, cement sheath, and steel casing to ascertain the life expectancy of the cement sheath. Results obtained from this model can be used to provide valuable information for subsequent wellbore integrity analysis and monitoring. The objectives are enumerated below.

1. Develop five models for calculating stress distribution in the oilwell cement sheath and predicting when failures may occur. The first two models developed are an analytical model and a finite element model, using data for downhole operating wellbore conditions, under steady-state conditions. Furthermore, this objective ascertains whether cement sheath failure prediction should be included as standard practice.

2. Extend the developed model(s) for a typical wellbore with multiple casings (i.e. conductor casing, surface casing, intermediate casing, and production casing). Since a wellbore with multiple casings is typically used in the industry, this extension is necessary and practically important.

3. Ascertain the factors that affect long-term integrity of the cement sheath. Parametric analysis is performed for the mechanical properties of the wellbore components (i.e. casing, cement, and rock formation) and the results are used to ascertain the best and worst combinations of the mechanical properties to avoid cement failure.

4. Investigate the effect of eccentricity, induced by high-angle/extended reach wellbores, on the long-term integrity of the cement sheath. Eccentricity is also determined as a function of time during the production-induced reservoir depletion phase.

5. Develop a geomechanical model using wellbore data to predict the effect of ductile formation on the cement sheath. The results of the model will provide definitive results for casing/cement stress and deformation as a function of time under downhole operating conditions.

6. Investigate the influence of well completion on critical drawdown, and ascertain the right direction of perforation through the casing, cement, and formation.

7. Propose a self-sensing monitoring system that is capable of monitoring the behaviour of the oilwell cement sheath. The proposed piezoresistive repair method would repair and regain the strength of a damaged oilwell cement sheath.

### 1.1.2 Methodology Overview

This research project utilised a combination of analytical, finite element, and experimental methods to achieve the objectives outlined in section 1.1.1. Three analytical models were developed for calculating stress distribution in the cement sheath under different operating wellbore conditions, three finite element models were developed to simulate the mechanical behaviour of the cement sheath under various downhole conditions, and two experimental programs were conducted to obtain input data for modelling and perform self-sensing monitoring, respectively.

### 1.1.3 Layout

This thesis is made up of five chapters. The chapters are briefly explained as follows.

1. The first chapter gives an overview of oilwell cement sheath integrity in the oil and gas industry and outlines the specific objectives of the thesis.

2. The second chapter discusses the literature review and scientific efforts in this field of research.

3. The third chapter presents the first experimental program used to obtain input data, and the analytical/numerical models used for predicting the mechanical behaviour of the cement sheath under downhole operating wellbore conditions.

4. The fourth chapter presents the geomechanical model for predicting cement sheath integrity and a proposed completion design for reducing differential stresses.

5. The fifth chapter discusses the experiments and analysis used to propose an innovative self-sensing system for monitoring the structural integrity of the oilwell cement sheath.

# Chapter 2

# Literature Review and Scientific Efforts

This chapter discusses scientific efforts and technical issues in the field of predicting and monitoring cement sheath integrity over the entire life cycle of the oil wellbore.

## 2.1 Introduction

This chapter presents vital information about the basics of well drilling and cementing and the importance of well cement integrity throughout the life of a well. To fully understand the importance of continuous well integrity monitoring, this chapter explains the challenges that the oil and gas industry currently face in monitoring cement sheath integrity, and the need for effective real time monitoring systems that monitor the structural health of oil-well cements. Furthermore, this chapter describes the different stages of the lifecycle of a wellbore (i.e. drilling and construction, production-induced reservoir depletion, and plugging and abandonment) and their unique geomechanical features.

Researchers in the past have conducted experiments on oilwell cement under pseudo-field conditions to ascertain causes of cement sheath failure, and ways to prevent these failures. Goodwin and Crook [37] conducted some experiments on Class G cement under simulated field conditions . Their cement system was mixed, pumped down the annular space, and cured at $350^oF$ by circulating hot oil through

the inner steel casing. They maintained annular pressure at 500 psi during the curing phase and increased the casing pressure from 2,000 psi to 10,000 psi in increments of 2,000 psi. The steel casing, cement sheath, and rock formation were assumed to be thermoelastic materials and the casing/cement and cement/formation interfaces were assumed to be fully bonded with no gaps (i.e. a perfectly bonded casing-cement-formation wellbore assembly with no gaps for leakages) [37, 82]. Two field cases were analysed with the first focusing on the effect of variations in wellbore pressure on the long term integrity of the cement sheath, and the second focusing on the effect of variations in wellbore temperature on the long term integrity of the cement sheath.

Other researchers [122–124] conducted further geothermal well studies with reinforced and plain cements to determine their mechanical properties under elevated temperature ($250^oF$) and pressure conditions (3,000 psi). The specimens used were placed inside pressure curing vessels and the vessels were preheated to about $645^oF$ and maintained at that temperature for the entire duration of the curing cycle. Recorded pressure inside the curing vessel was 2,133 psi at a recorded temperature of $645^oF$, and the curing vessels were removed from the oven at 4-month intervals over a 36-month period.

For the Finite Element Analysis (FEA), the models are not complex to build and some researchers have simulated the mechanical behaviour of the cement sheath under various downhole operating conditions [15,17,20,26,28,30,31,41,64,86]. However, FEA has not been extensively used in conjunction with lab tests/experiments to monitor the mechanical behaviour of the cement sheath in real time. Previous research shows that the most effective way to study the long-term mechanical behaviour of oilwell cement is to use a combined analytical-numerical-experimental approach, as the technical issues typically associated with oilwell cement are shear failures and casing-cement and cement-formation debonding. Restrepo et al. [112] studied the effect of eccentricity on the integrity of the cement sheath and the results show that the presence of channels and voids in the cement sheath increases the likelihood of casing collapse. The study, however, does not show the effect of eccentricity over a long period of time (i.e. years and months) and cannot be used

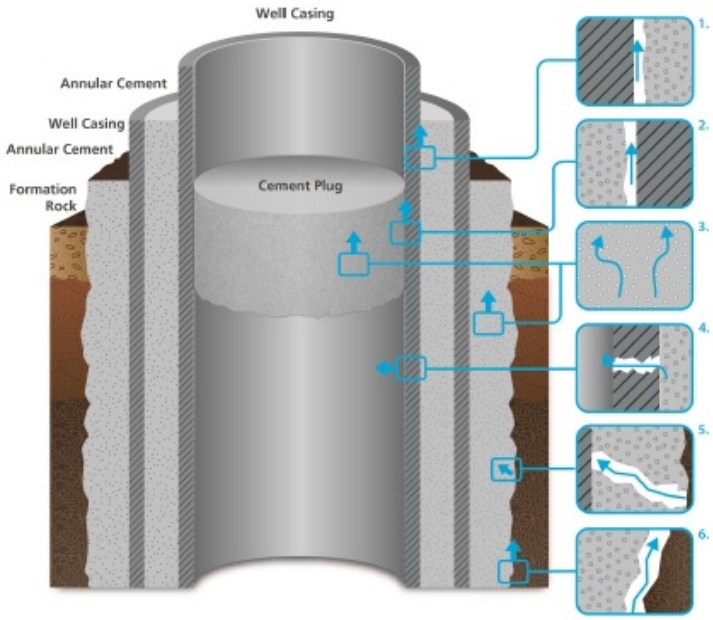


Figure 2.1: Schematic showing the various leakage paths that can be present in an oil wellbore (1. and 2. show the casing debonding from the oilwell cement sheath, 3. and 5. show fractures in the oilwell cement sheath, 4. shows fractures in the steel casing, and 6. shows the cement sheath debonding from the rock formation) [21,26].

to definitively tell how the casing would behave under high-angle conditions during the production phase of a well. Teodoriu [64] proposed an analytical model that can determine the mechanical interaction between the casing, cement, and rock formation, and the results were strongly affected by the different mechanical properties of all wellbore components, especially those of the cement. Numerical and analytical methods require precise input data to significantly improve the quality of results obtained. For this reason, it is important to measure the properties of the oilwell cement under *in situ* conditions.

## 2.2 Life Cycle of an Oil Well

The life cycle of an oil well, as shown in Figures 2.3 and 2.4, can be divided into four important stages: Exploration, Development, Production, and Plugging and Aban-

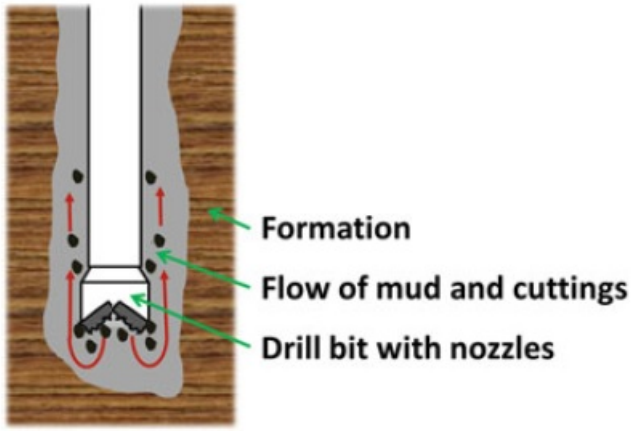


Figure 2.2: A schematic illustration of the oilwell drilling process that shows the drill bit breaking rocks into smaller pieces (i.e. cuttings) and transporting them to the surface, via the drilling mud, through the annular space between the drill string and rock formation (Lavrov and Torsaeter, 2016).

donment. This section presents some background information on the aforementioned stages in the life cycle of the wellbore.

To get an exploration license, petroleum companies need to satisfy some rigorous requirements stipulated by governing bodies. Once the exploration stage commences, geological surveys are performed to develop images of subsurface geological structures and identify potential oil-bearing sands (reservoirs). Exploration wells are then drilled to ascertain the presence of hydrocarbons based on the data gathered from the subsurface surveys. If commercial quantities of oil and/or gas are confirmed during the exploratory phase, appraisal wells are drilled to specifically determine the size and reservoir characteristics of the discovery.

The development phase is made up of drilling, well construction, and completion. The completion phase includes cementing and preparing the well for production in line with the characteristics of the reservoir fluids and production requirements (i.e. perforation, open-hole gravel packing). The production phase is the next stage and typically lasts between 15 years to 35 years [15, 26, 83, 115]. This phase is the most important stage in the life cycle of a well because it allows for operators to produce

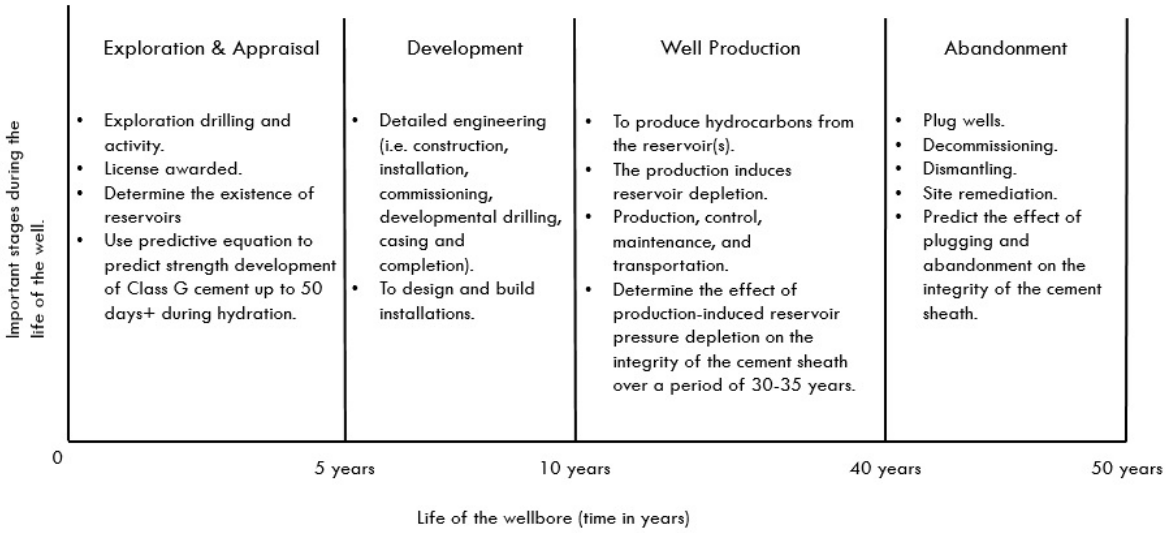


Figure 2.3: Important stages in the life cycle of an oil.

oil and/or gas to the surface for processing/commercial sale. More wells may be drilled to enhance production depending on the targeted rate of production and good cementing jobs are needed for integrity during production-induced reservoir depletion [26, 104, 115].

A decision will be made to abandon or shut-in a well when it reaches its economic limit (i.e. when the highest production rate significantly exceeds the operating expenses). At this stage, the abandoned wellbore is plugged with cement to ensure full isolation and prevent any future leakages.

### 2.2.1 Well Design and Production Casing Cement

Geologists and engineers alike analyse all available seismic data to determine the right type of steel casing, cement configuration, centralisers, reamers, shock absorbers, wellhead, and other equipments that will be needed to maintain well integrity. At specific depths, drilling will be halted temporarily to place steel casing into the ground in order to protect the hole and isolate surrounding aquifers and rock layers. The casing is made stable by pumping cement slurry down the inside the casing shoe and up the annular space between the steel casing and rock formation. Drilling does not resume until the cement slurry hardens and attains a minimum

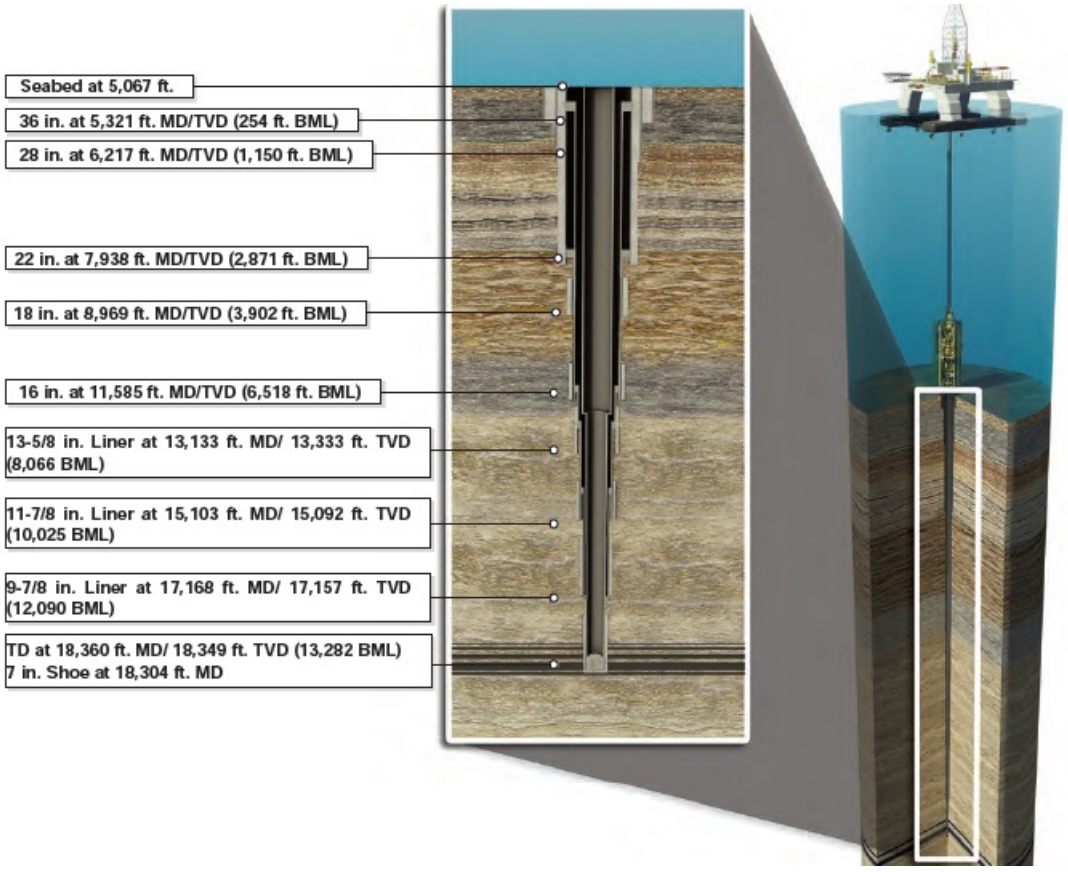


Figure 2.4: Schematic of the Macondo well [83].

compressive strength of 500 psi [79, 115].

There are different types of casings that serve different purposes – conductor casing, surface casing, intermediate casing, and production casing (see Figures 2.5 and 2.6). The casings with larger diameters (i.e. surface casing) are used in the uppermost part of the oil well architecture to ensure well integrity and well control. The production casing or liner is set when the well is about to be prepared for production. Depending on the completion process, a wellbore may be perforated at a depth close to oil-bearing sands/formation to allow oil and natural gas flow from the rock formation into the wellbore for production. Stimulation procedures, such as hydraulic fracturing and thermal injection, can be used to enhance productivity in tighter geological formations.

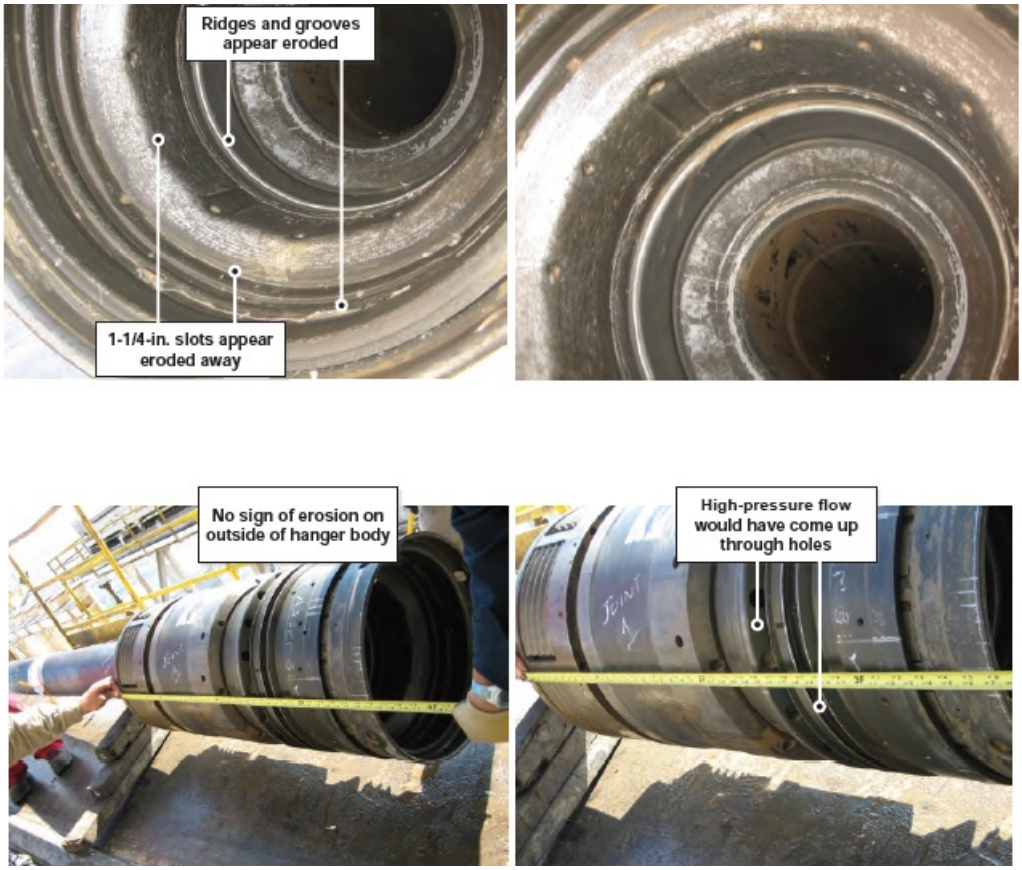


Figure 2.5: Interior (top) and exterior (bottom) of $9 \cdot \frac{7}{8}$-in. Casing Hanger [83].

### 2.2.2 Good Cementing Practices

Enumerated below are the best cementing practices in the industry. These practices currently satisfy the requirements of an ideally cased and cemented well for long term integrity.

1. The cement has to attain a compressive strength of 500 psi under 24 hours before resuming drilling operations. A leak-off test is performed during drilling to make sure the integrity of the oilwell cement is well maintained [79, 115].

2. The steel casing must be well centered in the wellbore using centralizer subs (see Figure 2.7). Centralizers are downhole devices that keep the casing(s) in the center of the wellbore in order to ensure efficient placement of the oilwell cement. If the casings are cemented off-center (eccentric) or not enough of them are used, there is a risk of creating an incomplete seal that could compromise long term integrity (see Figure 2.8).

3. The wellbore hole needs to be circulated until at least 85% of the annular volume is circulating [37, 115].

4. During drilling and cementing, the steel casing(s) should be rotated and reciprocated.

5. Lost circulation problems must be resolved before cementing in order to not lose cement and compromise well integrity [115].

6. Proper use of centralizers and using the right number of centralizers, cement plugs, scratchers, and other hardware of the casing.

### 2.2.3 Classification of Oil-Well Cement

The procedures for testing the performance of different types of construction cement were determined by the American Society for Testing and Materials (ASTM). However, the petroleum industry determined that the ASTM tests were inadequate for testing the performance of oilwell cements because these cements are made for

Figure 2.6: A typical centralizer sub used for centering the casing in the wellbore [83].

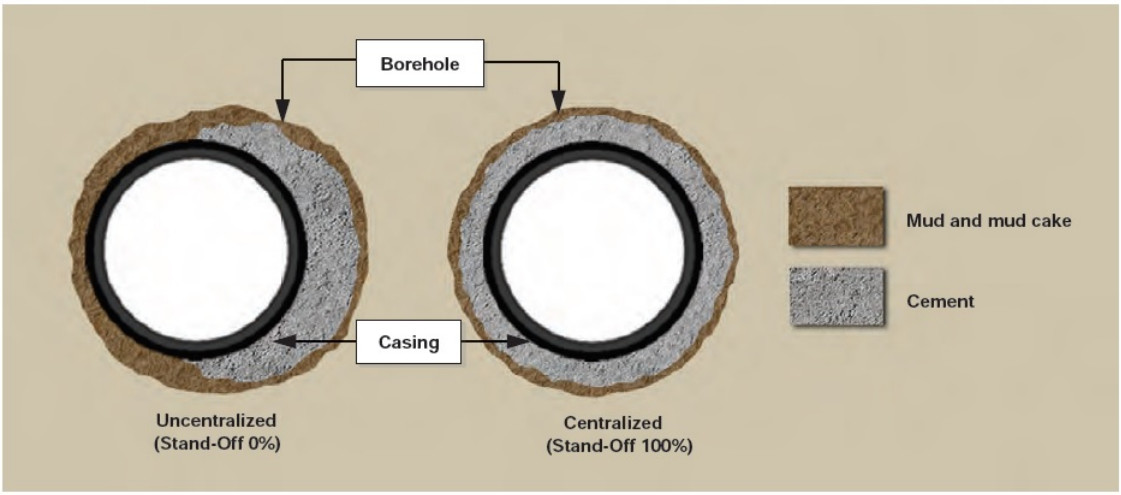


Figure 2.7: A schematic showing poor centralization (i.e. 0% stand-off) versus good centralization (i.e. 100% stand-off) of casing.

harsher downhole, operating wellbore conditions characterised by high pressures and high temperatures [82, 115].

API specifications are used to classify oilwell cement based on specific, required properties. This specification has nine classes of cement – lettered A, B, C, D, E, F, G, H, and J (see Table 2.1).

Table 2.1: Different classes of oil well cement and their properties. MSR represents Moderate Sulphate Resistance and HSR represents High Sulphate Resistance [115]
`[long]`

| Start of Table | | |
|---|---|---|
| API Class (ASTM Type) | Depth | Remarks |
| Class A (Type I) | Applied from surface to 6,000 ft. | No special properties required; w/c ratio of 0.46; specific gravity of 3.14; surface area of 1,500 $cm^2/gm$; Ordinary Portland Cement. |
| Class B (Type II) | Applied from surface to 6,000 ft. | Moderate Sulfate-Resistant (MSR) and High Sulfate Resistant (HSR); w/c ratio of 0.46; specific gravity of 3.14; surface area of 1,600 $cm^2/gm$; Ordinary Portland Cement. |

| Continuation of Table 2.1 | | |
|---|---|---|
| API Class (ASTM Type) | Depth | Remarks |
| Class C (Type III) | Applied from surface to 6,000 ft. | High Early Strength Moderate Sulfate-Resistant (MSR) and High Sulfate Resistant (HSR); w/c ratio of 0.56; specific gravity of 3.14; surface area of 2,200 $cm^2/gm$; High early cement. Finer than classes A and B. |
| Class D | Applied from 6,000 ft. to 10,000 ft. | MSR, HSR, High-Pressure/High-Temperature (HPHT); w/c ratio of 0.38; specific gravity of 3.16; surface area of 1,200 $cm^2/gm$; Retarded cement. |
| Class E | 10,000 ft. to 14,000 ft. | MSR, HSR, and HPHT; w/c ratio of 0.38; specific gravity of 3.16; surface area of 1,200 $cm^2/gm$; Retarded Cement. |
| Class F | 10,000 ft. to 16,000 ft. | HSR, Extremely HPHT; w/c ratio of 0.38; specific gravity of 3.16; surface area of 1,200 $cm^2/gm$; Retarded Cement. |

| Continuation of Table 2.1 | | |
|---|---|---|
| API Class (ASTM Type) | Depth | Remarks |
| Class G | Applied from surface to 8,000 ft. | MSR, HSR; w/c ratio of 0.44; specific gravity of 3.16; surface area of 1,400 $cm^2/gm$; Basic, commonly used well cement that can be used with accelerators and retarders to cover a good range of well depths and temperatures. |
| Class H | Applied from surface to 8,000 ft. | MSR, HSR; w/c ratio of 0.38; specific gravity of 3.16; surface area of 1,200 $cm^2/gm$; Basic, commonly used well cement that can be used with accelerators and retarders to cover a good range of well depths and temperatures. Coarser than Class G cement. |
| Class J | Intended for a depth range of 12,000 ft. to 16,000 ft. | Can be used with accelerators and retarders to cover a range of well depths and temperatures. No other addition other than water and calcium sulphate is necessary. |
| End of Table | | |

API classes D, E, F, G, H, and J are manufactured specifically for deep wells under harsh, operating wellbore conditions i.e. high pressure and high temperature. These types of oilwell cement are manufactured and distributed in North America

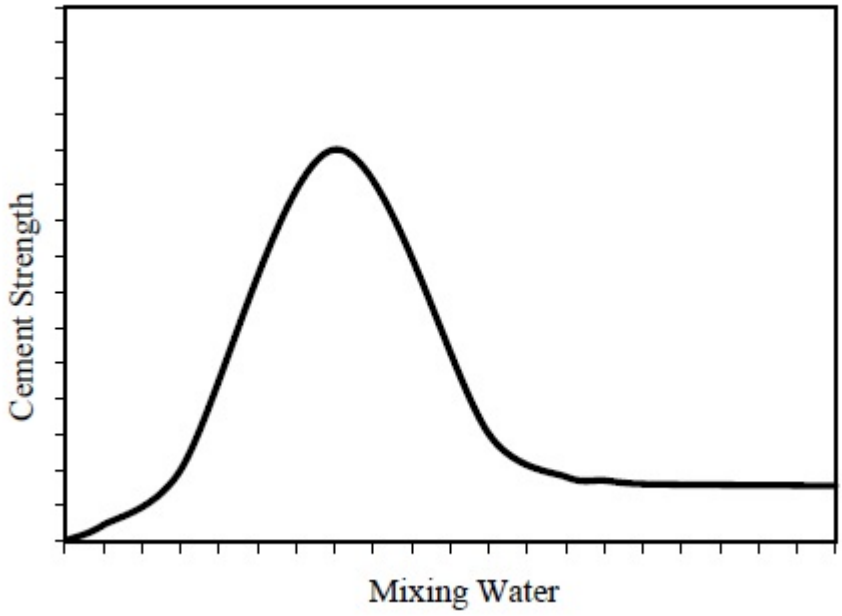


Figure 2.8: Plot showing variation of cement strength with mixing water.

– classes G and H being the most used and distributed (approximately 65% of the oilwell cement used in the US is class H cement). Outside North America, approximately 95% of the oilwell cement used is class G i.e. Europe, Middle East, South America, and Far East.

Even though the strength of the oilwell cement changes with water, strength is not the only criterion for deciding the water/cement ratio. Other factors to consider include, but are not limited to, flowability and pumpability.

The chemical reaction of cement and water causes hardening of the cement which is known as 'hydration' in the industry, and it starts as soon as the oilwell cement comes in contact with water [115]. When the cement mixes with water, the binding phases in Portland cement ($Ca_3SiO_5$ and $Ca_3Al_2O_4$) will react in different ways. During hydration, chemical reactions between the clinker components, calcium sulfate, and water would occur, leading to cement thickening and hardening. The products of hydration are calcium silicate hydrate and calcium hydroxide as shown in Equations (2.3.1) and (2.3.2). The final product "Calcium Silicate Hydrate" (C-S-H) is the principal binder of hardened cement and is made up of more than 70% fully hydrated Portland cement. During short hydration times, the aluminate phases

(i.e. $Ca_3Al_2O_4$) are the most reactive and have a strong impact on the rheology of the oilwell cement slurry and the early strength development of the set cement (see Equation 2.3.3).

$$2Ca_3SiO_5 + 7H_2O \rightarrow 3CaO \cdot 2SiO_2 \cdot 4H_2O + 3Ca(OH)_2 \tag{2.2.1}$$

$$2Ca_2SiO_4 + 4H_2O \rightarrow 3CaO \cdot 2SiO_2 \cdot 4H_2O + Ca(OH)_2 \tag{2.2.2}$$

$$2Ca_3Al_2O_4 + 27H_2O \rightarrow Ca_2 \cdot Al_2O_3 \cdot 8H_2O + Ca_4 \cdot Al_2O_3 \cdot 19H_2O \tag{2.2.3}$$

## 2.3 Technical Challenges Associated With Long Term Cement Sheath Integrity.

There are a number of technical issues associated with maintaining the integrity of the oil wellbore, starting with placement of the cement slurry in the annular space. If these issues are addressed early enough or in time, technical changes could be made – hence necessitating the need for an efficient real time monitoring system. Pertinent wellbore integrity issues are primarily in two stages: pre-production stage (i.e. drilling and well construction), production stage (production-induced reservoir depletion), and the plugging and abandonment phase. Technical issues found in literature and industry are discussed below in section 2.4.1.

### 2.3.1 Pre-Production Stage: Technical Issues

The pre-production stage is mainly related to the drilling and well construction process. After the cement sheath hardens, it is impossible to remove it – especially when it loses integrity. This necessitates the need for real time monitoring of the cement sheath over its entire life cycle. Itemised below are the technical issues associated with the pre-production stage;

1. Sometimes, the cement does not occupy the total annular space (100% annular space) and leaves pockets.

2. Oilwell cement contaminated with fluids such as drilling mud, spacer, or formation fluids have lesser density than is advised for optimum integrity and compressive strength [26, 37, 89, 115].

3. Channels within the cement sheath (and at the casing/cement and cement/formation interfaces) filled with liquid or gas.

4. Drilling induced vibrations could cause formation failure during drilling and well construction.

5. Poor and inadequate centralisation of the steel casing causes inconsistent cement sheaths and incomplete cementing. Cement will not fully displace the drilling mud from the eccentric parts of the annular space, leaving air pockets in narrow openings [26].

6. Entrapped drilling mud creates channels and forms mud cake. This typically happens when there is little to no circulation and subsequently weakens the integrity of the cement sheath (see Figure 2.8).

7. Under high-pressure/high-temperature conditions, water loss occurs which adversely affects the strength of the cement [79].

8. Pressure and leak-off tests exert stresses on the cement sheath, especially some days after cement placement. Typically, cementing operations require a minimum strength of about 500 psi to restart to drilling operations [79]. This waiting strength is known in the industry as wait-on-cement (WOC), which depends on the hydration time and is directly related to the drilling cost per hour. A shorter waiting time may contribute to cement failure (i.e. radial cracks and debonding at the casing/cement and cement/formation interfaces) due to imperfect setting of the cement sheath.

9. Variations in temperature induce a lot of stress on the cement sheath during drilling, logging, and injection tests. The loads induced by thermal processes exert stresses on the steel casing and cement sheath, causing an expansion of the steel casing against the cement sheath. This is investigated further in the methodology section of this research project.

### 2.3.2 Production Stage: Technical Issues

The production stage is characterised by production-induced reservoir depletion. The most pertinent wellbore integrity issues associated with the production phase are enumerated below;

1. Production can induce fractures in the rock formations and within the cement sheaths. These fractures create pathways for oil and gas to leak to the surface thereby compromising the integrity of the well (see Figure 2.2).

2. During the production phase, the HPHT conditions are more extreme. In the UK, HPHT is formally defined as a well having an undisturbed bottomhole temperature of greater than $300^oF$ and a pore pressure of at least 0.8 $psi/ft$ or requiring a Blowout Preventer (BOP) with a rating in excess of $10,000$ psi. These harsh downhole conditions cause significant expansion and contraction of the wellbore system, especially the cement sheath.

3. A micro-annulus could form at the casing/cement and cement/formation interfaces.

4. Weakening of the cement/formation bond due to production-induced reservoir depletion, as aforementioned. This causes leakage pathways around the interfaces and the formation of a micro-annulus.

5. During the life cycle of the wellbore, the casing-cement-formation assembly will be exposed to operating downhole conditions i.e. HPHT conditions. Cement with high sulfate resistance is typically used in the industry to maintain well integrity over its entire life cycle. High acidity downhole can induce corrosion of the steel casing and weakening of the cement sheath.

### 2.3.3 Plugging and Abandonment Stage: Technical Issues

All petroleum wells have to be plugged and abandoned at the end of their economic lives. This procedure must provide a thorough isolation of fluids along the wellbore to reduce the environmental risks of contamination and prevent costly remedial

jobs [36]. Enumerated below are some of the pertinent technical issues associated with the plugging and abandonment phase of a petroleum wellbore;

1. Even though previous research has analysed the mechanical behaviour of the plug when subjected to local pressure and thermal changes, little to no work has been done to accurately determine the effects of external pressure and stress changes on the cement plug after production-induced reservoir depletion ends.

2. Improperly abandoned wellbores pose a serious threat to the quality of groundwater and marine ecosystems [36]. Furthermore, remedial jobs are exorbitant and uneconomical for companies.

3. Deciding what sealing material to use for plugging and abandonment is not always obvious and depends on downhole operating conditions. Operating companies regularly develop novel cement formulations to ensure zonal isolation throughout the entire life of the wellbore, e.g. high compressive oilwell cements are not necessarily the best solution for plugging and abandoning the well.

4. From a mechanical perspective, the sealing plug typically loses integrity at the cement/rock interface via debonding. Several authors have analysed cement sheath failure during some phases of well completion and production but little work has been done to analyse the mechanical behaviour of the cement plug after abandonment [17, 31, 73, 82, 107].

5. Previous research in this field assumed no changes in pressure, temperature, and stress at the location of the cement plug and rock formation after setting. This assumption is not valid for plugged wellbores located in a field where pressure, heat, and stress states are not in equilibrium at the start of the abandonment phase.

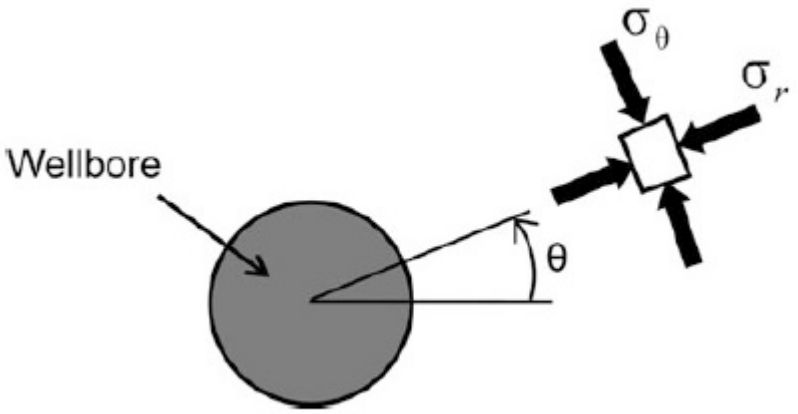


Figure 2.9: Directions of radial stress, $\sigma_r$, and hoop stress, $\sigma_\theta$, in the vicinity of the wellbore [26].

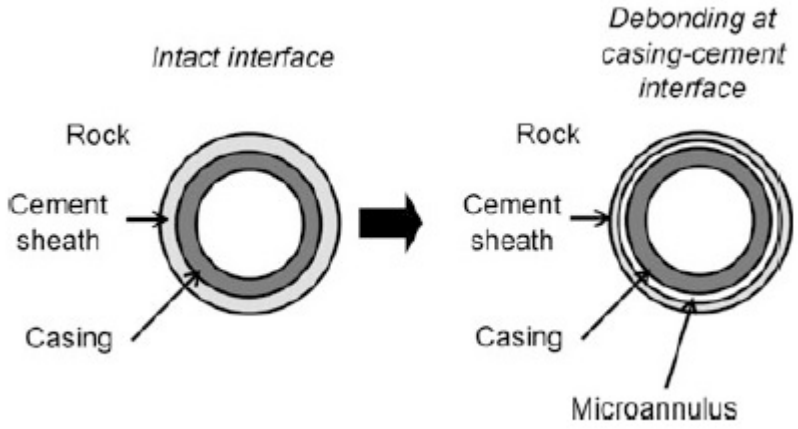


Figure 2.10: Debonding at the casing/cement interface.

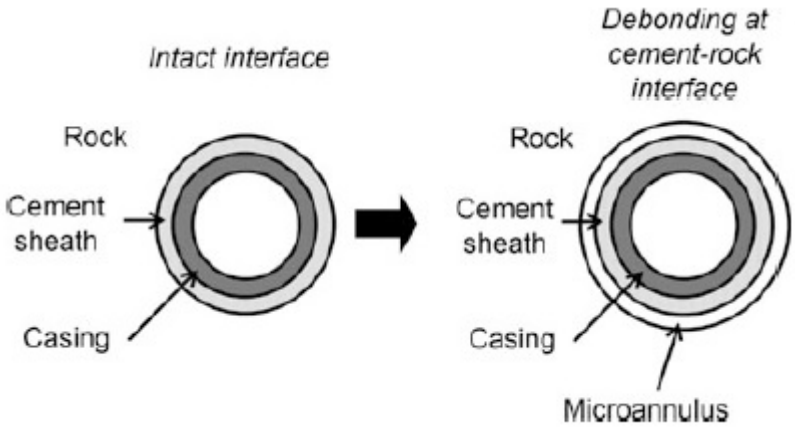


Figure 2.11: Debonding at the cement/formation interface.

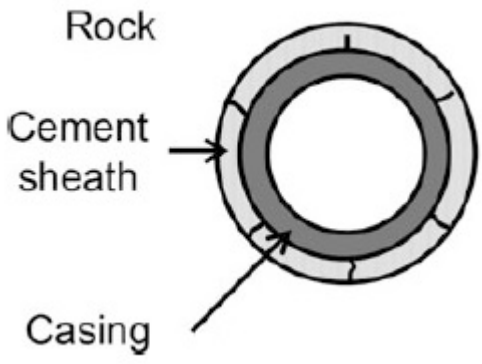


Figure 2.12: Schematic showing radial fractures in the cement sheath.

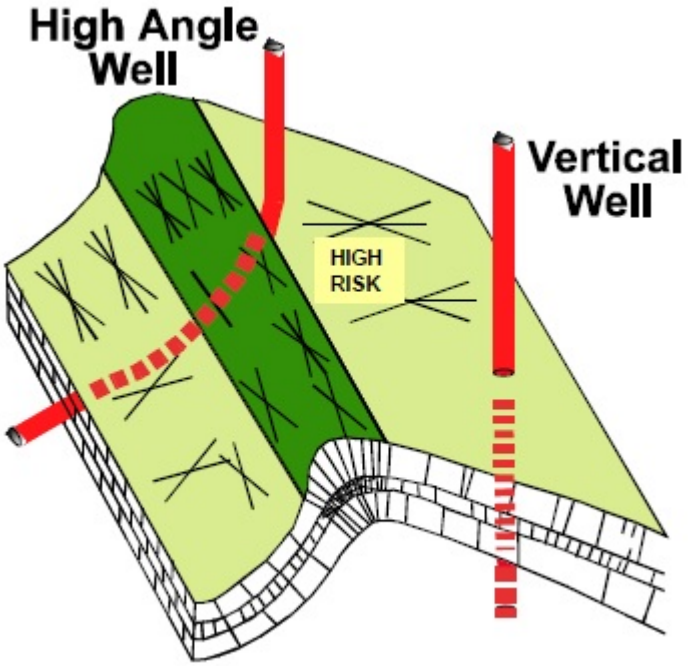


Figure 2.13: Trajectory for a high-angle well versus a typical vertical well.

## 2.4 Technical Issues With Casing Eccentricity.

High angles in wellbores induce casing eccentricity due to significant standoff, causing the cement sheath to be thinner in one side of the annular space (see Figures 2.14 and 2.15). Estimating casing design and safety factors based on stress calculations, that are under the assumption of a concentric casing placement, is erroneous and will produce inaccurate results. Mathematically, casing eccentricity $e$ is a dimensionless indicator that is directly related to the deflection of the casing in the borehole through the Equation (2.6.4);

$$e = \frac{\delta_r}{r_0 - r_i} \tag{2.4.4}$$

Where $\delta_r$ is the deflection of the steel casing from the center of the borehole (i.e. distance between the center of the wellbore and the center of the steel casing), $r_0$ represents the radius of the borehole, and $r_i$ represents the outer radius of the steel casing.

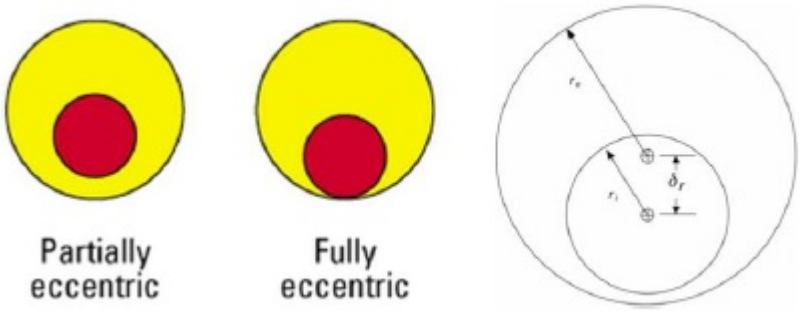


Figure 2.14: Schematic representation of different types of eccentricity, i.e. partial eccentricity and fully eccentricity.

## 2.5 Monitoring Well Behaviour In Real Time

Unlike construction cement that can be physically touched after setting and installation, oilwell cement sheath lies thousands of feet subsurface and cannot be regularly monitored with the naked eyes. For this reason, we have to depend on the results of measurements obtained from downhole tools to ascertain the integrity (i.e. quality) of the cement sheath placed around the steel casing. However, current research shows that the industry lacks efficient and cost-effective monitoring systems for real-time monitoring of cement sheath integrity during and after the production phase [104, 115].

If the annular space is filled with bad cement or not-well settled barite from drilling mud, no portion of the cement can be removed because it is in solid form, meaning that only cement in slurry/liquid form can be removed from the annular space for replacement. When cement mixes with either drilling mud or formation fluid in the annular space, the cement loses much needed density and compressive strength which could cause potential well integrity issues. This contamination produces a cement sheath that is not fully recognised as cement on a bond log measuring system, thereby necessitating an effective post-placement integrity monitoring system. A Cement Bond Log (CBL) uses variations in amplitude to ascertain the quality of cement bond on the outer (and inner) wall of the steel casing – based on the principle that the acoustic signal will be more attenuated in the presence of cement. However, the CBL measurement is mainly qualitative and struggles to

identify channelling within the cement sheath [115, 116].

### 2.5.1 Functions and Properties of the Real-Time Monitoring System

The proposed real-time monitoring method in this research thesis is based on electrical properties such as resistivity and impedance spectroscopy. Monitoring resistivity can help with the prediction of cement hydration because it changes with cement curing time. Very few studies have used electrical measurement methods to characterise the micro-structural evolution of hydrating cement, and its associated materials [117–121]. The piezoresistive effect, an important electrical property, measures the change in electrical resistivity of a metal (or semiconductor) when a mechanical strain is applied. This change in resistivity forms the basis for monitoring the integrity of the cement sheath in real time and is discussed in detail in a separate section of this research thesis.

The monitoring system needs to be capable of performing the following tasks;

1. Regularly monitor the placement and rising of cement slurry in the annular space and set off an alarm if something goes awry at a certain depth during and after placement.
2. Accurately detect free water level if present.
3. Detect air pockets and alert on time.
4. Set off alarm if water loss or a change in density are detected.
5. Ascertain stress levels at various depths along the cement sheath.
6. Detect cracks and accurately determine their depths.

## 2.6 Summary of Literature Review and Scientific Efforts

This section summarises the literature review discussed in the thesis. The summary points are enumerated below;

1. The lifecycle of a wellbore is made up of the well construction and development phase, the production phase (i.e. production-induced reservoir depletion), and the abandonment phase.

2. The cement sheath, which is the primary barrier in the wellbore, provides zonal isolation and holds the steel casing(s) in place. The cement sheath can get damaged over time due to variations in stress and should be monitored in real time for this reason.

3. A number of factors adversely affect the integrity of the cement sheath from placement through to abandonment. These technical factors are issues that need to be handled adequately using a robust monitoring system.

4. An effective monitoring system is needed to track the integrity of the cement sheath in real time and detect cracks and defects in the cement sheath in a timely manner.

5. Based on the principle of electrical resistivity, a monitoring system can track the integrity of the cement sheath by measuring the impedance and resistivity.

# Chapter 3

# Methodology

This chapter presents the methodology used in this research project. The research methods used for studying oilwell cement can be divided into analytical/numerical methods and experimental methods (i.e. laboratory tests). The first batch of experiments were performed to characterize oilwell cement (Class G) and measure its mechanical properties for relevant structural calculations such as compressive and tensile strength, Young's modulus, and Poisson's ratio.

## 3.1 Experimental Study

Since Class G cement is the preferred choice in western Europe, the focus was on generating a good data package for this cement to be used as a point of reference for other cement types. The cement composition had a water-cement factor of 0.45 and a slurry density of 15.77 lbm/gal. The procedures used for preparing the samples, measuring the mechanical properties, and determining the compressive strength of the cement are explained further in the next subsections.

### 3.1.1 Preparing Cement Samples

The cement mixture was blended for about twenty minutes and mixed under the API 10B mixture guidelines. The mixing process lasted about 50 seconds at a rate of $4,000$ rev/min, and was later increased to $12,000$ rev/min to create a fine cement blend. After mixing, the cement mixture was poured into a curing mould that is

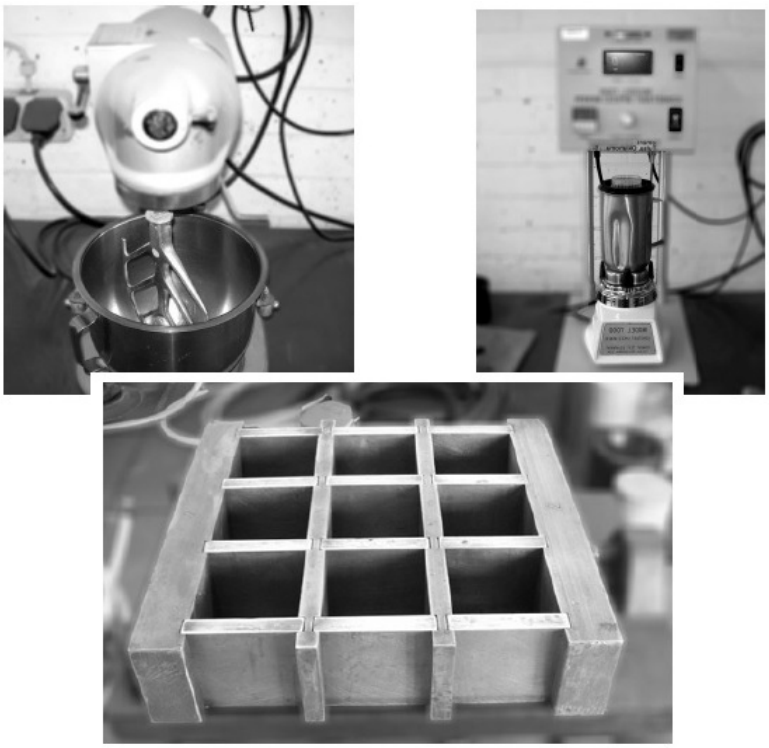

Figure 3.1: Photos of the curing mould, cement blender, and API mixer used for preparing the cement samples.

made up of nine $2 \times 2 \times 2$-in. blocks that are 5 inches in height (see Figure 3.1). The various cement samples were cured under three different conditions – (a) room condition, (b) $167^oF$ under atmospheric pressure, and (c) $212^oF$ under a pressure of $2,610$ psi. The samples were put in an oven and held at a temperature of $167^oF$ under atmospheric pressure with the aid of an autoclave. The cement samples were allowed to cool down and depressurise before measurements were taken.

### 3.1.2 Measuring Young's Modulus and Poisson's Ratio

Unconfined Compressive Strength (UCS) and compressive strength tests were performed on the aforementioned cubic samples to ascertain the compressive strength. A velocity measuring instrument (*Ultra Epoch 4*) was used to determine the Poisson's ratio and Young's modulus of the cement samples by measuring the velocities of shear and compressive waves (see Figure 3.2).

Figure 3.2: Instrument used for measuring the velocities of shear and compressive waves to determine the Poisson's ratio and Young's modulus.

$$\nu = \frac{1 - 2(V_T/V_L)^2}{2 - 2(V_T/V_L)^2} \tag{3.1.1}$$

$$E = \frac{V_L^2 \cdot \rho(1+\nu)(1-2\nu)}{1-\nu} \tag{3.1.2}$$

Where $V_L$ represents the shear velocity (ft/sec), $V_T$ represents the longitudinal velocity (ft/sec), and $\rho$ represents the density (lbm/gal).

### 3.1.3 Compressive Strength Test

A hydraulic press was used to measure the compressive strength of cement samples. The plot in Figure 3.3 (compressive strength development with time under different conditions) shows that after the first day, the recorded compressive strength is 865 psi and it increased significantly over the next eight to twenty days (i.e. from 865 psi to approximately $6,120$ psi). After the first twenty days, it was observed that the compressive strength increased very slightly. Under $167^oF$, the recorded compressive strength of the cement sample reached $5,110$ psi after the first twenty-four hours and increased progressively to $9,217$ psi after fourteen days. The compressive strength did not change much afterwards and remained relatively steady until the end of the experiment. For the cement samples cured under $212^oF$ and $2,610$ psi, the

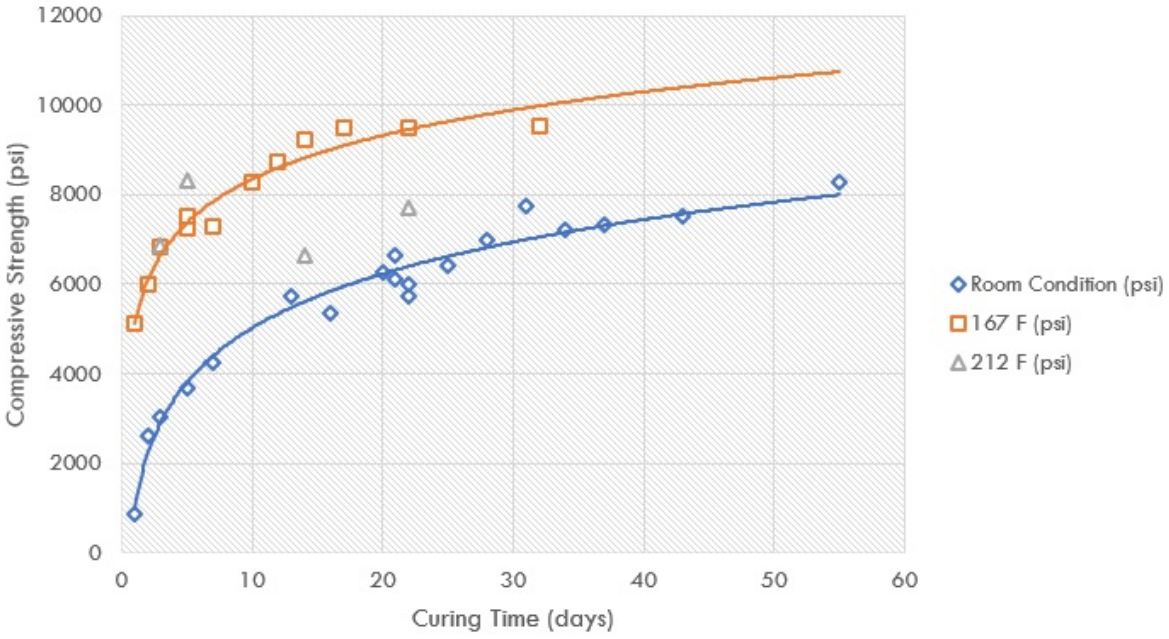


Figure 3.3: Compressive strength development of Class G cement with time.

recorded compressive strength after three days (6, 881 psi) was close to the recorded compressive strength after fourteen days (6, 654 psi).

Due to the limited sample size for the HPHT test, we inferred that the compressive strength would develop very quickly under HPHT conditions and remain relatively constant. Furthermore, all the samples were cured within a maximum of fourty days and the tests do not necessarily reflect the degradation of cement that is noticed in geothermal and injection wells.

The development of Poisson's ratio with time (Figure 3.4) shows that the ratio did not increase much over the experiment period and stayed relatively constant at approximately 0.29. Under $167^oF$, the ratio decreased from 0.312 to 0.205 over thirty days and remained steady. The ratio did not change much after twenty-one days under $212^oF$ and 2, 610 psi (approx. 0.2).

The plots showing the development of Young's modulus with time (Figure 3.5) shows that the Young's modulus increased from $1.75E6$ psi after eleven days to $2.33E6$ psi after fourty-five days, and remained steady. Under $167^oF$, the Young's modulus increased from $1.8E6$ psi after the first couple of days to $2.52E6$ psi after thirty days.

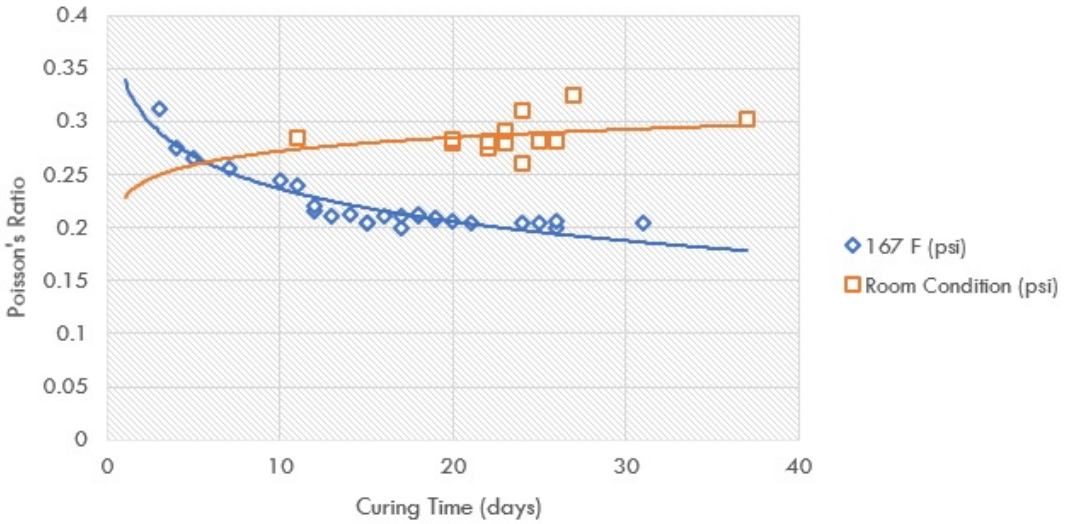


Figure 3.4: Poisson's ratio development of Class G cement with time.

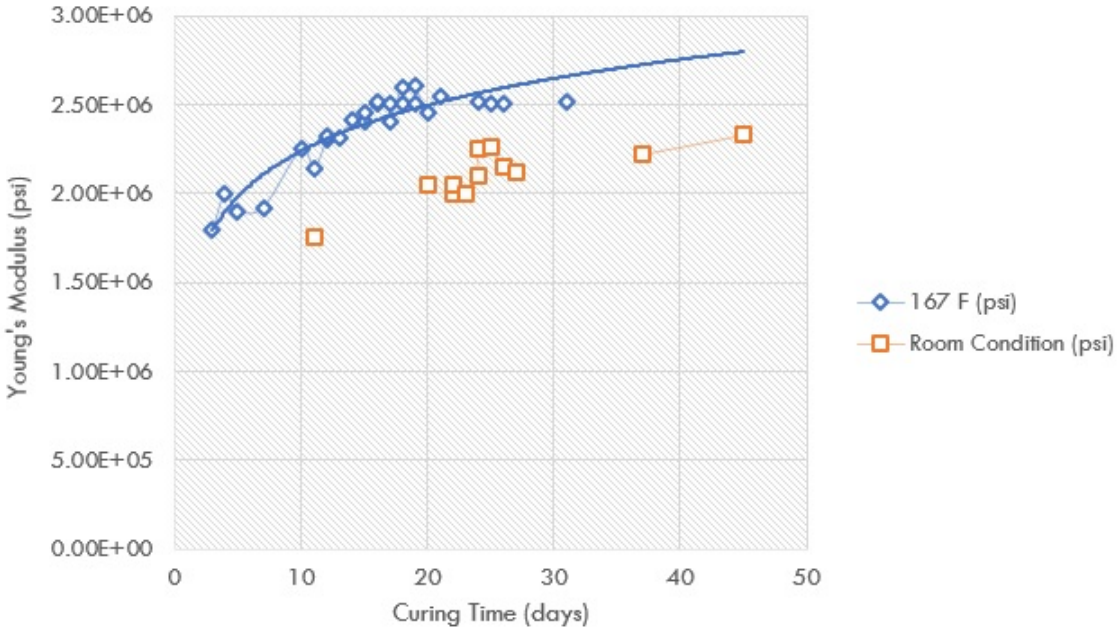


Figure 3.5: Young's Modulus development of Class G cement with time.

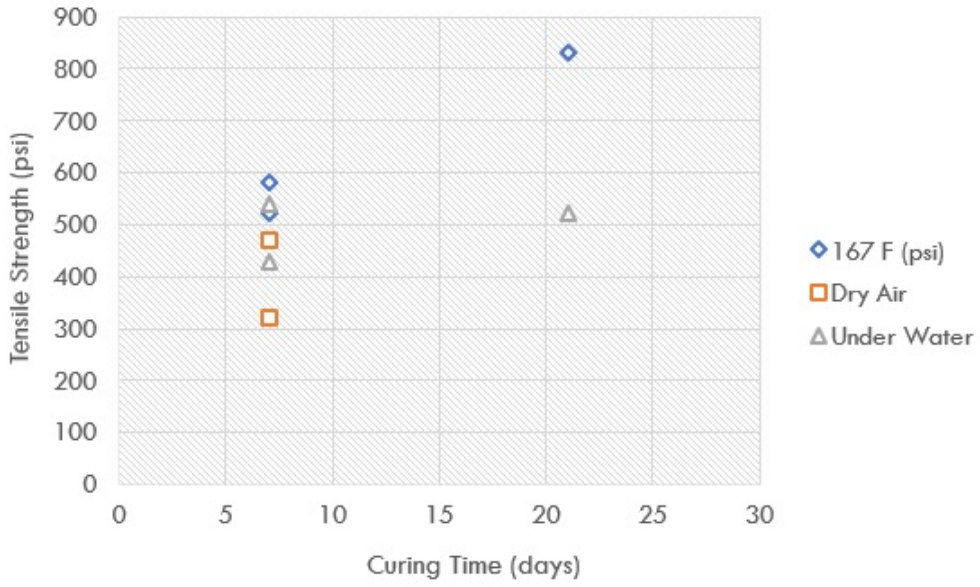


Figure 3.6: Tensile strength development of Class G cement over twenty-one days.

### 3.1.4 Tensile Strength Test

The tensile strength test for cement (also known as the Brazilian test) was performed under three different conditions: (a) dry air, (b) under water, and (c) $167^oF$. The cement samples were similar to the ones used for the compressive strength test (2 inches in diameter and 2 inches) and the tensile strength test was done in accordance to the ASTM D 3967 procedure. Tensile strength(s) of the samples were first measured after seven days and the ones cured under $167^oF$ had the highest recorded value (580 psi), while the sample cured under water had the second highest recorded tensile strength value (540 psi) and the sample cured in dry air conditions had the lowest recorded tensile strength value (320 psi). After twenty-one days, the recorded tensile strength of Class G cement cured under $167^oF$ increased significantly (830 psi), and the cement sample cured under water had a slightly lower recorded tensile strength value (521 psi).

## 3.2 Summary of Strength Test Results

This section presents a summary of the results and findings from the strength tests conducted on the cement samples.

### 3.2.1 Conclusions

The experiments provide a good set of data for Class G cement evaluation that can be used for numerical studies such as FEA and structural analysis. The results of the experiment show that under low-temperature conditions (i.e. room condition), the mechanical properties of cement did not change much with time. The compressive strength of the cement increased with temperature and showed stabilisation around $10,340$ psi. The stabilised Young's modulus of $2.55E06$ psi under high temperature conditions and $2.30E06$ psi are comparable to the input data of previous cement integrity research [28,31,86,104,107,112]. Lastly, the value of the recorded Poisson's ratio after stabilisation was approximately 0.21 under room condition and 0.3 under high temperature conditions.

### 3.2.2 Discussions

The extrapolated experimental value of compressive strength under room temperature reached a stabilised value of approximately $8,740$ psi after more than seventy days. Under elevated temperature conditions, the stabilised value attained a higher compressive strength value of between $10,152$ psi and $10,877$ psi. The test results showed that if extrapolated further, the Young's modulus will stabilise at $2.53E06$ psi after seventy days (under room conditions), and $2.52E06$ psi under elevated conditions.

The Poisson's ratio decreased from 0.312 to 0.205 over the span of thirty plus days under elevated temperature conditions (i.e. $167^oF$) and increased from 0.285 to 0.303 over thirty plus days under room condition. The tests conclusively show that a Poisson's ratio of approximately 0.2 is adequate for numerical analysis.

## 3.3 Analytical Model for Predicting Cement Sheath Failure.

It is necessary to calculate the state of stress in the cement sheath to ascertain if the cement will fail or debond at the interfaces (i.e. casing/cement interface and

| Parameters | Yuan [92] | Wang [113] | Bustgaard [104] | Restrepo [112] | Wilcox |
|---|---|---|---|---|---|
| Comp. Strength (psi) | 8,702 | 9,500 | 8,702 | | 10,340 |
| Tensile Strength (psi) | 435 | 603.08 | 3,000 | | 580 |
| Young's Modulus (psi) | 2.47E6 | 2E6 | 1.74E6 | 1.45E6 | 2.55E6 |
| Poisson's Ratio | 0.2 | 0.2 | 0.3 | 0.26 | 0.21 |

Table 3.1: Comparison of experimental values with different authors from the past ten years.

cement/formation interface). Elastic behaviour is assumed for the analytical and numerical models and the right boundaries such as the interfaces, pressure, and temperature conditions are inputted in the model.

This section discusses the development of an analytical model for predicting failure in or around the cement sheath (the theory is explained in further detail in Appendices A and B.

### 3.3.1 Principal Cylinder Stresses

In a cylinder subject to changes in temperature and pressure, three perpendicular principal stresses are set up in the material. The principal stresses are shown in Figure 3.7. The tangential stresses are the normal stresses that are in the azimuthal direction acting around the circumference of the cylindrical material. For this reason, pressure differentials across a cylindrical pipe generate hoop stress. Longitudinal stresses are the stresses along the axis of the cylinder while radial stresses are acting away from or towards the axis of the cylinder. The thick-walled cylinder theory suggests that the internal pressure is equivalent to the radial stress at the inner wall of the cylinder while the external pressure is equivalent to the radial stress at the outer wall of the cylinder.

### 3.3.2 Thin-Walled and Thick-Walled Cylinder Theories

The thin-walled cylinder theory can not be used for the steel casing and cement sheath because it assumes that the radial and axial stresses are constant across the

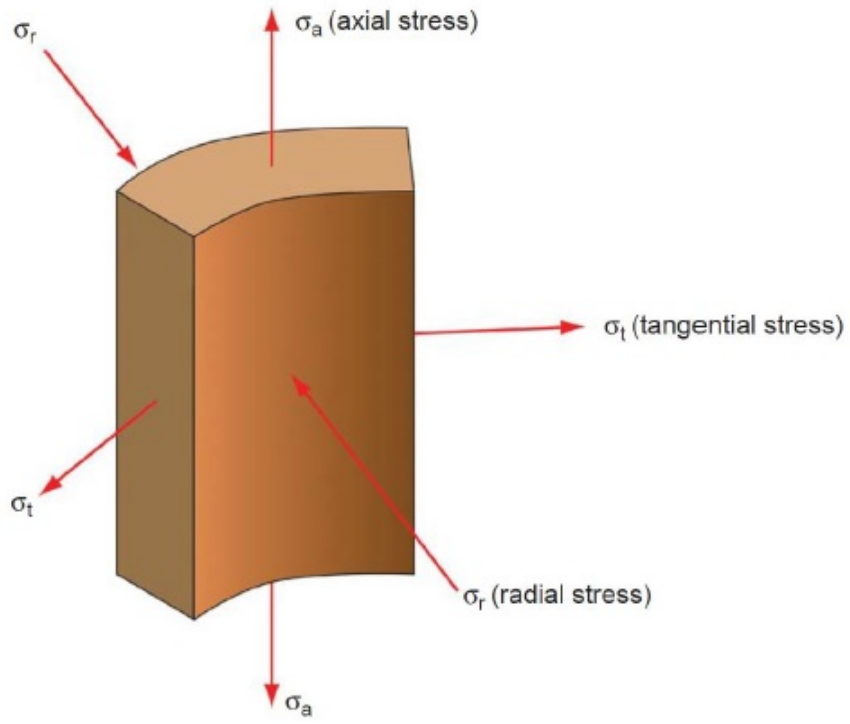


Figure 3.7: Schematic showing the principal stresses in a cylinder section i.e. the hoop stress (tangential), axial stress (longitudinal), and radial stress.

thickness of the wall. The thick-walled cylinder theory is much more applicable as a stress theory for modelling the stress states in casing-cement-formation wellbore system. The stress theory developed by Lam was used in this project as it accounts for pressure differences across the wall of the cylinder and changes in the hoop stress across the thickness of the cylinder.

### 3.3.3 Lame's Cylinder Theory

The derivation of Lame's theory is shown in detail in the Appendices. Equations (3.3.3) and (3.3.4) are the main results of the derivation and can be used for any radius to calculate the hoop and radial stresses in a thick-walled cylinder.

$$\sigma_r = A - \frac{B}{r^2} \tag{3.3.3}$$

$$\sigma_H = A + \frac{B}{r^2} \tag{3.3.4}$$

Where $\sigma_r$ represents the radial stress (psi), $\sigma_H$ represents the hoop stress (psi), $r$ represents the radius (m), and $A$ and $B$ represent Lam's constants (the constants are determined for the right boundary conditions).

### 3.3.4 Boundary Conditions

As aforementioned, Lame's cylinder stress equations can be used for a cylinder subjected to internal and external pressures. Equations (3.3.5) and (3.3.6) are the boundary conditions applied to the cylinder.

$$\sigma_r(\sigma_i) = -P_i \tag{3.3.5}$$

$$\sigma_r(r_o) = -P_o \tag{3.3.6}$$

Where $r_i$ represents the internal radius of the cylinder (m), $r_o$ represents the outer radius of the cylinder (m), $P_i$ represents the internal pressure of the cylinder (psi), and $P_o$ represents the external pressure (psi). By inputting the boundary

conditions (Equations 3.3.5 and 3.3.6) into Lam's equations (Equations 3.3.3 and 3.3.4), the constants A and B can be calculated using Equations (3.3.9) and (3.3.10) shown below;

$$-P_i = A - \frac{B}{r_i^2} \tag{3.3.7}$$

$$-P_o = A - \frac{B}{r_o^2} \tag{3.3.8}$$

$$A = \frac{(r_i^2 P_i - r_o^2 P_o)}{(r_o^2 - r_i^2)} \tag{3.3.9}$$

$$B = \frac{(P_i - P_o) r_i^2 \cdot r_o^2}{(r_o^2 - r_i^2)} \tag{3.3.10}$$

The radial, tangential, and axial stresses in a cylinder can be calculated using Equations (3.3.11), (3.3.12), and (3.3.13);

$$\sigma_r = \frac{r_i^2 P_i - r_o^2 P_o}{r_o^2 - r_i^2} - \frac{(P_i - P_o) r_i^2 \cdot r_o^2}{(r_o^2 - r_i^2) \cdot r^2} \tag{3.3.11}$$

$$\sigma_H = \frac{r_i^2 P_i - r_o^2 P_o}{r_o^2 - r_i^2} + \frac{(P_i - P_o) r_i^2 \cdot r_o^2}{(r_o^2 - r_i^2) \cdot r^2} \tag{3.3.12}$$

$$\sigma_z = \nu \cdot (\sigma_r + \sigma_H) \tag{3.3.13}$$

### 3.3.5 Determining Equations for Casing-Cement-Formation System.

Lam's equations for radial and tangential stress (Equations 3.3.11 and 3.3.12) need to be used for the casing-cement-formation system of a wellbore. The schematic in Figure 3.8 shows the system where $r_a$ represents the inner radius of the steel casing, $r_b$ represents the outer radius of the steel casing and/or the inner radius of the cement sheath, $r_c$ represents the outer radius of the cement sheath, $r_d$ represents the outer radius of the rock formation, and the contact pressures are represented by $P_{c1}$ and $P_{c2}$.

To obtain accurate stress equations for the casing-cement-formation system, it is imperative to determine the aforementioned contact pressures (i.e. casing/cement interface and cement/formation interface). The detailed derivation of the contact pressures is shown in Appendix A.2 (section A.2.1). Furthermore, it is important to consider the changes in temperature induced by operational loads during well construction and production-induced reservoir depletion.

$$\Delta T_{cas} - \Delta T_{cem} = \frac{Q}{2\pi} \cdot \frac{\ln \frac{r_c}{r_b}}{K_{cem}} \tag{3.3.14}$$

$$\Delta T_{cem} - \Delta T_{for} = \frac{Q}{2\pi} \cdot \frac{\ln \frac{r_d}{r_c}}{K_{for}} \tag{3.3.15}$$

Where $\Delta T_{cas}$ represents change in casing temperature ($C^o$); $\Delta T_{cem}$ represents change in cement temperature ($C^o$); and $\Delta T_{for}$ represents change in formation temperature ($C^o$); $Q$ represents heat ($W$); $K_{cem}$ represents the thermal conductivity of cement ($W/m \cdot C^o$); and $K_{for}$ represents the thermal conductivity of cement ($W/m \cdot C^o$).

The hoop stress(es) and radial stress(es) in the steel casing can be calculated using Equations (3.3.16) and (3.3.17);

$$\sigma_{r-cas} = \cdot \frac{r_a^2 P_i - r_b^2 P_{c1}}{r_b^2 - r_a^2} - \frac{(P_i - P_{c1}) r_a^2 \cdot r_b^2}{(r_b^2 - r_a^2) \cdot r^2} \tag{3.3.16}$$

$$\sigma_{h-cas} = \cdot \frac{r_a^2 P_i - r_b^2 P_{c1}}{r_b^2 - r_a^2} + \frac{(P_i - P_{c1}) r_a^2 \cdot r_b^2}{(r_b^2 - r_a^2) \cdot r^2} \tag{3.3.17}$$

The hoop stress(es) and radial stress(es) in the cement sheath can be calculated using Equations (3.3.18) and (3.3.19);

$$\sigma_{r-cem} = \cdot \frac{r_b^2 P_{c1} - r_c^2 P_{c2}}{r_c^2 - r_b^2} - \frac{(P_{c1} - P_{c2}) r_b^2 \cdot r_c^2}{(r_c^2 - r_b^2) \cdot r^2} \tag{3.3.18}$$

$$\sigma_{h-cem} = \cdot \frac{r_b^2 P_{c1} - r_c^2 P_{c2}}{r_c^2 - r_b^2} + \frac{(P_{c1} - P_{c2}) r_b^2 \cdot r_c^2}{(r_c^2 - r_b^2) \cdot r^2} \tag{3.3.19}$$

The hoop stress(es) and radial stress(es) in the rock formation can be calculated using Equations (3.3.20) and (3.3.21);

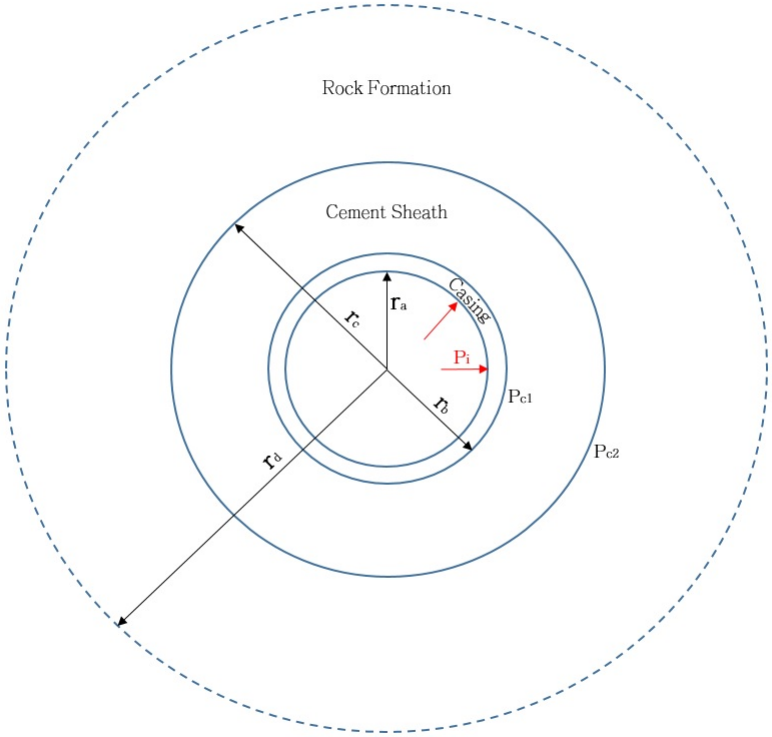


Figure 3.8: Schematic of the casing-cement-formation wellbore system showing the radii of the elements ($r_a$, $r_b$, $r_c$, and $r_d$) and the interfacial contact pressures ($P_{c1}$ and $P_{c2}$).

$$\sigma_{r-for} = \cdot\frac{r_c^2 P_{c2} - r_d^2 P_f}{r_d^2 - r_c^2} - \frac{(P_{c2} - P_f) r_c^2 \cdot r_d^2}{(r_d^2 - r_c^2) \cdot r^2} \tag{3.3.20}$$

$$\sigma_{r-for} = \cdot\frac{r_c^2 P_{c2} - r_d^2 P_f}{r_d^2 - r_c^2} + \frac{(P_{c2} - P_f) r_c^2 \cdot r_d^2}{(r_d^2 - r_c^2) \cdot r^2} \tag{3.3.21}$$

If cement expands during curing, the stresses in the cement sheath is equivalent to the sum of the initial hydrostatic pressure (initial stress) and degree of restriction of the expansion in the wellbore. This necessitates the addition of initial stresses to the variation of stress induced from different loads in the lifecycle of the wellbore, and further used by a failure criterion.

### 3.3.6 Cement Failure Criteria

The analytical model for predicting the mechanical behaviour of the cement sheath under different loads can be applied to the steel casing and the rock formation. However, the focus is on cement failure because less research has been conducted in this area as compared to casing and rock failure. Typically, there are two kinds of failure: tensile failure and shear failure. Tensile failure happens when stresses exerted on the cement exceed the tensile strength of the cement. In similar style, shear failure occurs when stress exceeds the shear strength of the cement. The cement sheath behaves differently under compression and tension, so different failure criteria are needed for both types of failure.

This research project uses a combination of the Mogi-Coulomb criterion and the maximum tensile stress criterion to characterise failure in the cement sheath with the analytical model. The next section(s) describes failure (tensile and shear) and the criteria in more detail.

### 3.3.7 Tensile Failure and Shear Failure

The experiments conducted show that the tensile strength of the cement is approximately ten to fifteen times less than the value of compressive strength. This is consistent with industry standards which shows that concrete is weak in tension because of the existence of a weak link within the concrete matrix known as the

Interfacial Transition Zone (ITZ). The tensile failure criterion is described using the following equation;

$$\sigma_p - P_o \leqslant -T_s \tag{3.3.22}$$

Where $\sigma_p$ represents the principal stress, $P_o$ represents the pore pressure of the cement, and $T_s$ represents the tensile strength of the cement. Since it is assumed that the cement is elastic;

$$\sigma_p + T_s \leqslant O \tag{3.3.23}$$

If any part of the cement satisfies Equation 3.3.23, tensile failure will occur. The Mohr Coulomb criterion has been used extensively to examine shear failure because it is straightforward. However, it underestimates rock strength by neglecting the influence of intermediate stress ($\sigma_2$). Even though the Drucker Prager criterion is preferred to the Mohr Coulomb criterion in a bid to consider the effect of intermediate stress, it overestimates rock strength [31]. The Mogi-Coulomb criterion uses the octahedral shear stress ($\tau_{oct}$) and mean stress ($\sigma_{m,2}$), while the Mohr-Coulomb criterion consists of the shear stress ($\tau$) and the normal stress ($\sigma_n$), and the Drucker-Prager criterion has the octahedral shear stress ($\tau_{oct}$) and the octahedral normal stress ($\sigma_{oct}$). The octahedral shear stress and the mean stress can be calculated using Equations 3.3.24 and 3.3.25.

$$\tau_{oct} = \frac{1}{3}\sqrt{(\sigma_1 - \sigma_2)^2 + (\sigma_2 - \sigma_3)^2 + (\sigma_3 - \sigma_1)^2} \tag{3.3.24}$$

$$\sigma_{m,2} = \frac{\sigma_1 + \sigma_3}{2} \tag{3.3.25}$$

Figure 3.9 shows the Mogi-Coulomb failure envelope and can be represented mathematically as shown in Equation 3.3.26;

$$\tau_{oct} = a + b\sigma_{m,2} \tag{3.3.26}$$

Where $a$ and $b$ represent the Mogi strength parameters and are normally obtained experimentally. Shear failure is determined with the aid of the Mogi-Coulomb cri-

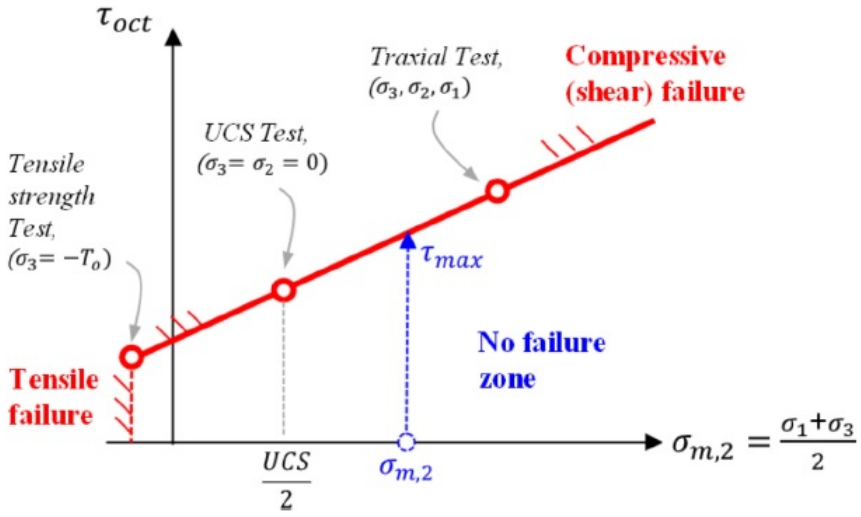


Figure 3.9: Mogi-Coulomb failure envelope [28, 29]

terion and the tensile stress criterion is used to determine failure by debonding and radial cracks. Debonding can happen during production-induced reservoir depletion, subsidence, and variations in pressure and temperature. Failure would occur if the radial stresses reaches a critical value or if the shear stress is larger than normal. If the hoop stress exceeds the tensile strength, cracks will start to develop in the radial direction and unavoidably compromise the integrity of the cement sheath. The third failure mode, shear failure, is caused by an increase in effective stresses around the wellbore during production, and will increase with further reservoir depletion.

## 3.4 Model for Predicting Cement Failure

### 3.4.1 Flowchart for Analytical Model

The flowchart in Figure 3.11 shows how the analytical model for predicting cement failure works. The main input categories are the wellbore data, wellbore geometry, and mechanical data (the wellbore data are in terms of change from initial conditions). The output of the model is the type of cement failure and their respective safety factors (SFs) to ascertain if the cement sheath fails before the cement under a particular loading scenario.

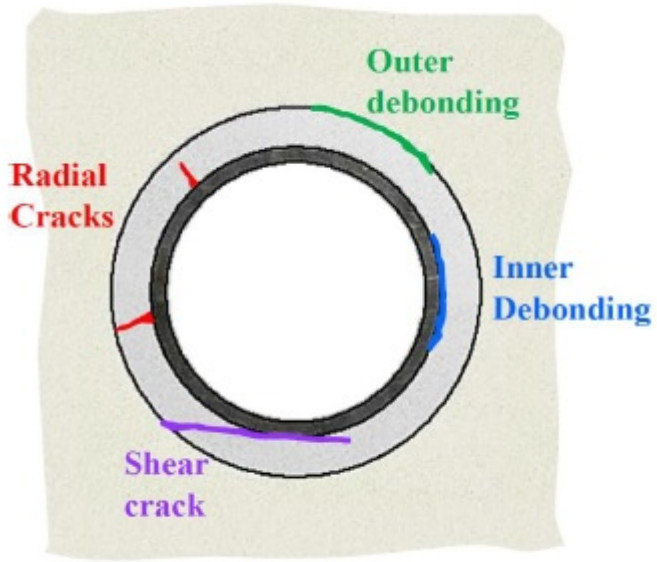


Figure 3.10: Failure modes in the cement sheath [29]

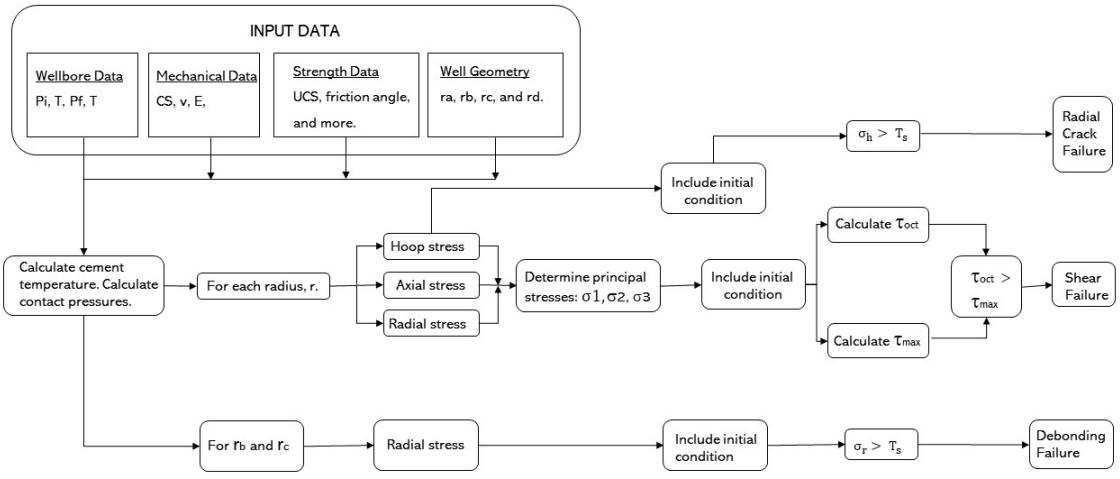


Figure 3.11: Flowchart showing the calculations for the analytical cement model.

### 3.4.2 Well Loading

Industry standards advises that static and dynamic loading cases for well barrier elements should be defined for each wellbore. The loading varies according to the type of oil well and its purpose during its entire life. The operational standard also emphasises the need for design calculations to be done by well trained and competent personnel using software that has been vetted by the industry. In a typical industry leading software, loads can be generated from custom downhole scenarios on different grades of steel casing, and the software can generate outputs in the form of safety factors (the safety factors can be studied to know if the design is good for long term use or not).

### 3.4.3 Initial Conditions

The initial condition refers to the state of the steel casing immediately after the cement sets. The initial temperature of the well will be similar to the geothermal gradient of the rock formation. The initial internal pressure of the production casing will be analogous to the pressure of the fluid column in the annular space (initial fluids column is drilling mud used when running the casing). To calculate the changes in pressure and temperature, the initial values of pressure and temperature must be deducted from the final values of temperature and pressure induced by the respective loading scenario, as shown in Equations (3.4.27) and (3.4.28).

$$\Delta P_i = P_{i,final} - P_{i,initial} \tag{3.4.27}$$

$$\Delta T_i = T_{i,final} - T_{i,initial} \tag{3.4.28}$$

Where $\Delta P_i$ represents change in internal pressure from the initial state to final state ($psi$); $P_{i,final}$ represents the internal pressure at its final state ($psi$); $P_{i,initial}$ represents the internal pressure at its initial state ($psi$); $\Delta T_i$ represents the change in internal temperature from initial to final condition ($^oC$); $T_{i,final}$ represents the internal temperature at its final state ($^oC$); and $T_{i,initial}$ represents the internal temperature at its initial state ($^oC$).

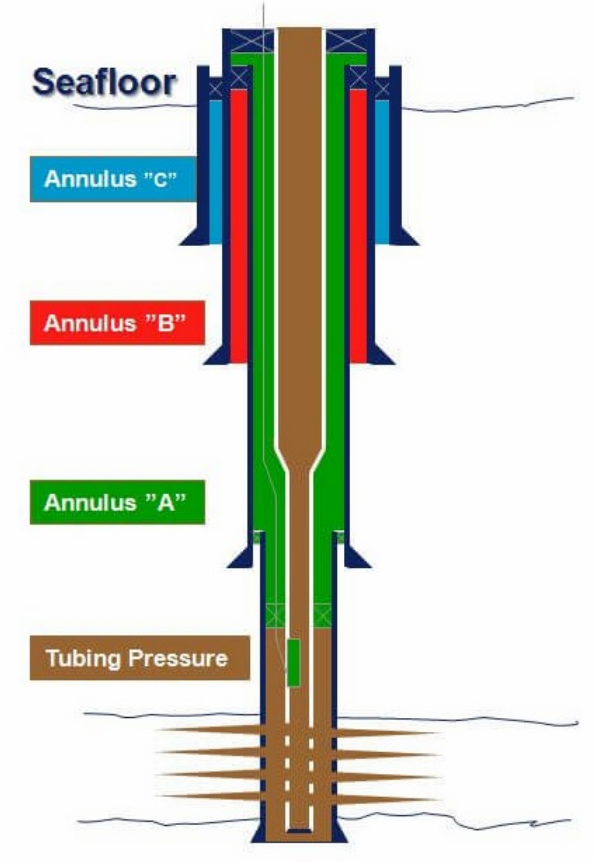


Figure 3.12: Schematic of subsea well showing Annulus "A", Annulus "B", Annulus "C", and the tubing pressure.

### 3.4.4 Pressure Test

As standard procedure, the steel casing must be tested for the highest possible burst load it may experience during the entire life of the well. A leak in the tubing poses the worst loading scenario for the production casing and typically occurs below the wellhead [26]. For this reason, pressure is applied to the fluid column in Annulus "A" and the testing pressure is adjusted to the highest possible burst load pressure, and a *kill margin* is included (see Figure 3.12). The kill margin for a $9\frac{5}{8}$-in production casing is set to approximately 508 psi [104]. The internal pressure can be calculated using Equation 3.4.29.

$$P_z = P_s + \mu_m \cdot z \tag{3.4.29}$$

Where $P_z$ represents the pressure at depth, $z$ (psi); $P_s$ represents pressure at test

surface (psi); $\mu_m$ represents mud weight (psi/m); and $z$ represents depth (m).

### 3.4.5 Safety and Design Factors

The Safety Factor (SF) must be significantly higher than the Design Factor (DF) in any engineering design project. For this reason, it is important to determine the maximum permissible load that the oil well can be exposed to (the DF differs based on the company or the wellbore).

$$SF = \frac{IS}{DL} \tag{3.4.30}$$

Where $IS$ represents the Intrinsic Component Strength, $DL$ represents the Design Load, and $SF$ represents the Safety Factor. The SF for different failure modes are shown in Equations (3.4.31), (3.4.32), and (3.4.33) – shear failure, debonding, and radial cracks respectively;

$$SF = \frac{\tau_{max}}{\tau_{oct}} \tag{3.4.31}$$

$$SF = \frac{-T_o}{\sigma_r} \tag{3.4.32}$$

$$SF = \frac{-T_o}{\sigma_h} \tag{3.4.33}$$

## 3.5 Results (I)

This results chapter presents the assumptions and preliminary findings based on the analytical and numerical model(s) presented in Appendix B (A.2). There are three main sections: (i) modelling assumptions are presented, (ii) resulting stresses in the cement sheath through the cross section of the wellbore under different loading scenarios, and (iii) a comparison of the cement sheath model with an industry leading cement integrity software.

### 3.5.1 Modelling Assumptions

The following assumptions are required for a proper application of the failure criteria and to facilitate the analytical/numerical modelling of the casing-cement-formation wellbore;

1. The coordinate system used in this research project is a borehole coordinate system (see Figure 3.13 for details). The directions of principal stresses are in tandem with the global coordinates.

2. The casing, cement sheath, and rock formation are modelled as concentric circles. The steel casing is analysed as a thin-walled pressure vessel, while the cement sheath and rock formation are both analysed as thick-walled pressure vessels.

3. The casing, cement sheath, and rock formation are assumed to be perfectly bonded at the casing/cement interface and cement/formation interface. The complete bonding at the interfaces means mathematically that radial displacements and stresses are satisfied at both contacts/interfaces.

4. The steel casing and cement sheath are assumed to be isotropic, linearly elastic materials, while the rock formation is assumed to be a linear, poroelastic material. Furthermore, the casing and cement are assumed to be non-porous while the rock formation is modelled as porous.

5. The variation in wellbore temperature is assumed to be steady-state i.e. it is not a function of time.

6. Axisymmetric deformation is assumed for the composite casing-cement-formation cylinder.

7. The effects of cement shrinkage and invasion were ignored and the cement column is assumed to be a hydraulic column before setting.

8. The casing-cement-formation composite cylinder setup undergoes plane strain deformation, implying that the wellbore is under a triaxial stress state.

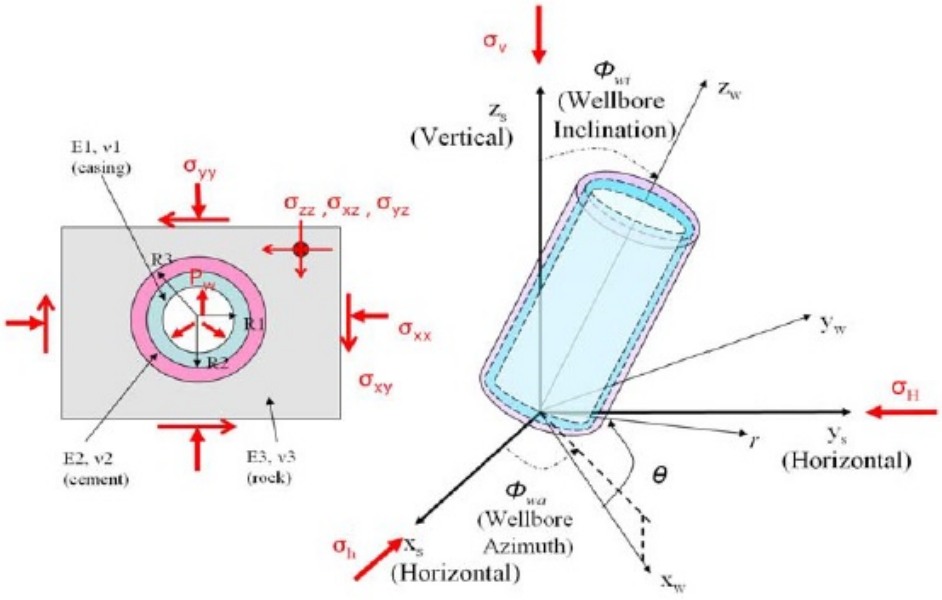


Figure 3.13: Principal stresses (*in situ*) and wellbore coordinate system i.e. $[(x, y, z) = (x_w, y_w, z_w)]$.

9. Each of the factors affecting failure of the cement sheath acts independently of each other.

### 3.5.2 Methodology

Based on the assumptions outlined in section 3.5.1, the following steps are implemented to investigate failure of cement;

1. Calculate the stresses in the cement sheath around the specific area of interest. The stresses can be determined using the developed analytical model and the numerical model.

2. Determine the least principal stress at a number of points in the area of interest within the cement sheath.

3. Investigate tensile failure of the cement sheath by checking that Equation 3.3.23 is satisfied.

4. Determine the octahedral shear stress $\tau_{oct}$ and mean stress $\sigma_{m,2}$ within the area of interest in the cement sheath. Afterwards, plot shear stress $\tau_{oct}$ against mean stress $\sigma_{m,2}$.

5. Plot a failure envelope (linear failure envelope) for shear failure and investigate shear failure of the oilwell cement sheath.

6. Perform steps 1 through to 5 to study the influence of the following parameters on cement failure;

    - Young's modulus of the cement sheath.
    - Azimuth of the wellbore.
    - Inclination of the wellbore.
    - Variation in wellbore temperature.
    - Wellbore pressure.
    - In situ stresses ratio.
    - Ratio of the variation of tectonic stresses.
    - Effect of casing eccentricity on cement integrity induced by high-angle wellbores; where $e = d/(r_b - r_c)$ and $d$ represents the distance between the centers of the casing and cement.

Tensile failure can be investigated using steps 2 and 3 while shear failure can be investigated using steps 4 and 5. The results are based on the input data for the oilwell cement model listed in Table 3.2 and 3.3.

### 3.5.3 Results (I)

The following findings were deduced from the results obtained from the predictive steady-state analytical model;

1. Based on the plots in Figures 3.15 to 3.27, the ductile cement sheath (cement 1) has a significantly lower probability of failure compared to the brittle cement

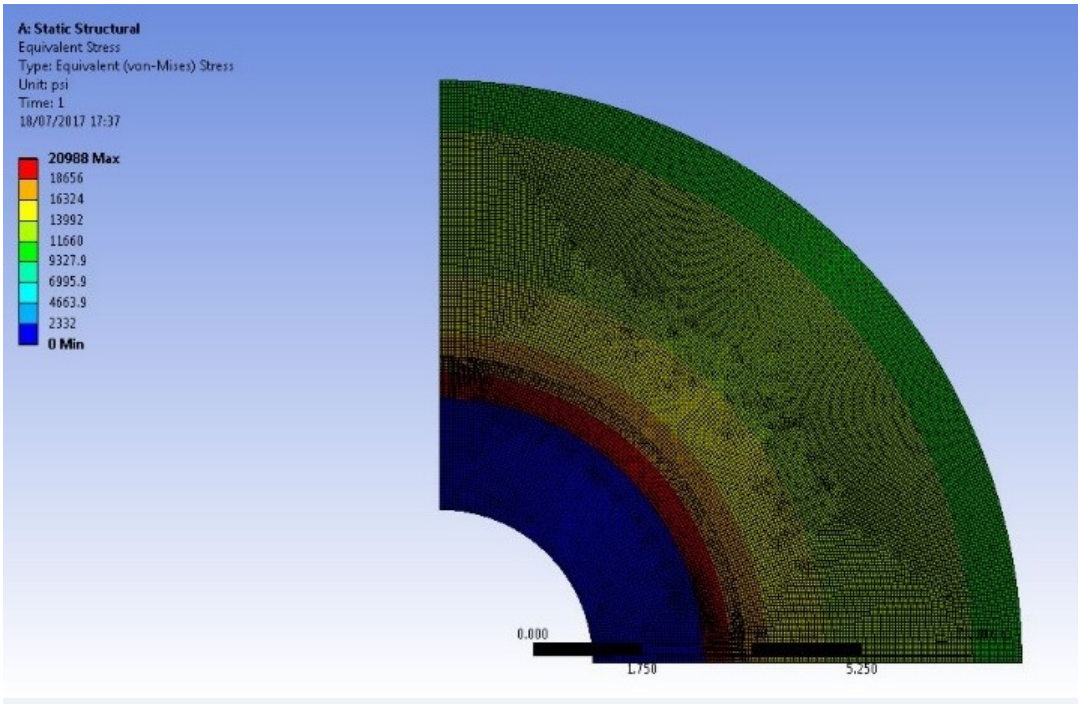


Figure 3.14: Numerical model of equivalent stress for casing-cement-formation model with adequate meshing.

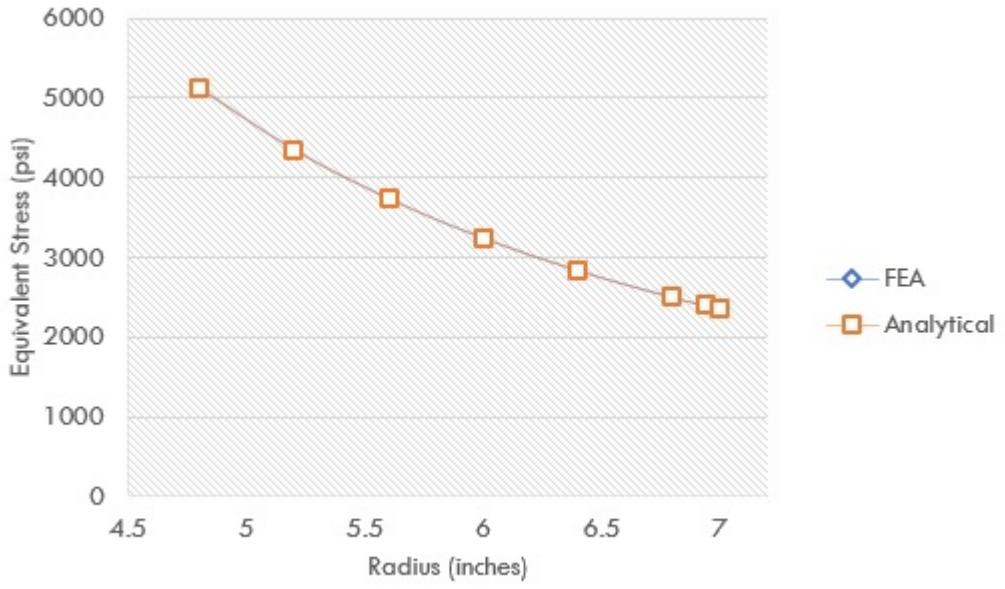


Figure 3.15: Comparison of equivalent stress for FEA and analytical models.

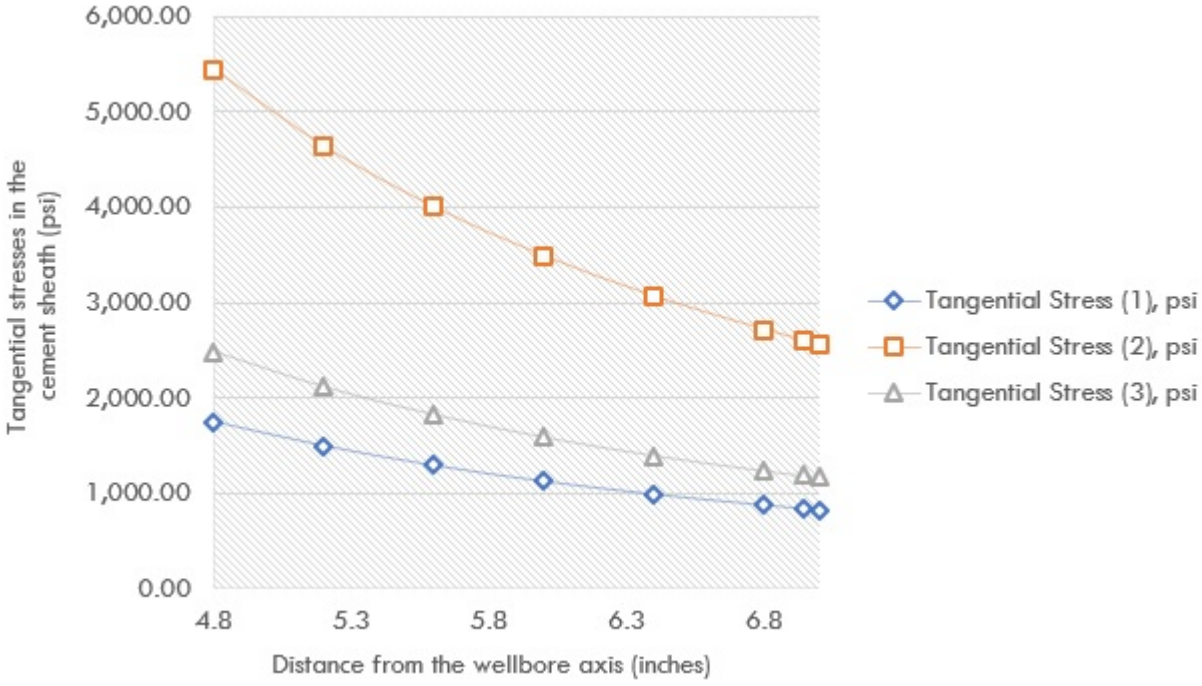


Figure 3.16: Plot of tangential stresses as a function of the distance from the wellbore axis for oilwell cements (1), (2), and (3). Wellbore pressure = 15,000 psi, rock formation pressure = 1,000 psi, and $\Delta T = 0^o F$.

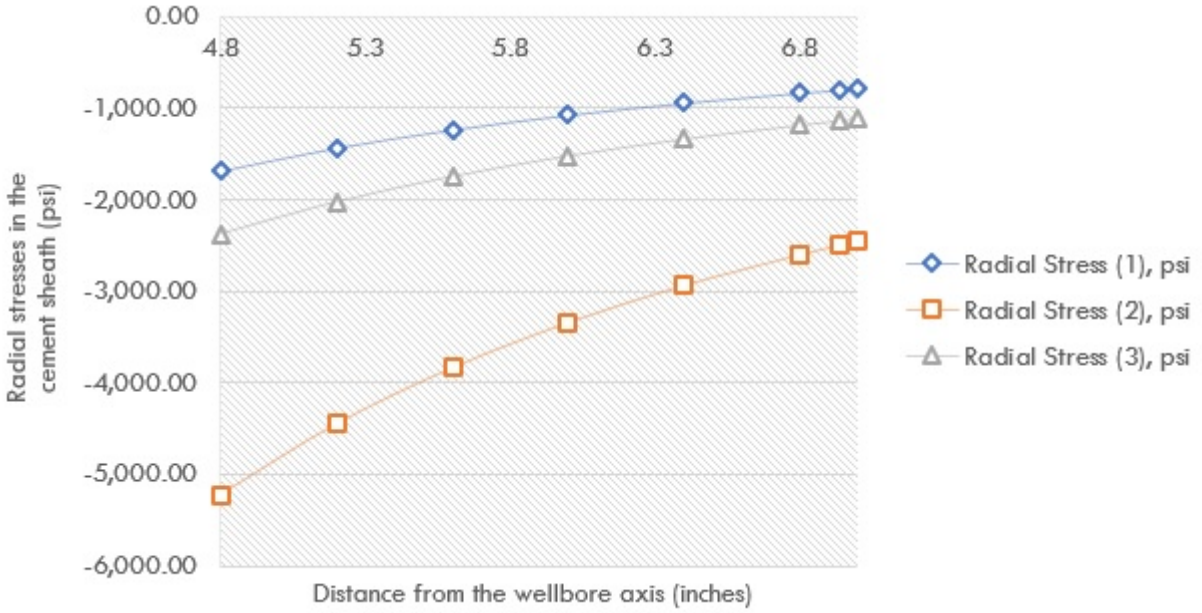


Figure 3.17: Plot of radial stresses as a function of the distance from the wellbore axis for oilwell cements (1), (2), and (3). Wellbore pressure = 15,000 psi, rock formation pressure = 1,000 psi, and $\Delta T = 0^o F$.

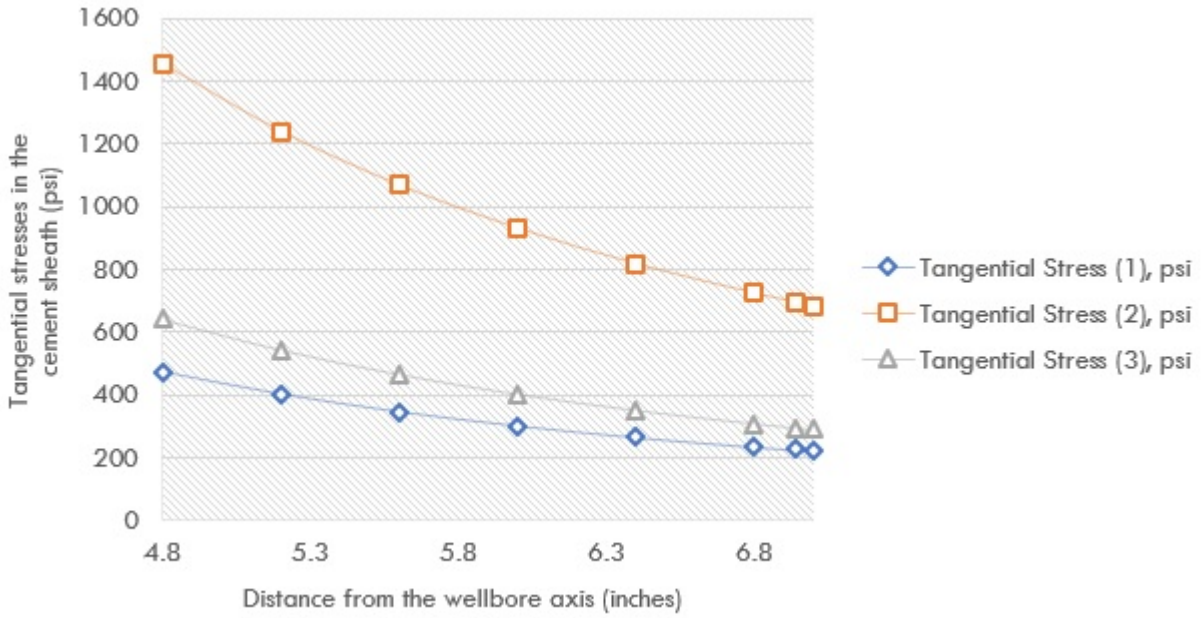


Figure 3.18: Plot of tangential stresses as a function of the distance from the wellbore axis for oilwell cements (1), (2), and (3). Wellbore pressure = 4,000 psi, rock formation pressure = 10,000 psi, and $\Delta T = 0^o F$.

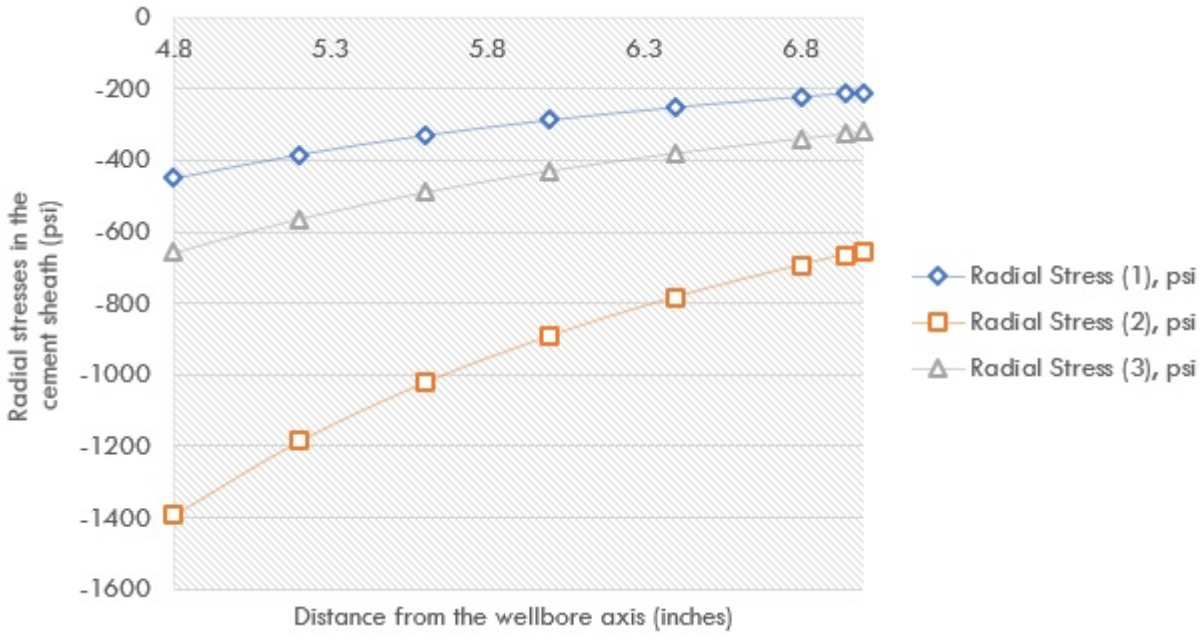


Figure 3.19: Plot of radial stresses as a function of the distance from the wellbore axis for oilwell cements (1), (2), and (3). Wellbore pressure = 4,000 psi, rock formation pressure = 10,000 psi, and $\Delta T = 0^o F$.

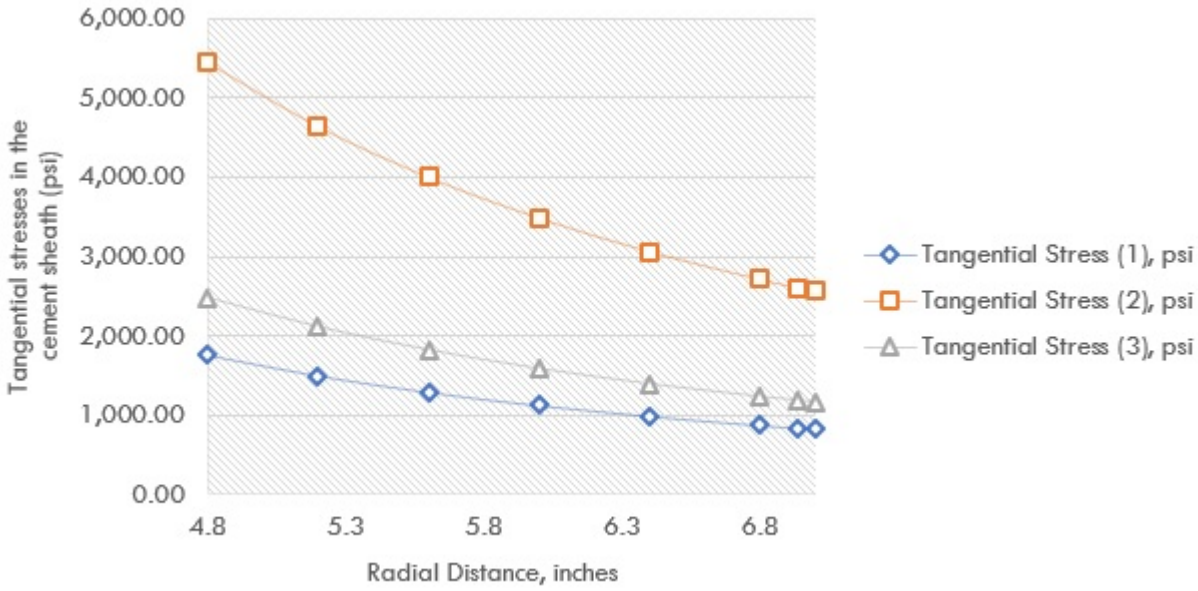


Figure 3.20: Plot of tangential stresses as a function of the distance from the wellbore axis for oilwell cements (1), (2), and (3). Wellbore pressure = 15,000 psi, rock formation pressure = 12,000 psi, and $\Delta T = 0^o F$.

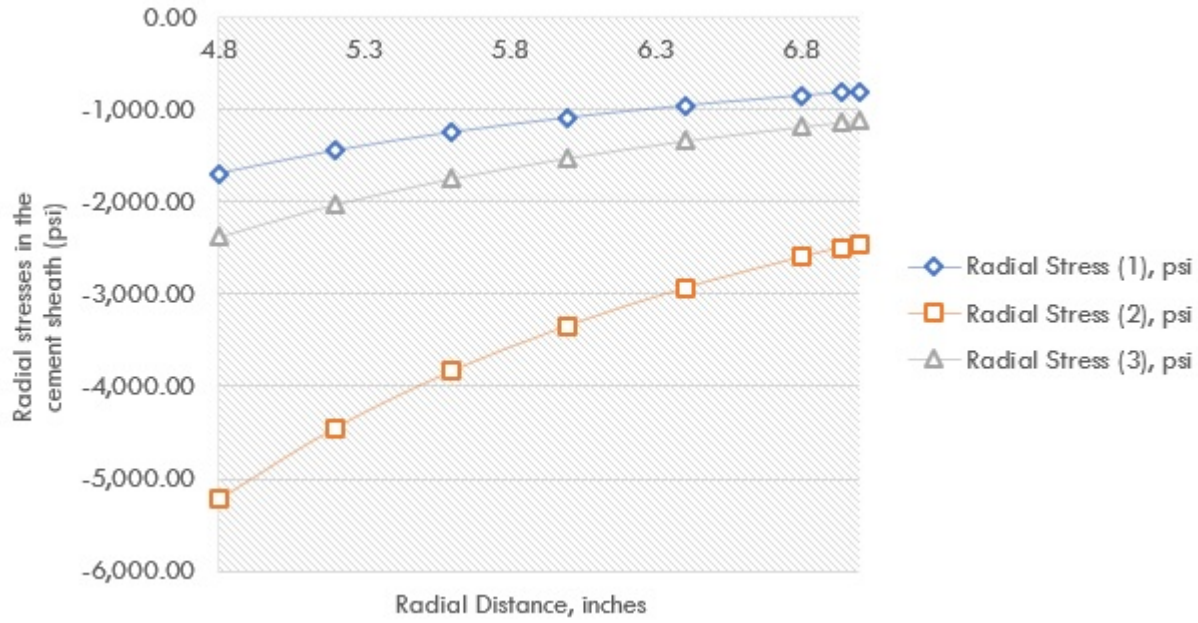


Figure 3.21: Plot of radial stresses as a function of the distance from the wellbore axis for oilwell cements (1), (2), and (3). Wellbore pressure = 15,000 psi, rock formation pressure = 12,000 psi, and $\Delta T = 0^o F$.

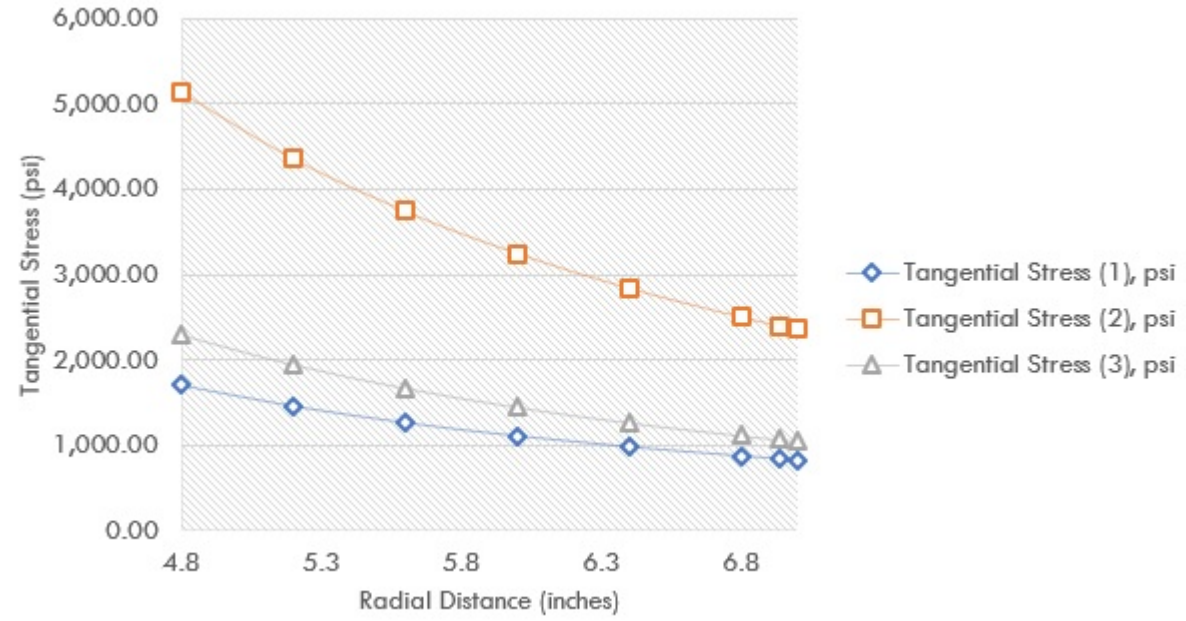


Figure 3.22: Plot of tangential stresses as a function of the distance from the wellbore axis for oilwell cements (1), (2), and (3). Wellbore pressure = 15,000 psi, rock formation pressure = 1,000 psi, and $\Delta T = 250^o F$.

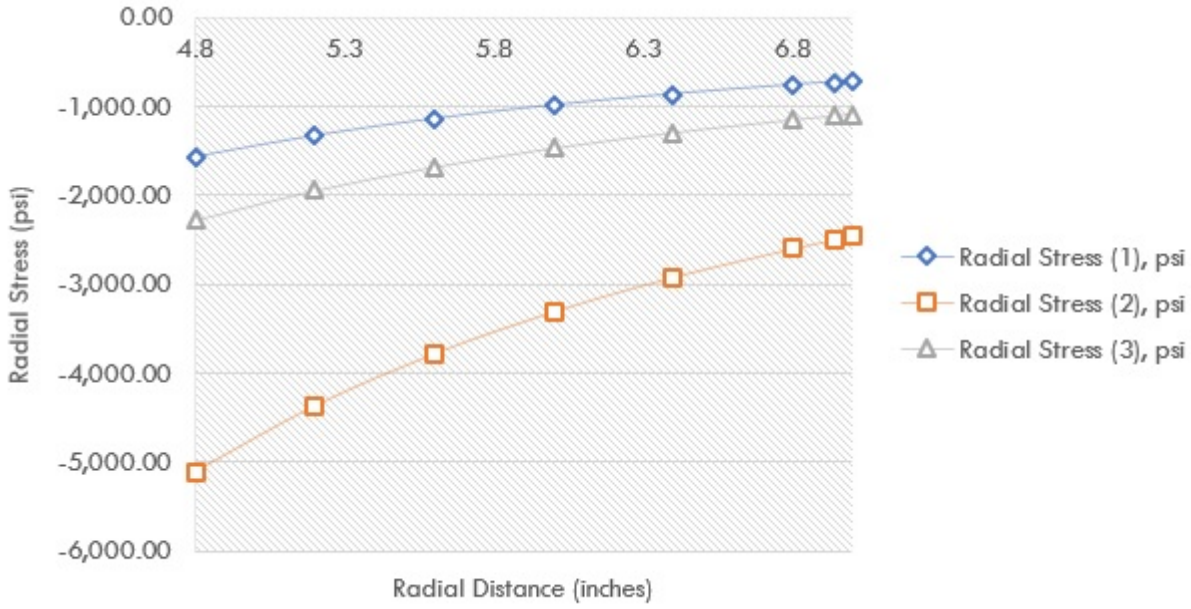


Figure 3.23: Plot of radial stresses as a function of the distance from the wellbore axis for oilwell cements (1), (2), and (3). Wellbore pressure = 15,000 psi, rock formation pressure = 1,000 psi, and $\Delta T = 250^o F$.

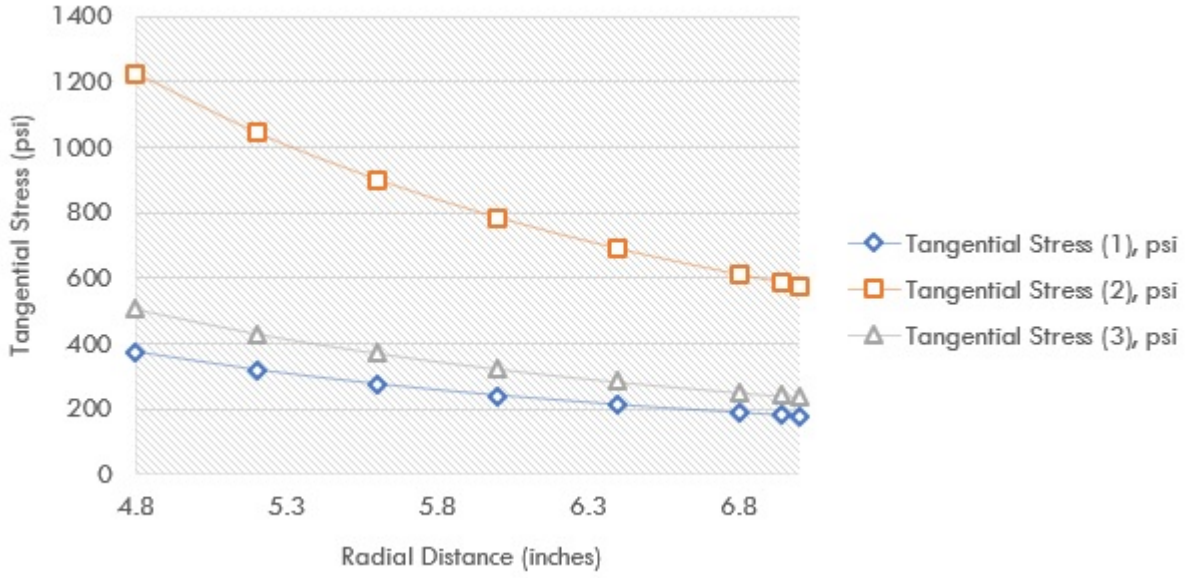


Figure 3.24: Plot of tangential stresses as a function of the distance from the wellbore axis for oilwell cements (1), (2), and (3). Wellbore pressure = 4,000 psi, rock formation pressure = 10,000 psi, and $\Delta T = 250^o F$.

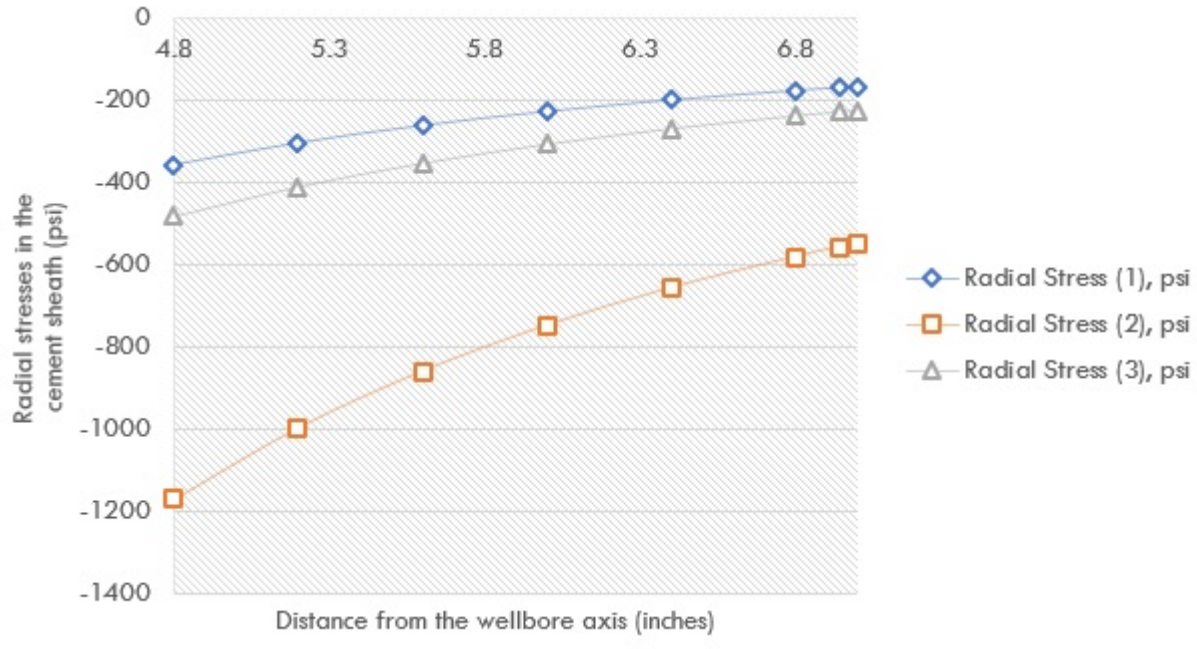


Figure 3.25: Plot of radial stresses as a function of the distance from the wellbore axis for oilwell cements (1), (2), and (3). Wellbore pressure = 4,000 psi, rock formation pressure = 10,000 psi, and $\Delta T = 250^o F$.

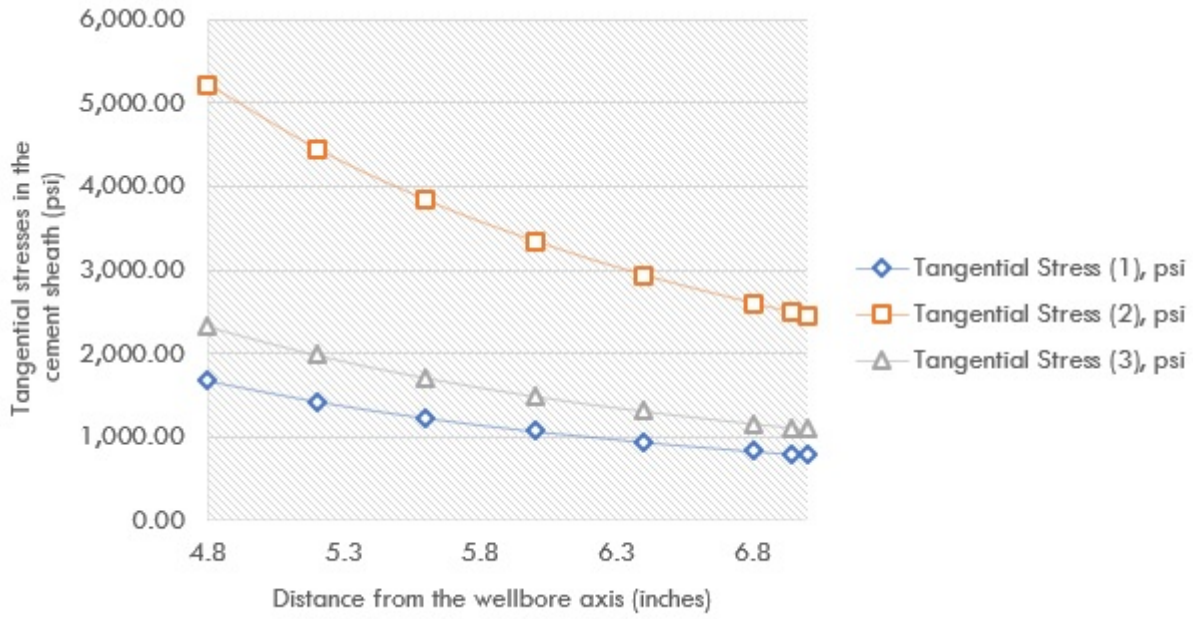


Figure 3.26: Plot of tangential stresses as a function of the distance from the wellbore axis for oilwell cements (1), (2), and (3). Wellbore pressure = 15,000 psi, rock formation pressure = 12,000 psi, and $\Delta T = 250^o F$. The casing/cement interface is at 4.81 inches and the cement/rock interface is at 6.94 inches.

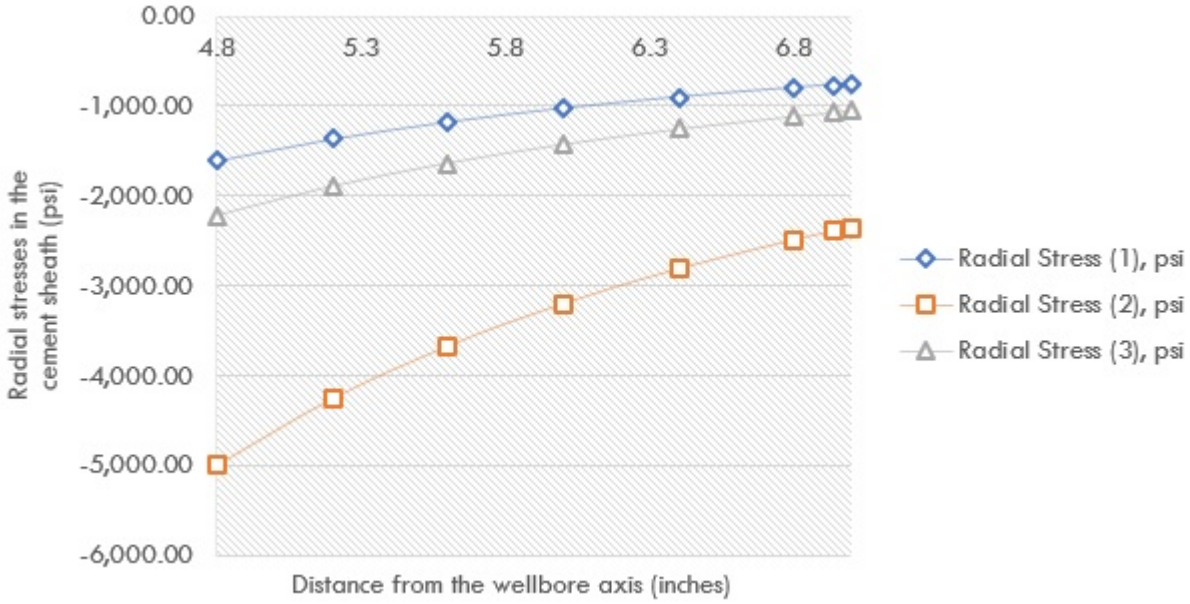


Figure 3.27: Plot of radial stresses as a function of the distance from the wellbore axis for oilwell cements (1), (2), and (3). Wellbore pressure = 15,000 psi, rock formation pressure = 12,000 psi, and $\Delta T = 250^o F$. The casing/cement interface is at 4.81 inches and the cement/rock interface is at 6.94 inches.

sheath (cement 2). This was observed in the aforementioned plots for all variations in pressure.

2. The brittle cement sheath (cement 2) is more compressive than the ductile cement sheath (cement 1). Due to oilwell cement being weaker in compression, this buttresses the preliminary finding that the ductile cement sheath has a lower probability of failure.

3. Very little changes in the stress behaviour were observed from the results that considered change in temperature. This is due to the steady-state configuration of the analytical model.

4. Despite the limitations of the steady-state analytical model, it can be configured with different values of pressure to give a near-accurate representation of the mechanical behaviour of the oilwell cement sheath and its probability of failure.

5. The analytical results show the importance of the mechanical properties of the oilwell cement sheath as cement 1 (ductile cement sheath with a low Young's modulus and high Poisson's ratio) has a lower chance of failure as compared to the brittle cement which has a higher Young's modulus (cement 2). The ductile cement generated lower values of tangential stress and higher value of radial stress (i.e. less tensile).

## 3.6 Results

Results using the analytical and numerical methods are presented in this section. Even though the models can be configured for any case, a representative case is used to show the effect of different properties on failure of the oilwell cement.

### 3.6.1 Influence of Young's modulus on cement failure.

For this mechanical property, this research considers the interaction between the tensile strength of the cement and Young's modulus of the cement. This study utilises Lacy's empirical correlations as presented in Equation (3.6.34)

$$UCS(C_o) = 0.2787E_s^2 + 2.458E_s \tag{3.6.34}$$

Where $E_s$ represents the Young's modulus ($10^6$ psi) and the Mogi strength parameters are expressed in Equations (3.6.35) and (3.6.36);

$$a = \frac{2\sqrt{2}}{3}\frac{C_o}{q+1} \tag{3.6.35}$$

$$b = \frac{2\sqrt{2}}{3}\frac{q-1}{q+1} \tag{3.6.36}$$

The plot in Figure (3.28) shows the influence of Young's modulus on tensile failure of the cement. It shows that tensile failure declines (and becomes zero) as Young's modulus increases. In addition, the analytical and numerical results have similar patters for the shape and slope of the results, albeit having different values.

Also, the plot shows that an increase in the Young's modulus is accompanied by a steep decline in the numerical results (steeper than the analytical results).

For shear failure, the Mogi-Coulomb failure criterion was utilised to ascertain the influence of the aforementioned mechanical properties on shear failure of the cement at the interfaces (casing/cement interface and cement/formation interface). The analytical and numerical results show that as Young's modulus increases, shear failure decreases but tensile failure increases. Furthermore, the numerical results are much closer to the failure envelope than the analytical results for tensile and shear failure.

### 3.6.2 Influence of azimuth on cement failure.

The plots for the effect of wellbore azimuth on tensile and shear failure of oilwell cement (Figure 3.29) shows that an increase in azimuth causes no variation to the tensile strength (both analytical and numerical methods). Since changes in wellbore inclination and wellbore azimuth occur prior to cementing, they have little to no effect on cement failure, thereby explaining the results. Furthermore, the results show that the numerical results are closer to the failure envelope than the analytical results.

### 3.6.3 Influence of inclination on cement failure.

The wellbore inclination, unlike azimuth, defines the deviation of the wellbore from the vertical axis irrespective of compass direction. Figure 3.30 shows the effect of wellbore inclination on cement failure. The result is not consistent with industry knowledge and would require further research.

### 3.6.4 Influence of temperature variation on cement failure.

Figures (3.31) and (3.32) show the effect of downhole wellbore temperature variation on tensile and shear cement failure. The results show that as downhole temperature increases, the probability of tensile cement failure decreases due to a significant increase in tensile strength. The result also shows that the probability of shear cement

failure at the interfaces decreases as downhole temperature increases. Furthermore, the plots show a discrepancy in the results as the numerical results are further away from the failure envelope at a much greater rate than the analytical results. This difference is due to the analytical model using generalised plane strain (pseudo 3D) while the numerical model uses a finite box that is a full 3D model.

### 3.6.5 Influence of wellbore pressure on cement failure.

Figures (3.33) and (3.34) show the influence of wellbore pressure on cement failure. The plots clearly show that the probability of tensile cement failure increases as wellbore pressure increases. The results also show slightly different trends for the analytical and numerical results – the numerical results come closer to the failure envelope while the analytical results are nearer to the failure envelope after a wellbore pressure of $7,000$ psi.

### 3.6.6 Influence of eccentricity on cement failure.

The plot in Figure (3.37) shows the variation in maximum stress induced by different values of eccentricity under downhole operating conditions. The results of the numerical simulation show that high eccentricity induces stress in the steel casing and oilwell cement sheath. The results also show a linear relationship between eccentricity and stress increase, meaning that good casing centralisation will lead to a reduction in maximum stress.

## 3.7 Sand Production

This section presents the application of an appropriate failure criteria for predicting sand production in a perforated wellbore. The production of formation sands is undesirable because it poses a well integrity problem by impeding well productivity, eroding completion components, and interfering with downhole equipments.

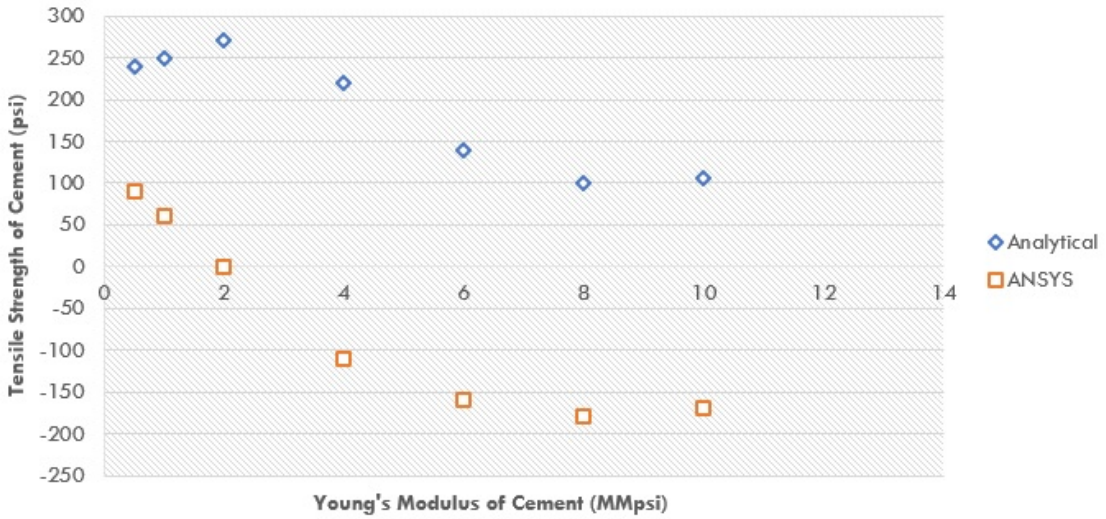


Figure 3.28: Plot showing the effect of Young's modulus on tensile failure of oilwell cement.

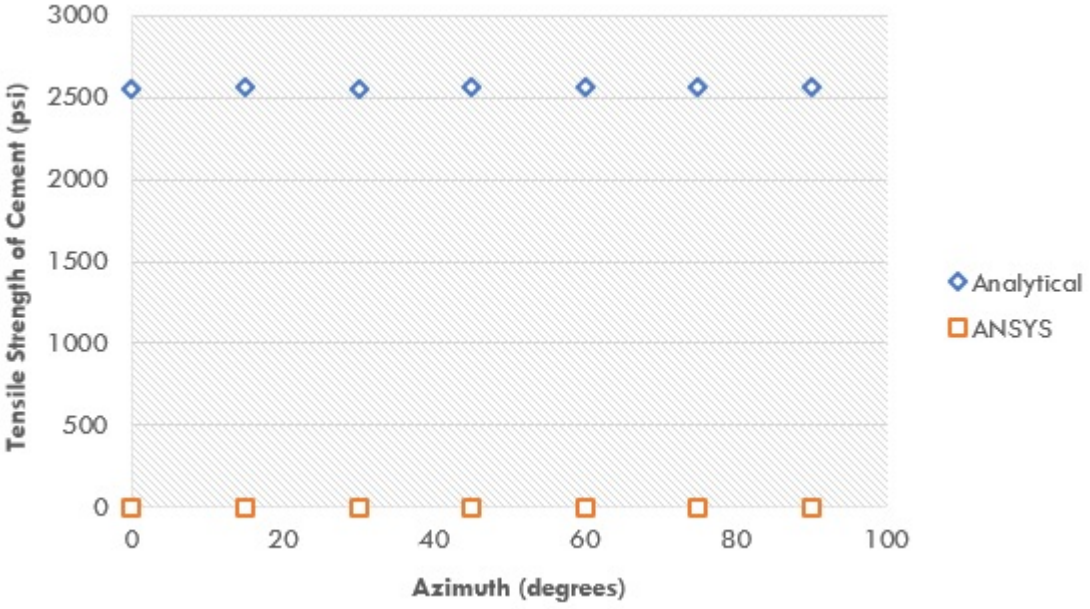


Figure 3.29: Plot showing the effect of wellbore azimuth on tensile failure of oilwell cement.

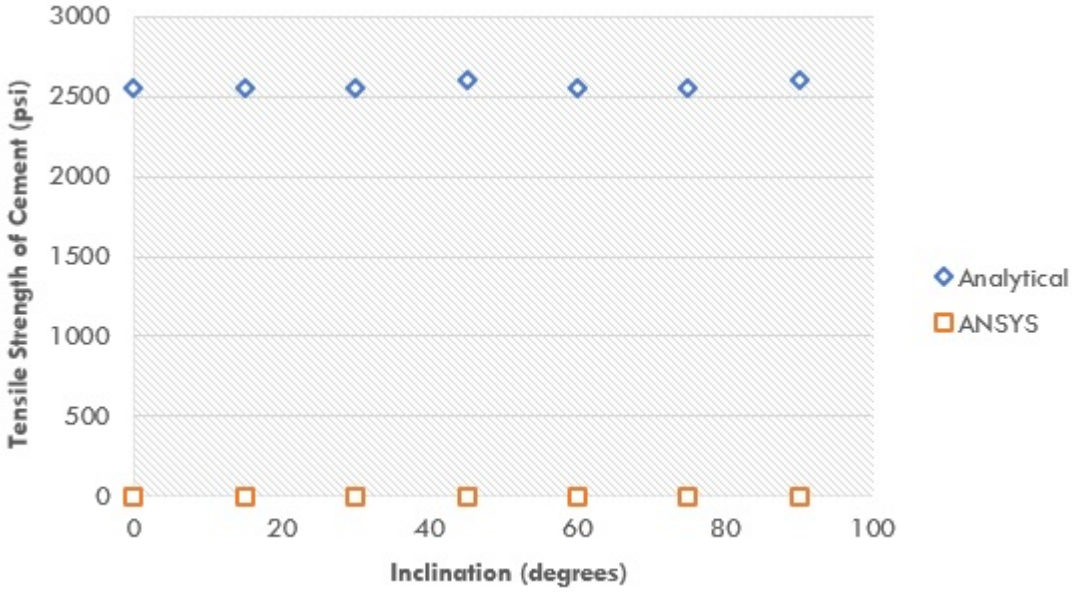


Figure 3.30: Plot showing the effect of wellbore inclination on tensile cement failure.

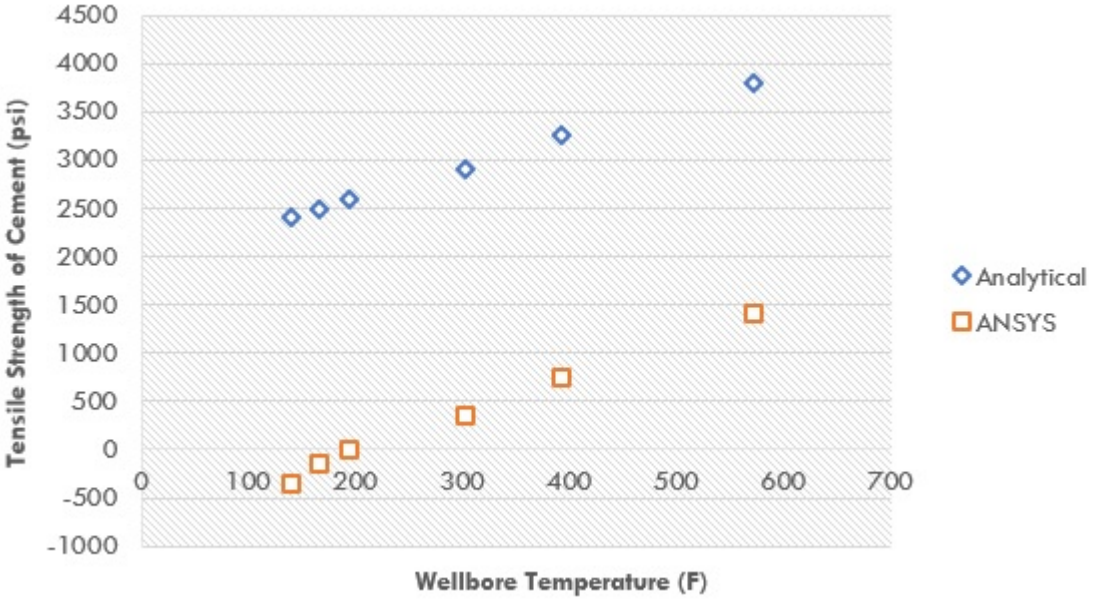


Figure 3.31: Plot showing the effect of wellbore temperature on tensile failure of cement.

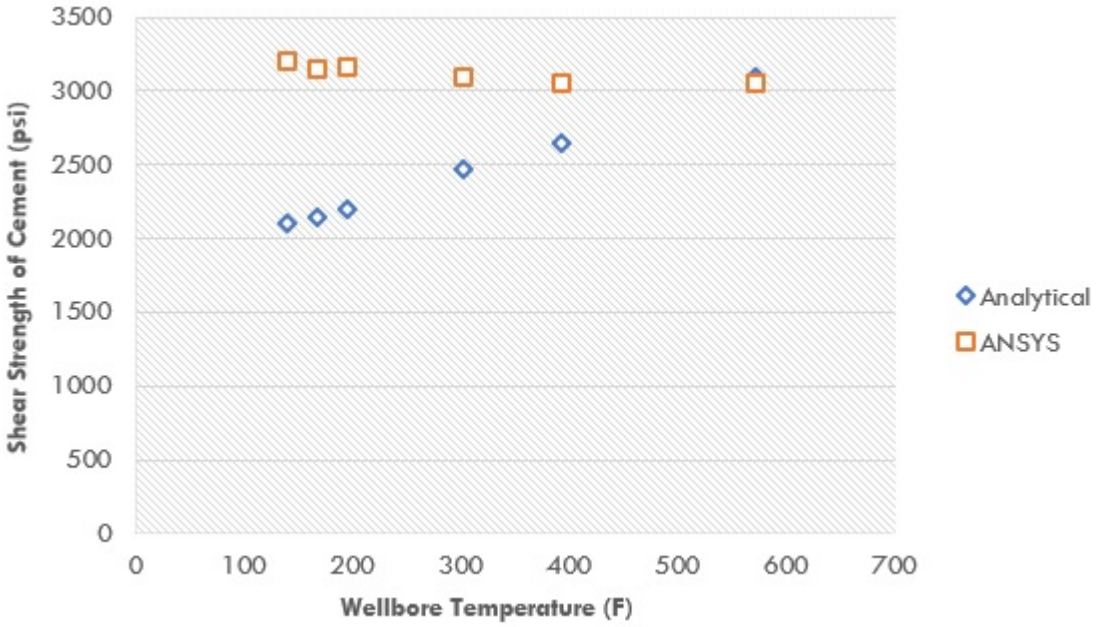


Figure 3.32: Plot showing the effect of wellbore temperature on shear failure of oilwell cement.

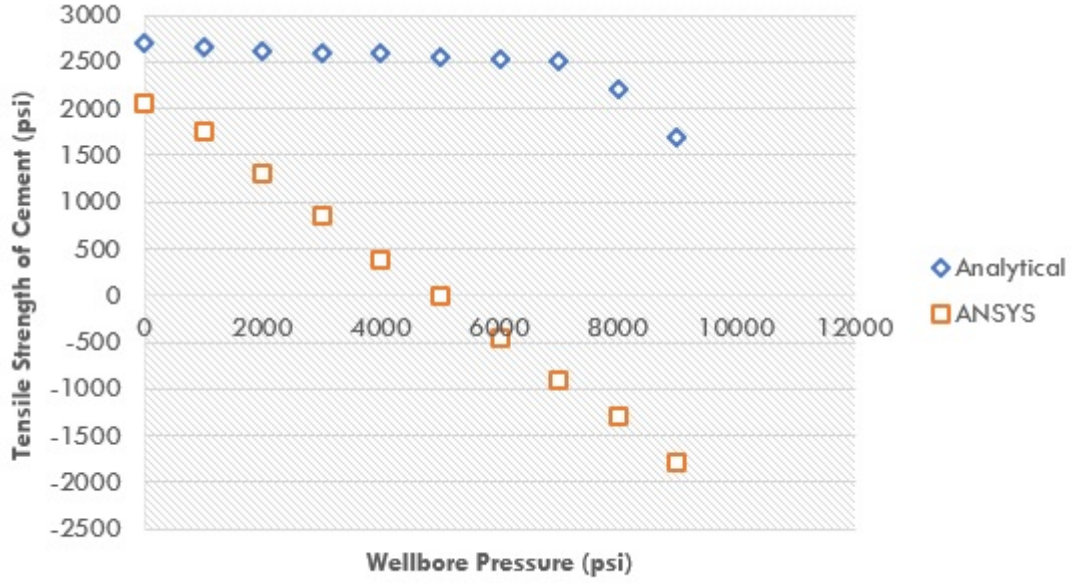


Figure 3.33: Plot showing the effect of wellbore pressure on tensile failure of oilwell cement.

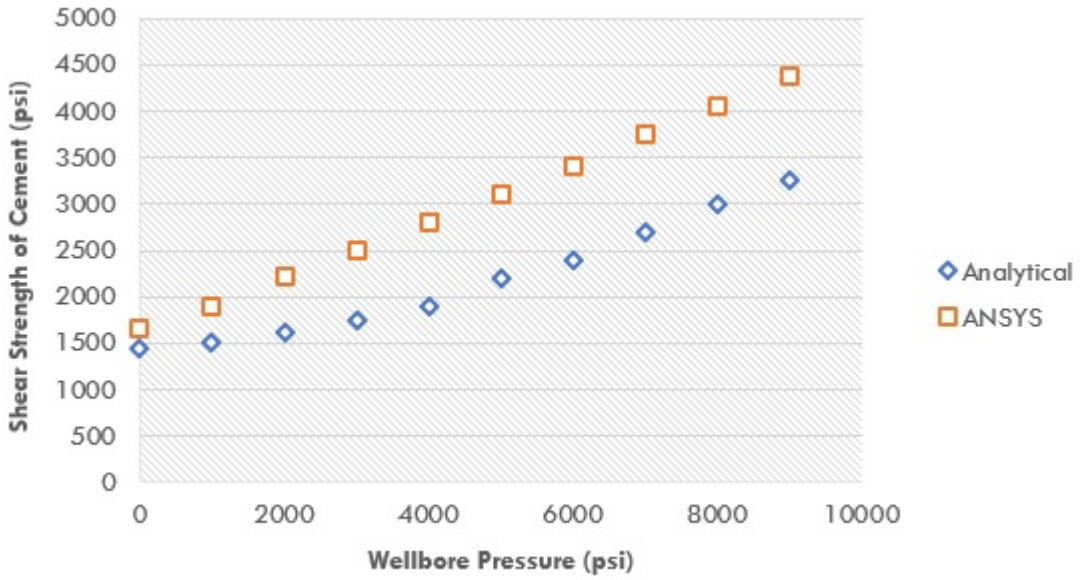


Figure 3.34: Plot showing the effect of wellbore pressure on shear failure of oilwell cement.

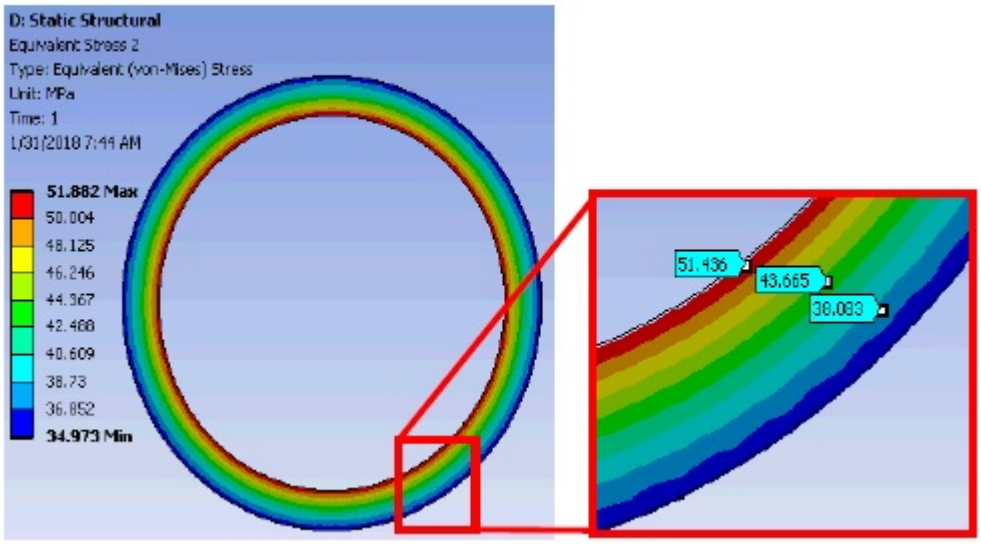


Figure 3.35: Stress distribution in the oilwell cement sheath for fully concentric casing-cement-formation wellbore system (0% eccentricity).

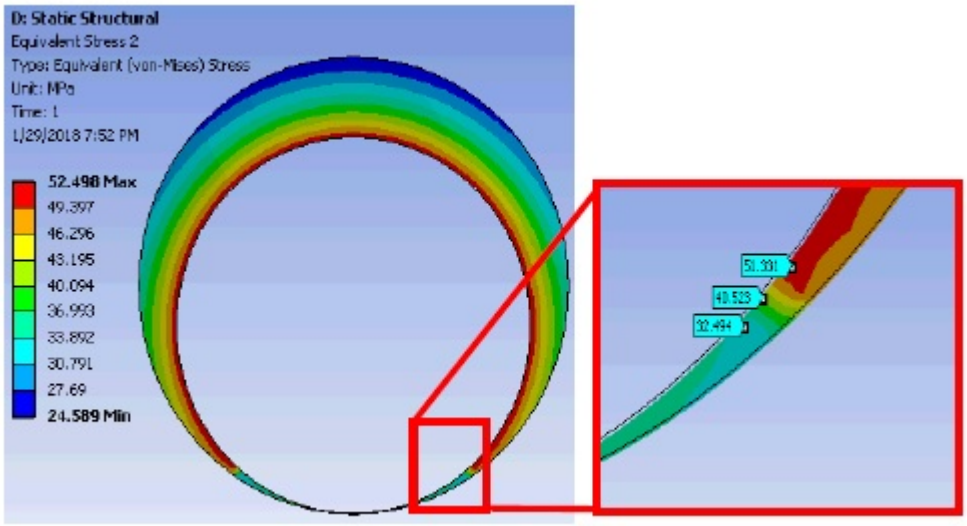


Figure 3.36: Stress distribution in the oilwell cement sheath for fully eccentric casing-cement-formation wellbore system (90% eccentricity).

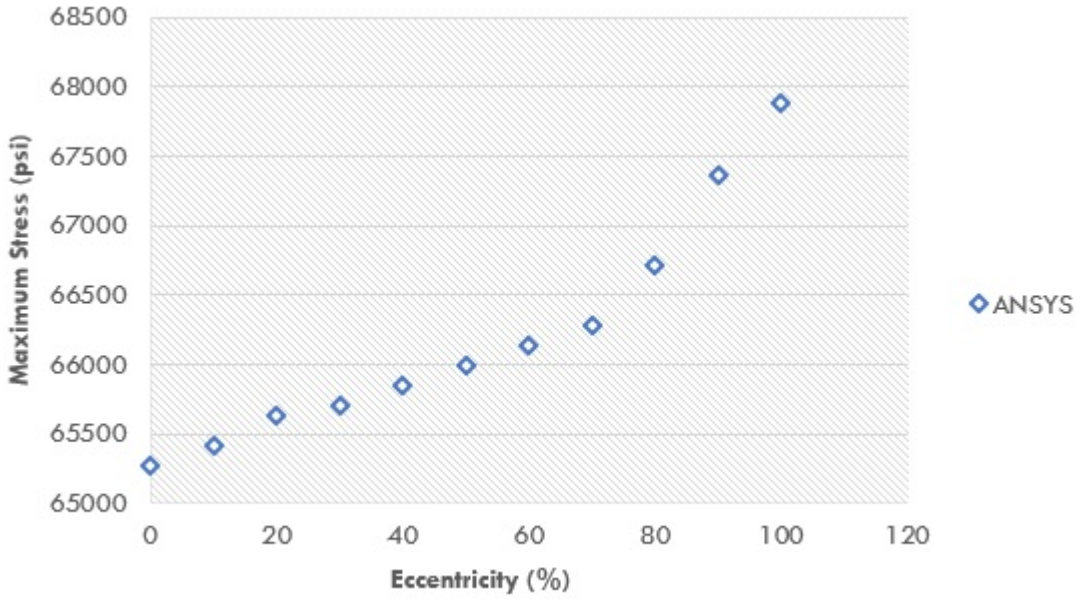


Figure 3.37: Maximum stress generated at different values of eccentricity.

### 3.7.1 Distribution of stress in the perforated region.

Perforation creates a communication medium from the casing (or liner) into the reservoir formation through which oil and gas is produced. This communication tunnel induces some disturbance in the wellbore system, especially around the perforated region. In this scenario, the initial stress state is the stress distribution around the cased and cemented wellbore. However, a plane strain condition is utilised to reduce the complexity of the solution, and the final stress is obtained by adding the initial stress to the disturbed stress as shown in Equation 3.7.37.

$$\sigma_{final} = \sigma_{initial} + \Delta \cdot \sigma_{disturbed} \tag{3.7.37}$$

### 3.7.2 Poroelasticity

The analysis for predicting sand production includes the effect of poroelasticity by coupling rock and fluid interaction. Cui et al. [105, 106] divided the loading conditions into three separate loading problems: (i) a plane strain problem, (ii) a uni-axial stress problem, and (iii) an elastic shear problem. The stress equations are expressed in detail in the appendices.

### 3.7.3 Assumptions

The following assumptions are needed for predicting sand production in a perforated wellbore;

1. Given the cylindrical shape of the perforation tunnel, a cylindrical coordinate system is used (see Figure 3.38)

2. Two angles are required to specify the orientation of the perforated region – a perforation inclination (i.e. angle from the wellbore) and a perforation azimuth (i.e. angle perpendicular to the wellbore).

3. The tensor for permeability is assumed to be isotropic and homogeneous ($k_{ij} = k$).

4. The radius of perforation is significantly smaller than the radius of the wellbore. For this reason, the initial stresses are assumed to be uniform on a cross-section that is perpendicular to the perforated region.

5. Fluid flow is assumed to be in the radial direction as that is the prevalent flow during production-induced reservoir depletion.

6. Fluid is mostly incompressible (or slightly compressible) and is assumed as such to avoid complexities associated with high fluid compressibility.

7. Given the smaller radius of the perforated region, the pressure in the perforation tunnel is assumed to be considerably higher than the wellbore pressure.

8. Due to the time difference between well completion and perforation (approx. four hours), the initial formation pressure is assumed to be uniform prior to perforation.

9. Rocks are generally characterised as either brittle or ductile. The distance between the yield point and failure point is shorter for brittle rocks but longer for ductile rocks, meaning that only the failure criteria is needed for brittle rocks.

10. Unlike the Mohr-Coulomb criterion, the Drucker-Prager criterion considers the effect of intermediate principal stress on the strength of the rock. A combination of the Drucker-Prager criterion and the Lade criterion is used to characterise rock failure.

11. The pressure in the perforation tunnel is assumed to be in an underbalanced state to aid production. This also means that the maximum pressure of the perforation tunnel is assumed to be the initial reservoir pressure.

### 3.7.4 Methodology

The following steps are required to calculate the stress distribution around the perforation tunnel in the wellbore. Firstly, the stresses around an inclined wellbore

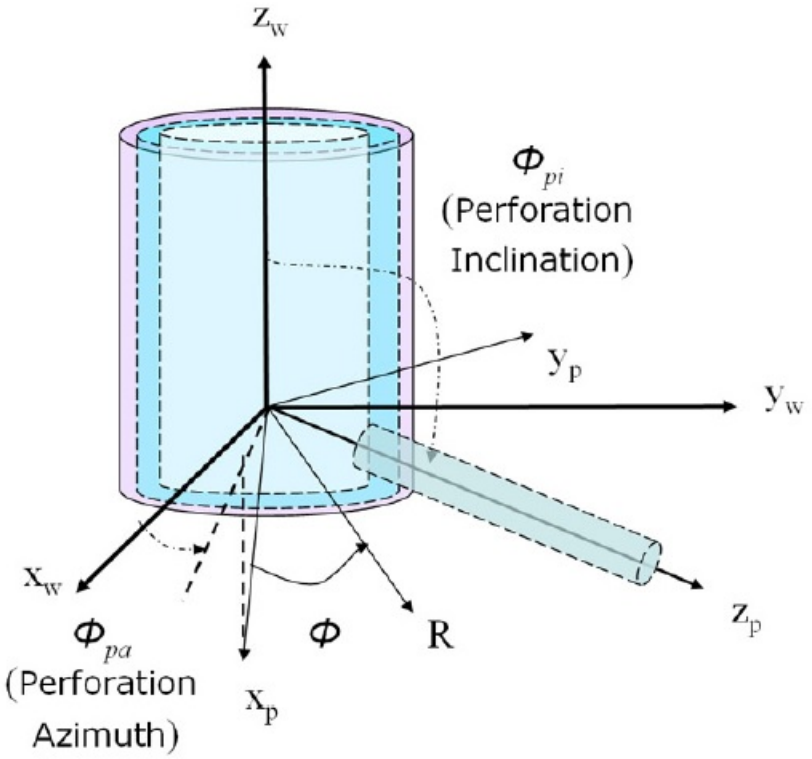


Figure 3.38: Cylindrical coordinate system for the perforation tunnel.

are mathematically changed from borehole coordinates to the coordinates for the perforation tunnel using second order tensor matrices (see Appendices). Secondly, the stresses generated in the perforated region are derived from the work of Cui et al. [105,106]. Finally, the stresses generated around the perforated tunnel are added to the initial stresses in the wellbore, as presented in Equation (3.7.37).

### 3.7.5 Critical Drawdown

If the right combination of assumptions and failure criteria is applied, failure around the perforated interval can be predicted. If the prediction is performed well, critical drawdown can be calculated to avert the possibility of sand production.

### 3.7.6 Results

The results of the study on sand production and critical drawdown focus on the behaviour of critical drawdown over time, and the orientation of the perforation

Table 3.2: Data for predicting sand production in a cased wellbore.

| INPUT PARAMETER | VALUE |
|---|---|
| Inner radius of casing | 2.5 inches |
| Inner radius of cement | 2.8 inches |
| Inner radius of rock formation | 3.2 inches |
| Young's modulus of casing | $30 \times 10^6$ psi |
| Young's modulus of cement | $3 \times 10^6$ psi |
| Young's modulus of rock | $2 \times 10^6$ psi |
| Poisson's ratio of casing | 0.3 |
| Poisson's ratio of cement | 0.25 |
| Poisson's ratio of rock | 0.219 |
| Friction Angle, $\Phi$ | $35^o$ |
| Unconfined Compressive Strength, UCS | $3,500$ psi |
| Consolidation coefficient, $c$ | 23.97 $in^2/day$ |
| Biot-Willis coefficient, $\alpha$ | 0.968 |
| Depth | $5,000$ ft. |
| Max. horizontal stress, $\sigma_H$ | $4,500$ psi |
| Min. horizontal stress, $\sigma_h$ | $3,500$ psi |
| Min. vertical stress, $\sigma_v$ | $5,000$ psi |
| Initial pore pressure, $P_o$ | $2,250$ psi |
| Time after perforation, $t$ | 0.0001, 0.01, 1, and 100 days |

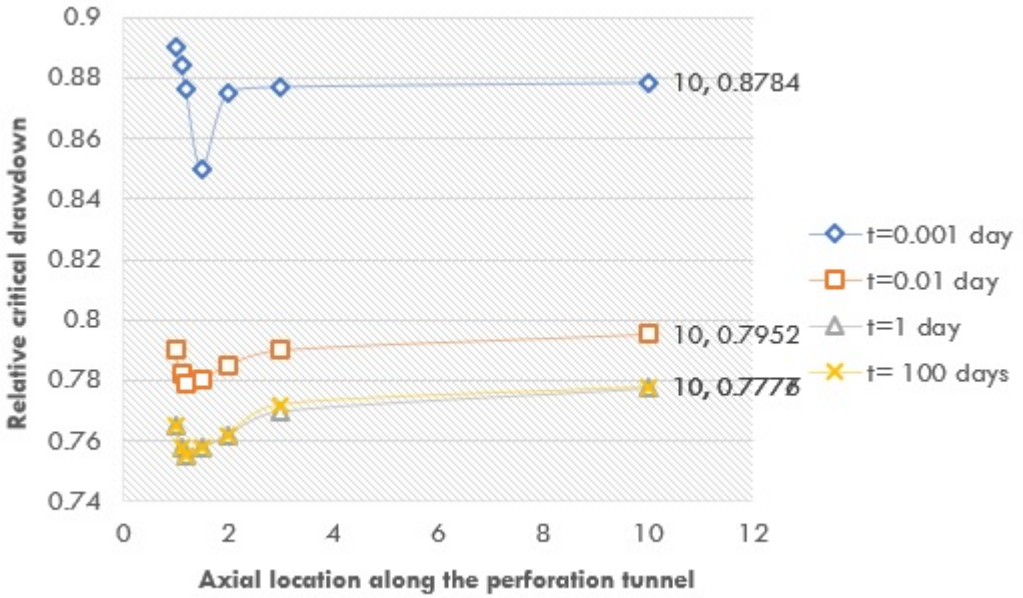


Figure 3.39: Plot showing distance from the centre of the perforation interval ($r/R_3$) versus the critical drawdown ($\Delta P_c/P_o$) in the direction of maximum horizontal stress. This plot is for a cased wellbore scenario.

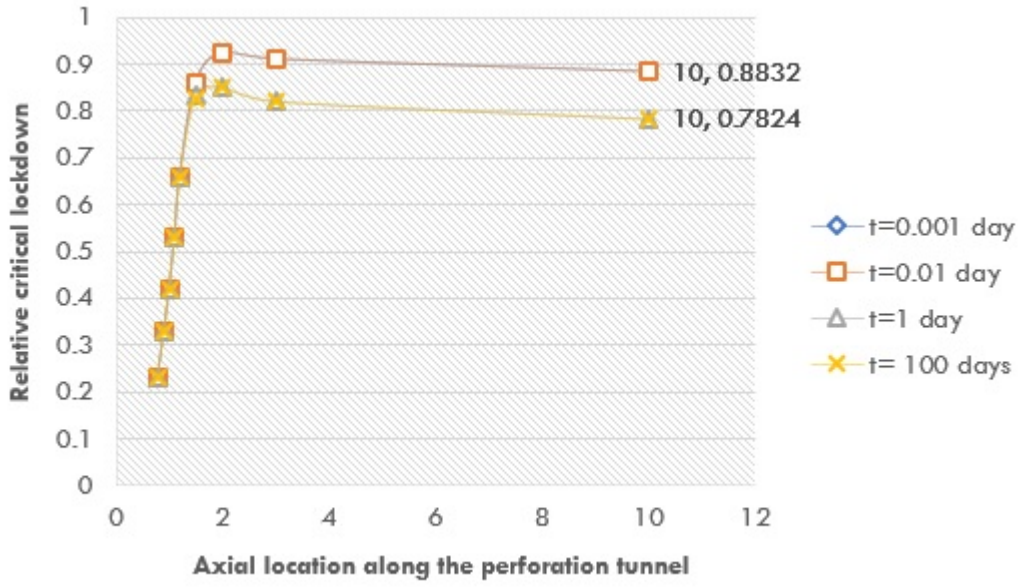


Figure 3.40: Plot showing distance from the centre of the perforation interval ($r/R_3$) versus the critical drawdown ($\Delta P_c/P_o$) in the direction of maximum horizontal stress. This plot is for an uncased/open-hole wellbore scenario.

interval. The data used for analysis is outlined in Table 3.4 and Figure 3.39 shows the transient behaviour of the critical drawdown of a cased wellbore perforated in the direction of maximum horizontal stress ($\sigma_H$). For every duration ($t$), the pattern for relative critical drawdown has a U-shape close to the wellbore meaning that there is a high critical drawdown near the wellbore. This is in line with industry standards as stress concentration increases with higher proximity to the wellbore. Furthermore, the results show that relative critical drawdown decreases as time increases for cased and uncased (open-hole) wellbores. The result for a cased wellbore has a relatively flatter pattern than the open-hole result due to a lower concentration of stress.

## 3.8 Discussion and Recommendation

This section presents a summary of results, conclusions, and suggestions for future research. Up to this point, the objectives of this research project are – (i) to ascertain if elastic models can be used to model the mechanical behaviour of an inclined and cased wellbore, (ii) to develop analytical and numerical models for the life cycle of a wellbore (i.e. completion, production-induced reservoir depletion, and variations in temperature), (iii) to predict cement failure using the developed models, and (iv) use developed models to predict sand production and critical drawdown behaviour.

This section further characterises the results obtained from previous sections and presents potential applications and limitations for further research.

### 3.8.1 Analytical Model (Discussion)

The results thus far show that an elastic model can be used to model the mechanical behaviour of the cement sheath in an inclined, cased wellbore under steady state conditions. As aforementioned, there were some discrepancies in the analytical results and numerical results because the analytical models are not 3D models while the numerical model (ANSYS) used 3D models. Furthermore, the model includes post-completion activities i.e. variation of wellbore temperature and variation of tectonic stresses.

The analytical model is a very useful tool for obtaining stress distribution in the

casing-cement-formation system without needing a numerical simulator. This analytical model can also be used for a typical wellbore with multiple, concentric casings using straightforward superposing principles. The **FEATURES** of the analytical model are outlined as follows;

1. It utilises generalised plane strain.
2. It incorporates poroelastic interaction/coupling.
3. It uses straightforward superposition principles that can be extended to a typical wellbore with multiple, concentric casings. Details are presented in the Appendix.
4. The analytical model considers completion and post-completion activities, including variations in temperature and tectonic stress.

**LIMITATIONS** of the analytical model are outlined as follows;

1. It does not consider plasticity.
2. It does not utilise full 3D solutions.
3. It ignores the interaction between fluid and temperature in the rock formation.

### 3.8.2 Cement Failure (Discussion)

The developed analytical and numerical models were used to predict failure of the cement sheath (tensile and shear), and ascertain the influence of certain mechanical properties on the behaviour of the cement. The mechanical properties investigated include, but are not limited to, the Young's modulus, wellbore pressure, wellbore temperature, wellbore azimuth, wellbore inclination, and casing eccentricity. The following conclusions are based on the results generated from the analytical and numerical investigation;

1. An increase in Young's modulus significantly decreases the probability of shear failure while the chance of tensile failure increases.

2. The results show that wellbore azimuth and inclination have no clear influence on failure, both shear and tensile. This finding, however, is not in tandem with industry standards because cement stress typically changes when wellbore azimuth changes. This is most likely due to errors in modelling.

3. The analytical and numerical results for the influence of wellbore pressure on cement failure show very distinct trends. As aforementioned, the analytical models used the generalised plane strain (pseudo-3D condition) while the numerical models used a 3D box model. For this reason, the analytical model cannot consider in-plane stresses which have a direct relationship with wellbore pressure.

4. The results show that casing eccentricity increases the probability of tensile and shear cement failure. However, further investigation is needed to fully ascertain the influence of casing eccentricity on cement failure over a long period of time. The results of this suggestion are in the next chapter.

5. The results of the numerical analysis are more conservative than the analytical results because the numerical results are closer to the failure envelope than the analytical results. This further suggests that the numerical models are better suited for safely predicting cement failure than the analytical model.

6. Even though the numerical analysis provides a much more realistic assessment of failure in the casing-cement-formation system, the analytical model is faster and requires very little to no computing power. It is therefore necessary to balance both approaches and make an informed decision for engineering applications.

### 3.8.3 Sand Production (Discussion)

Sand production was investigated analytically and the results obtained provide some insight into critical drawdown behaviour in closed and open-hole wellbores. The conclusions are outlined below;

1. The results of the sand production analysis show that the critical drawdown behaviour of the cased and open hole wellbores are different. However, the critical drawdown behaviour looks very different beyond an average point of $6r/R_3$ from the perforation interval.

2. The results show that the critical drawdown decreases as time increases for both closed and open-hole scenarios, meaning that a possible collapse of the perforation interval can be considerably delayed at a short time. This phenomenon is in tandem with previous research.

3. There is a possibility that an optimal perforation direction exists, but further research is needed to fully ascertain this (not the core focus of this research project).

**LIMITATIONS** of the sand production study are outlined below;

1. Industry study shows that most sand production problems occur in ductile rock formations. Because ductile rock formations exhibit plasticity, a plastic model is needed to predict sand production in this kind of formations.

2. The distribution of stress is not fully 3D because the analytical model is based on a plane strain model.

### 3.8.4 Suggestions for Further Research

Suggestions for further research related to this aspect of well integrity are enumerated below;

1. Even though the models (analytical and numerical) provided some useful findings to further understand the mechanical behaviour of a casing-cement-formation system, the utilised models in this research project use elastic approaches which is not entirely realistic. The wellbore system in field applications exhibit elasticity and plasticity (non-linear behaviour). This fact necessitates further study with a particular focus on the plasticity of the wellbore elements.

2. The results presented thus far do not consider the time-dependent mechanical behaviour of the wellbore elements which is necessary to fully ascertain failure resistance during life cycle of the wellbore.

3. The results do not consider the influence of phenomenon associated with the well completion stage i.e. cement shrinkage. This phenomenon may have a significant impact on the mechanical behaviour of the cement and further studies are required to investigate this thoroughly.

The next chapter will look to address some of the aforementioned limitations.

# Chapter 4

# Geomechanical Modelling

## 4.1 Introduction

This chapter furthers the investigation of the mechanical behaviour of wellbore components (especially the cement sheath) under downhole wellbore conditions by addressing some of the limitations outlined in the previous chapter i.e. the time-dependent behaviour of the wellbore elements, and plasticity. For these reasons, a 3D geomechanical model is developed with useful data to predict the life expectancy of the oilwell cement sheath under downhole operating conditions. The numerical results of this model can provide definitive information for analysis of long-term wellbore integrity.

To address the limitation of plasticity outlined in the previous chapter, a salt formation is used for the analysis in this chapter. Salt formations are ductile in nature and deform in unique ways that create impermeable traps, acting as strategic reserves for hydrocarbons. A significant number of reservoirs in the North Sea are either surrounded by or above salt. One of the major problems associated with salt formations is that it creeps and deforms over time. In geological time, salt reservoirs creates walls and diapirs that exhibit visco-plasticity and pose significant drilling/completion problems. More technical issues associated with salt reservoirs are enumerated below;

1. Well completion does not halt salt creep, meaning that movement of salt can displace wellbore tubulars thereby causing restricted access to flow of oil and

gas.

2. During drilling in salt reservoirs, the borehole walls become weakened and increase wellbore instability.

3. Intrusion of salt distorts the stress field and makes it harder to predict wellbore instability using conventional geomechanical models. This is due to the fact that the steel casing across salt formations is subjected to not just compression and tension, but a combination of non-uniform loads and hydrostatic loads – both of which must be included in design calculations to fully ascertain well integrity.

4. Production induced reservoir depletion causes reservoir compaction which compresses the axes of the casing (i.e. along the horizontal or radial directions). This makes casing collapse one of the main wellbore integrity issues in salt reservoirs (which would adversely affect cement integrity).

5. From a geomechanical perspective, salt creep can cause differential sticking (stuck pipe) which could lead to significant problems for well construction and associated downhole operations.

Even though some researchers have investigated the integrity issues associated with wellbores in salt reservoirs, very little has been done to develop a comprehensive model that considers variations in temperature and other wellbore components as an integrated system [1–3]. More so, previous research are based on two-dimensional models that assume plane strain conditions (as presented in the previous chapter) which is not valid for time-dependent, ductile formations. The next section examines the visco-plastic behaviour associated with ductile formations such as salt reservoirs.

### 4.1.1 Ductile Formations

Ductile formations exhibit visco-plasticity that show a tendency to creep when subject to stress. The rate of creep depends on a number of factors that include, but are not limited to, temperature, differential stress, grain size, and confining pressure. Figure 4.2 shows a plot for a typical creep deformation in a salt reservoir.

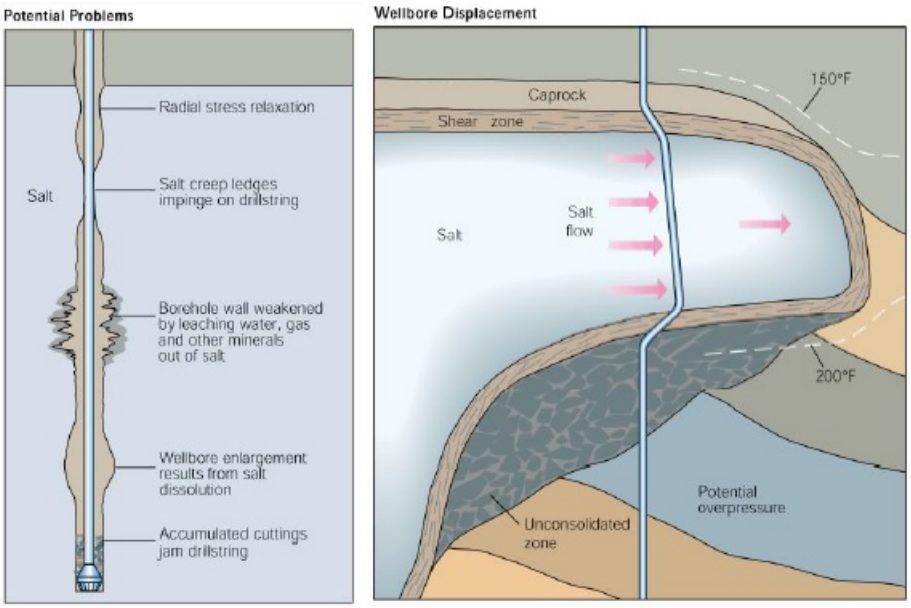


Figure 4.1: Challenges associated with drilling and completion in a salt formation.

The tertiary creep (shown as accelerative creep in Figure 4.2) seldom occurs in a salt formation because the deformations are constrained. For this reason, the creep rate is primarily defined by the transient creep rate ($\bar{\dot{\varepsilon}}_t$) and the steady-state creep rate ($\bar{\dot{\varepsilon}}_s$). The total strain rate caused by salt creep is given by Equation (4.2.1). The transient creep normally lasts for a short time and dissipates during the drilling and well completion phase which usually takes days (sometimes weeks) to complete. Hence, the total strain rate is equivalent to the steady-state strain rate after well completion in the ductile formation (i.e. $\bar{\dot{\varepsilon}} = \bar{\dot{\varepsilon}}_s$).

$$\bar{\dot{\varepsilon}} = \bar{\dot{\varepsilon}}_t + \bar{\dot{\varepsilon}}_s \tag{4.1.1}$$

Munson [5] presented a mathematical relationship for creep whose results show that the creep behaviour primarily depends on the temperature and stress under which the salt is subjected (Equation 4.2.2)

$$\bar{\dot{\varepsilon}}_s = \bar{\dot{\varepsilon}}_o \left(\frac{\sigma_{eff}}{\sigma_o}\right)^n \cdot e^{\left(\frac{Q}{RT_o} - \frac{Q}{RT}\right)} \tag{4.1.2}$$

Where $\bar{\dot{\varepsilon}}_s$ represents steady-state creep under reference conditions, $\sigma_{eff}$ represents the effective stress of creep, $\sigma_o$ represents effective stress at reference conditions,

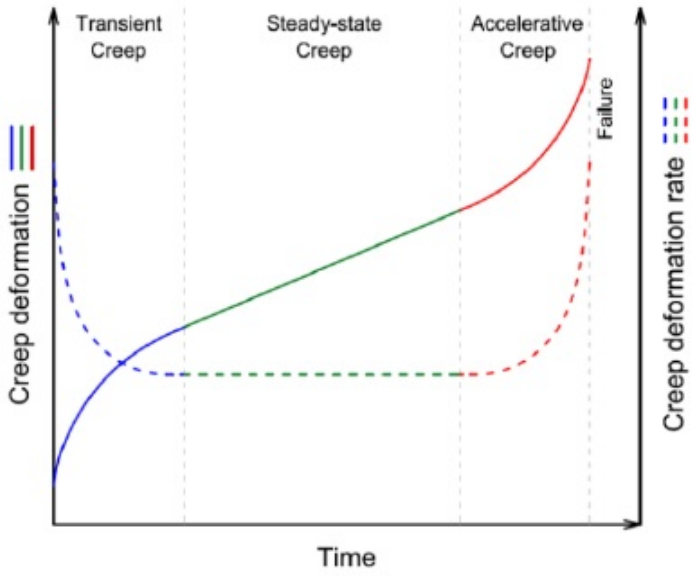


Figure 4.2: Creep deformation results from a typical salt reservoir.

$n$ represents the exponent constant obtained from lab experiments, $Q$ represents the activation energy, $R$ represents the universal gas constant (0.003574 kcal/mol $\cdot^o F$), $T_o$ represents temperature at reference conditions, and $T$ represents temperature of the rock formation.

However, the mathematical relationship put forward by Munson [5] only considers rapid creep and neglects the long-term well integrity issues associated with ductile reservoirs. The next section investigates this technical issue.

## 4.2 Modelling

A thorough geomechanical investigation of wellbore integrity issues in visco-plastic ductile reservoirs entails: (i) wellbore modelling to investigate the behaviour of the casing, cement, and ductile rock (e.g. salt), (ii) applying lab data to develop and validate predictive models, and (iii) reservoir modeling to ascertain the influence of loads and boundary conditions on the long term integrity of the wellbore components. In a bid to not focus on rapid creep behaviour, this section examines the period after the ductile formation has been cased and cemented during which there

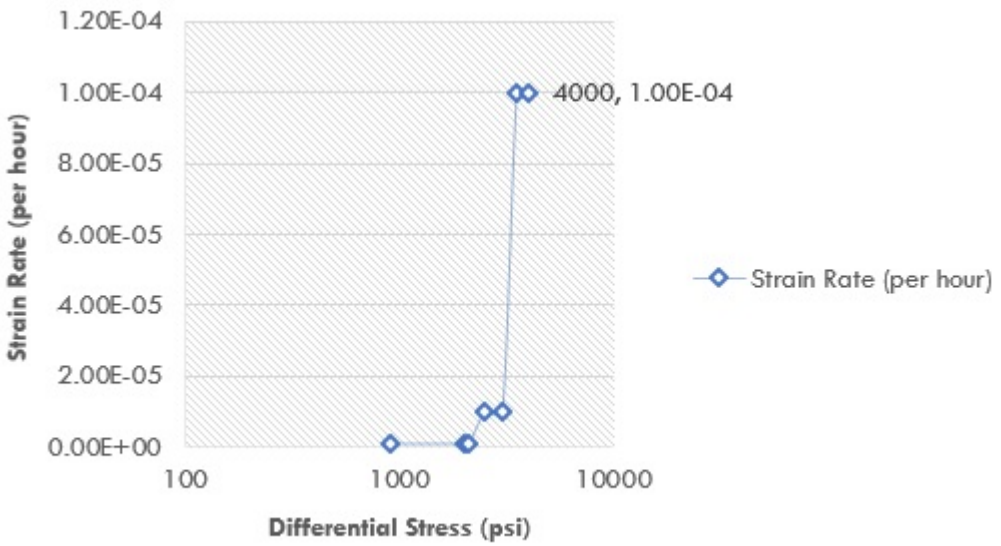


Figure 4.3: Plot of steady-state creep strain rate versus differnetial stress for a ductile formation (halite reservoir). Modified from Costa et al. [6].

is predominantly slow, lengthy creep behaviour.

This section presents the application of a three-dimensional geomechanical model to a field case scenario that has a cased and cemented wellbore, under downhole operating conditions. The model includes an integrated concentric casing-cement-salt wellbore system, as shown in Figure 4.4, whose inner casing diameter is 7.92 inches, outer casing diameter is 8.625 inches, and outer cement diameter is 12.25 inches. As shown in Figure 4.4, boundary conditions are applied along the symmetric plane line and the outer boundary (non-displacement conditions).

After applying the boundary conditions, the casing-cement-salt wellbore system is simulated for different phases of the life cycle of the well using the following three steps;

1. Drilling Phase: This phase is simulated by applying uniform pressure on the inner surface of the steel casing. To account for fluid circulation, a low-temperature boundary condition was applied and a hundred days of the drilling process were simulated in this phase.

2. Intermediate Phase: This phase simulates the variations in pressure prior to production that is characterised by a decline in pressure. Fifty days were

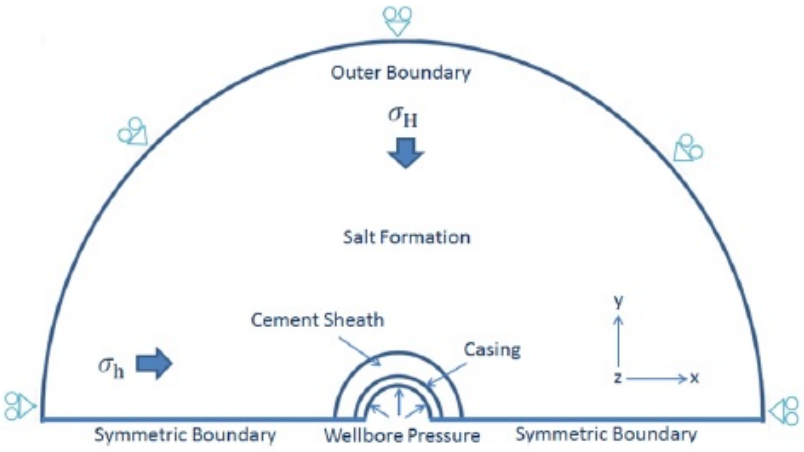


Figure 4.4: Schematic of the casing-cement-salt simulation model.

simulated for this phase.

3. Production Phase: This phase is characterised by production-induced reservoir depletion over a simulated period of five hundred days. For the boundary conditions, high temperature was applied on the inner surface of the steel casing to simulate the flow of high temperature hydrocarbons.

The mathematical relationship for the underlying physics (and mechanism) in this geomechanical investigation are presented in the following equations. The equation for energy balance is based on the work of Carslaw and Jaegar [7].

$$\rho C \frac{\partial T}{\partial t} + \nabla \cdot (-\lambda \nabla T) = q \tag{4.2.3}$$

Where $\rho$ represents the density of the ductile rock formation, $C$ represents the heat capacity of the ductile rock formation, $\lambda$ represents the thermal conductivity, $T$ represents the temperature, $\nabla$ represents the divergence operator. For steady-state analysis, $\rho C \frac{\partial T}{\partial t}$ and $q$ are equal to zero. The mathematical relationship for stress equilibrium is presented in Equation (4.3.4) based on the work of Zienkiewicz and Taylor [8];

$$\int_v \sigma : \delta\varepsilon dV = \int_s \gamma \cdot \delta v dS + \int_v f \cdot \delta v dV \tag{4.2.4}$$

Where $\delta v$ represents the field of virtual velocity, $\delta\varepsilon$ represents the rate of deformation, $\gamma$ represents traction, and $f$ represents force per unit volume. This mathematical relationship is discretized using Lagrangian formulation. The mathematical equation for the solid is expressed as Equation (4.3.5);

$$d\sigma = Ed\varepsilon + \int_0^t (t-\tau)\frac{d\varepsilon}{d\tau}d\tau \tag{4.2.5}$$

Where $\sigma$ represents stress, $\varepsilon$ represents strain, $E$ represents material stiffness, and $\tau$ represents the time of relaxation. The equation for the mechanical behaviour of the salt reservoir, based on the aforementioned creep law, can be solved using the following iteration method;

1. The field of displacement, $[\delta_i]$, and the stress field, $[\sigma_i]$, are solved at the end of the equilibrium. The solutions are passed on to the production phase as the initial values.

$$[K][\delta_i] = [F] \tag{4.2.6}$$

$$[\sigma_i] = [D][B][\delta_i] \tag{4.2.7}$$

   Where $[K]$ represents the stiffness matrix, $[F]$ represents the nodal force, $[B]$ represents the geometric stiffness matrix, and $[D]$ represents the elasticity matrix.

2. Assuming the field of stress does not change during each increment, the stress is $\sigma_t$ from $t$ to $t + \Delta t$. Calculating the change in creep strain;

$$[\Delta\varepsilon_t^c]_{\Delta t} = \Delta t[\dot{\varepsilon}_t] \tag{4.2.8}$$

   Where $[\dot{\varepsilon}_t]$ represents the rate of creep. The constituents of $[\dot{\varepsilon}_t]$ are represented using the following mathematical equations;

$$\dot{\varepsilon_1} = \frac{\bar{\dot{\varepsilon}}}{\sigma_{eff}}[\sigma_1 - \frac{1}{2}(\sigma_2 + \sigma_3)] \tag{4.2.9}$$

$$\dot{\varepsilon_2} = \frac{\bar{\dot{\varepsilon}}}{\sigma_{eff}}[\sigma_2 - \frac{1}{2}(\sigma_1 + \sigma_3)] \tag{4.2.10}$$

$$\dot{\varepsilon_3} = \frac{\bar{\dot{\varepsilon}}}{\sigma_{eff}}[\sigma_3 - \frac{1}{2}(\sigma_1 + \sigma_2)] \tag{4.2.11}$$

The mathematical relationship for $\sigma_{eff}$ is given by Equation (4.3.12);

$$\sigma_{eff} = \frac{1}{\sqrt{2}}[(\sigma_1 - \sigma_2)^2 + (\sigma_2 - \sigma_3)^2 + (\sigma_3 - \sigma_1)^2 + 6(\tau_{12}^2 + \tau_{23}^2 + \tau_{13}^2)]^{0.5} \tag{4.2.12}$$

3. The mathematical relationship for force in a time interval is expressed in Equation (4.3.13). It is applied to the entire domain of the salt reservoir;

$$[\Delta F_c(t)] = \int_\Omega [B]^T [D][\Delta \varepsilon_t^c] d\Omega \tag{4.2.13}$$

4. Solve the equilibrium equation;

$$[K][\Delta \delta^c]_t = [\Delta F_c(t)] \tag{4.2.14}$$

The equations were solved using the Newton's method (Newton-Raphson technique) to determine a good approximation, and a Jacobian matrix was generated for all first order partial derivatives. The input parameters, properties, and boundary conditions are presented in Table 4.1.

## 4.3 Results and Discussion

This section presents the numerical results of the long term effect of salt-induced creep on wellbore integrity under downhole operating conditions. The results of the simulation (2D and 3D) are compared, and the long-term effect of casing eccentricity is also presented in this results section. At the end of this section, conclusions and limitations are discussed based on the results.

Table 4.1: Input data for geomechanical model.

| PROPERTY PARAMETERS | INPUT VALUE |
|---|---|
| Casing Specification | $8\ \frac{5}{8}$ in. K-55 |
| Cement Specification | API Class G |
| Salt Rock Specification | Halite |
| Young's Modulus, Steel casing | 3E7 psi |
| Young's Modulus, Oilwell Cement | 2E6 psi |
| Young's Modulus, Salt Rock | 3E6 psi |
| Poisson's Ratio, Steel Casing | 0.3 |
| Poisson's Ratio, Oilwell Cement | 0.2 |
| Poisson's Ratio, Salt Rock | 0.36 |
| Steel Casing Density | 0.284 lb/in$^3$ |
| Oilwell Cement Density | 0.0683 lb/in$^3$ |
| Salt Rock Density | 0.08 lb/in$^3$ |
| Specific Heat, Steel Casing | 0.113 BTU/lb $\cdot F$ |
| Specific Heat, Oilwell Cement | 0.422 BTU/lb $\cdot F$ |
| Specific Heat, Salt Rock | 0.221 BTU/lb $\cdot F$ |
| Thermal Conductivity, Steel Casing | 34.09 BTU/hr $\cdot ft \cdot F$ |
| Thermal Conductivity, Oilwell Cement | 0.8 BTU/hr $\cdot ft \cdot F$ |
| Thermal Conductivity, Salt Rock | 2.31 BTU/hr $\cdot ft \cdot F$ |
| Initial Temperature | $320^O F$ |
| Wellbore Temperature (Drilling) | $200^o F$ |
| Wellbore Temperature (Production) | $380^o F$ |
| Wellbore Pressure (Drilling) | 3,500 psi |
| Wellbore Pressure (Production) | 1,500 psi |
| Horizontal Stress | 2,300 psi |

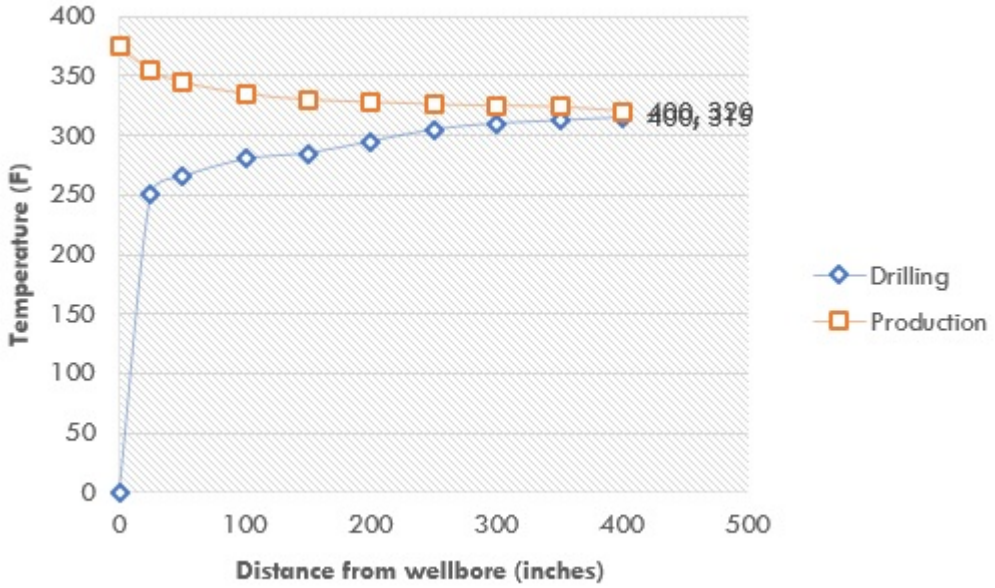


Figure 4.5: Profile of temperature along the radius of the wellbore in the simulation model.

### 4.3.1 Temperature Distribution

Figure 4.5 shows the distribution of temperature during drilling and production-induced reservoir depletion. The plot clearly shows that temperature is considerably lower during drilling but higher during the production phase because of the flow of hydrocarbons from HPHT reservoir formation(s). The result also shows that variation in temperature is high near the wellbore region but plateaus further away from the wellbore.

### 4.3.2 Stress and Strain Distribution

Figures 4.6 to 4.9 show the simulation results of the distribution of maximum principal stress. The result shows that at the start of the drilling phase (Figure 4.6), highest value of maximum principal stress exists within the steel casing. As the salt formation begins to deform, stress is exerted around the wellbore and the highest value of compressive principal stress occurs within the oilwell cement sheath (Figure 4.7). The results clearly show that as time progresses, the compressive principal stresses in the oilwell cement sheath increases during the drilling and production

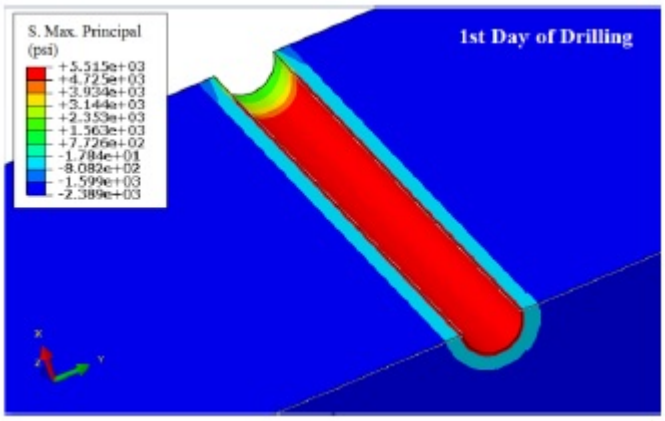


Figure 4.6: Distribution of maximum principal stress after first day of drilling.

phases. As aforementioned, the most probable case of wellbore failure in salt reservoirs is plastic yield caused by salt rock creep, as opposed to the development of cracks. For this reason, the best indicator of casing (and cement) failure is the von mises stress. Figures 4.10 to 4.13 show the simulation results for the distribution of von mises stress. The results show that the maximum von mises stress exists in the steel casing, but the stress declines during the drilling phase and significantly increases the production phase due to the flow of hydrocarbons from HPHT reservoirs.

Figures 4.14 and 4.15 show the axial strain and radial strain in the steel casing respectively. The simulation results show that the radial strain is higher than axial strain, and there is a sharp spike in strain (radial and axial) during the first two hundred days.

### 4.3.3 Comparison of 2D and 3D Models

The analysis in the previous chapter assumes plane strain conditions and only used two-dimensional models for the analytical and numerical investigation. A 2D model was developed alongside the 3D model in order to compare both and present the differences. Figures 4.16 and 4.17 show the von Mises stress and radial displacement results from the 2D and 3D models. The results show similar patterns for both models. During the drilling phase, the wellbore pressure is higher than the horizontal stress, thereby increasing the von Mises stress over time. During the production

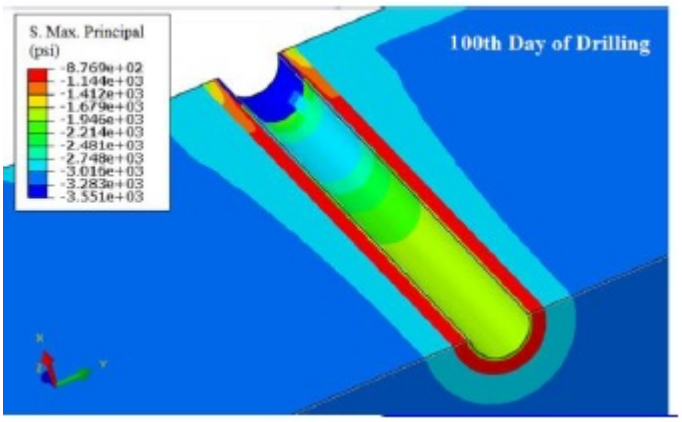


Figure 4.7: Distribution of maximum principal stress after one hundred days of drilling.

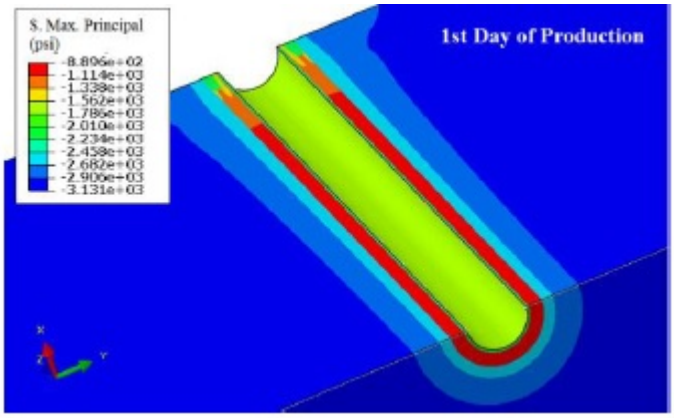


Figure 4.8: Distribution of maximum principal stress after first day of production.

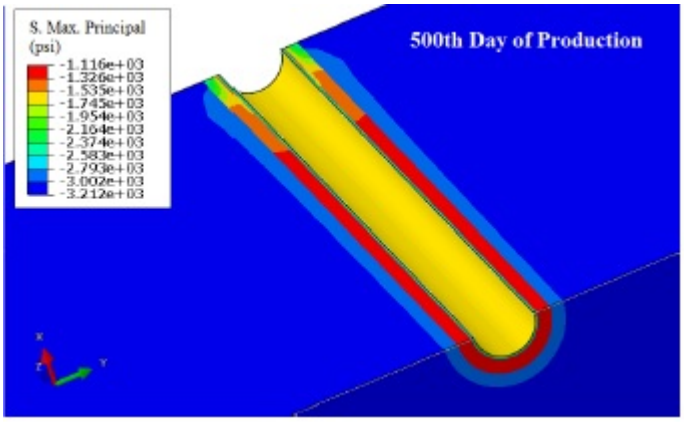


Figure 4.9: Distribution of maximum principal stress after five hundred days of production.

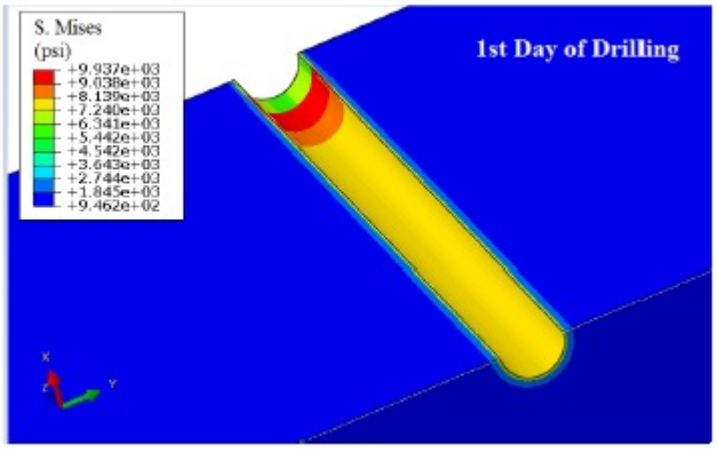


Figure 4.10: Distribution of von mises stress after first day of drilling.

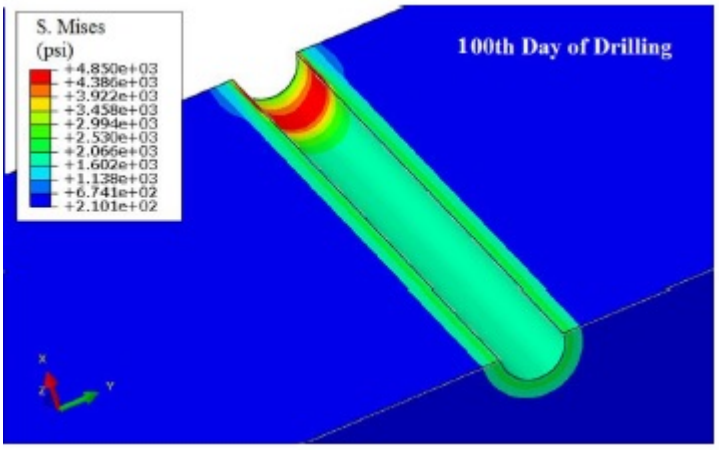


Figure 4.11: Distribution of von mises stress after one hundred days of drilling.

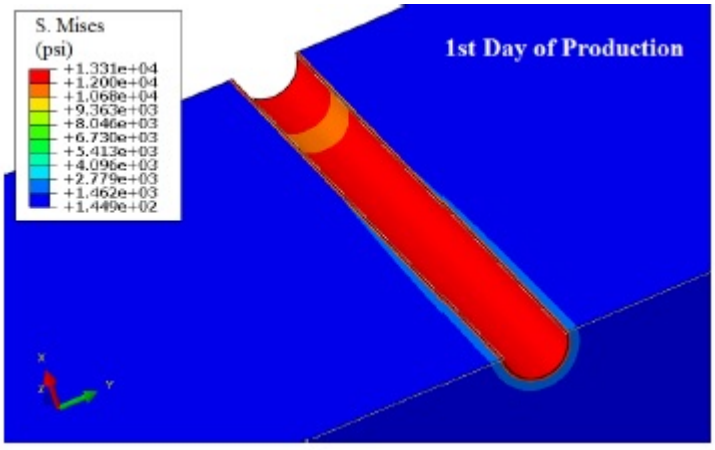


Figure 4.12: Distribution of von mises stress after first day of production.

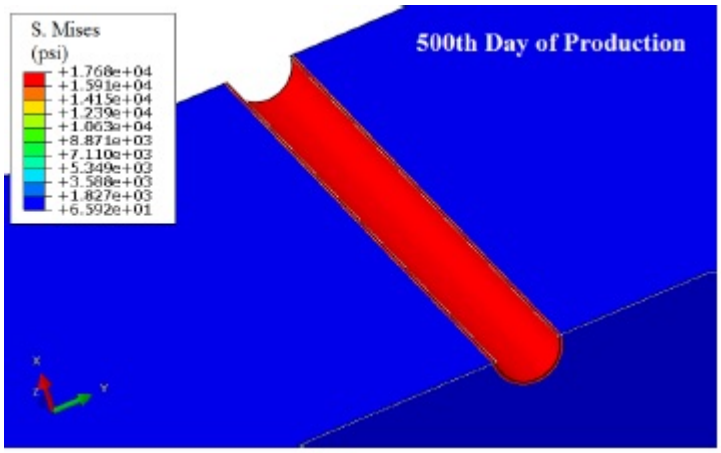


Figure 4.13: Distribution of von mises stress after five hundred days of production.

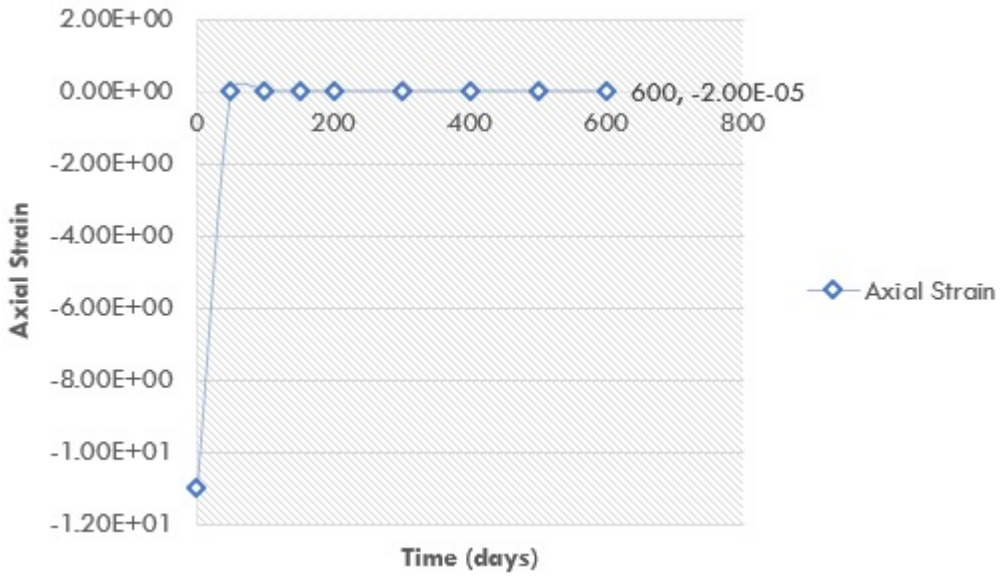


Figure 4.14: Plot showing simulation results for axial strain in the steel casing during the drilling phase and production phase.

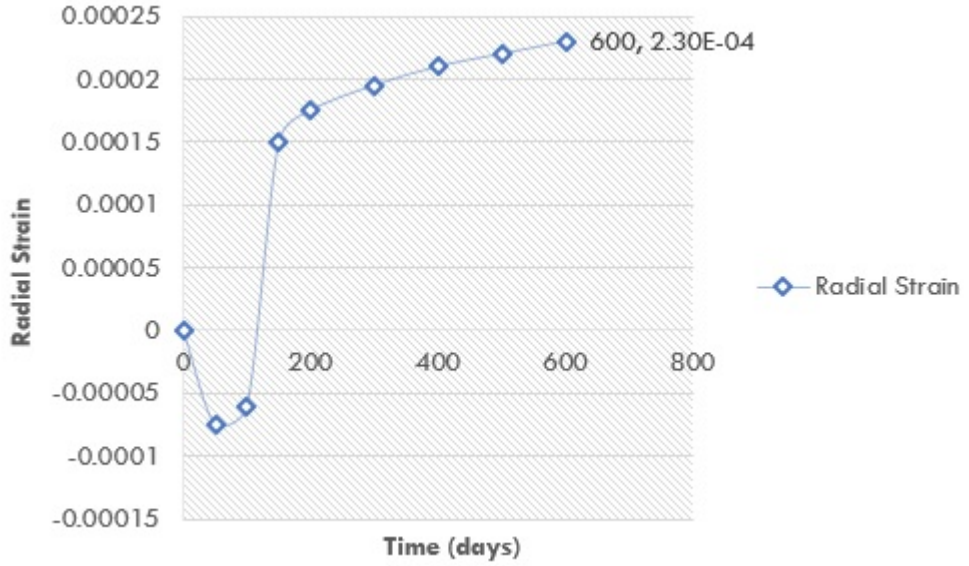


Figure 4.15: Plot showing simulation results for radial strain in the steel casing during the drilling phase and production phase.

phase, the wellbore pressure is lower than the horizontal stress, thereby causing a decline in the von Mises stress over time. However, results of the 2D model clearly underestimate the effect of salt rock creep as time progresses, even though the result is similar to the 3D result at the start of the simulation. Transient temperature did not have a major influence on the results obtained from the simulation models, so steady-state temperature is sufficient for modelling of wellbore integrity analysis.

### 4.3.4 Effect of Casing Eccentricity

The influence that casing eccentricity has on long term well integrity was investigated in the previous chapter, albeit under elastic and static conditions. This section considers casing eccentricity, in a visco-plastic salt reservoir, over a long period of time in order to determine a more realistic effect of eccentricity on long term well integrity. Figure 4.18 shows casing eccentricity induced by fast salt creep and a lack of sufficient centralisers. As aforementioned, the focus of this investigation is beyond fast creep behaviour and, instead, is focused on the long term mechanical behaviour of the casing-cement-formation wellbore system. The mathematical relationship for casing eccentricity, $\varepsilon$, is shown in Equation (4.4.15);

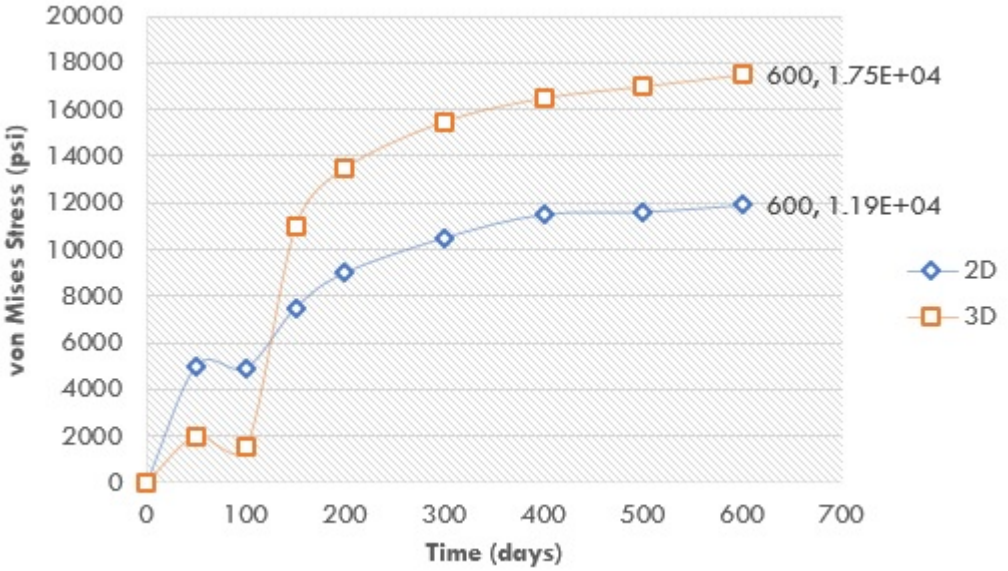


Figure 4.16: Plot showing von Mises stress in the steel casing predicted by the 2D and 3D models.

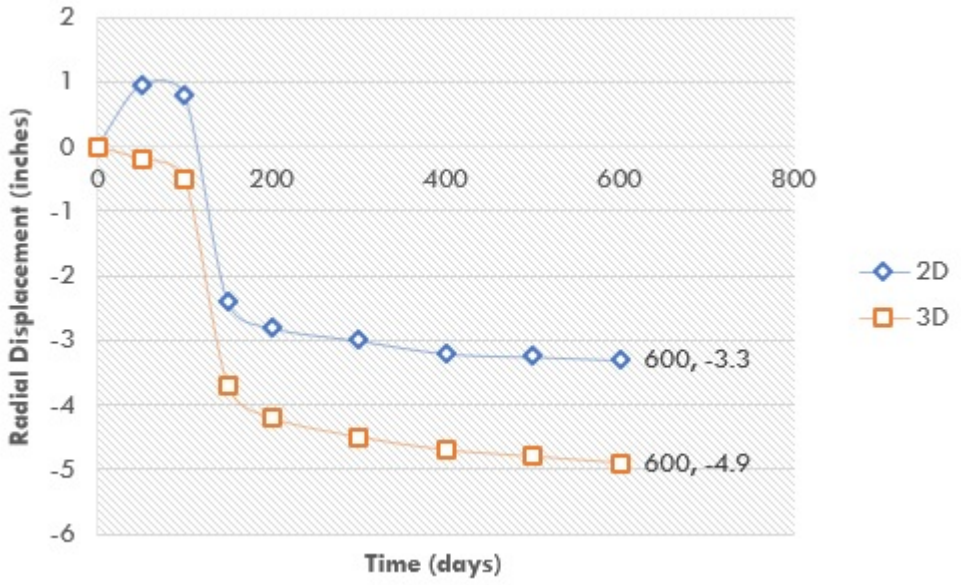


Figure 4.17: Plot showing radial displacement predicted by the 2D and 3D models.

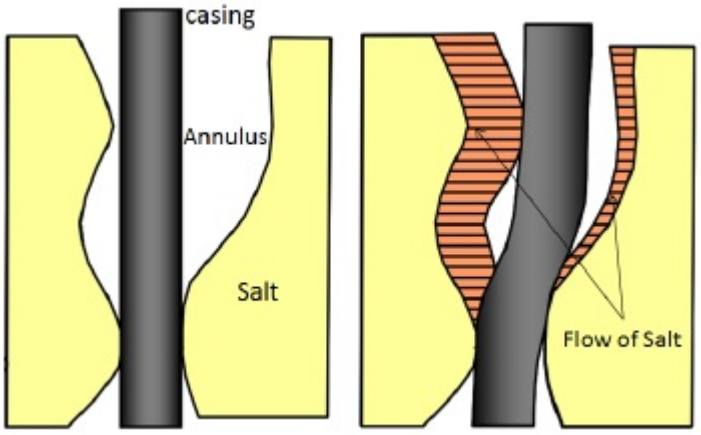


Figure 4.18: Eccentricity of the casing induced by salt creep. Figure on the left shows the initial condition of the steel casing in the salt reservoir, and figure on the right shows casing eccentricity induced by salt creep.

$$\varepsilon = \frac{\delta_r}{r_o - r_i} \tag{4.3.15}$$

Where $\delta_r$ represents casing deflection from the center of the wellbore (i.e. distance from the center of the wellbore to the center of the steel casing), $r_o$ represents the radius of the wellbore, and $r_i$ represents the outer radius of the steel casing. Various eccentricity scenarios were simulated to investigate the influence of eccentricity on stress distribution in the casing-cement-formation wellbore in a ductile, visco-plastic salt reservoir. Based on the previous results, maximum stress occurs in the steel casing during production-induced reservoir depletion. For this reason, the stresses in the casing were analysed after about five hundred days of production. The simulation result in Figure 4.20 clearly shows that stress increases as the eccentricity increases, more so after lengthy wellbore production. It also shows how eccentricity induces non-uniform stress distribution in the casing-cement-formation wellbore system over time. It is therefore important to have tight control on drilling fluids in order to prevent the dissolution of salt rock, and ensure that there are enough centralizers in place to significantly lower the chances of casing eccentricity.

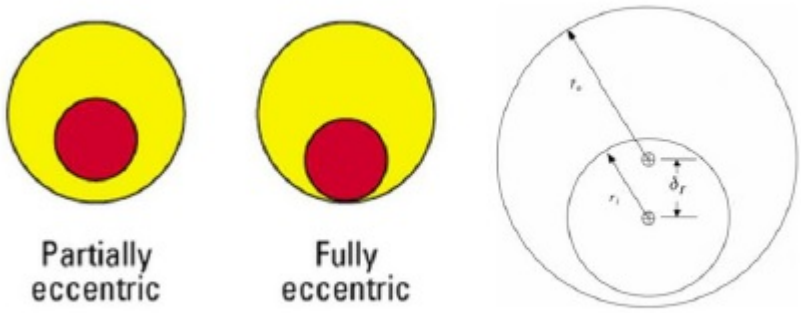


Figure 4.19: Schematic of partially eccentric and fully eccentric casings.

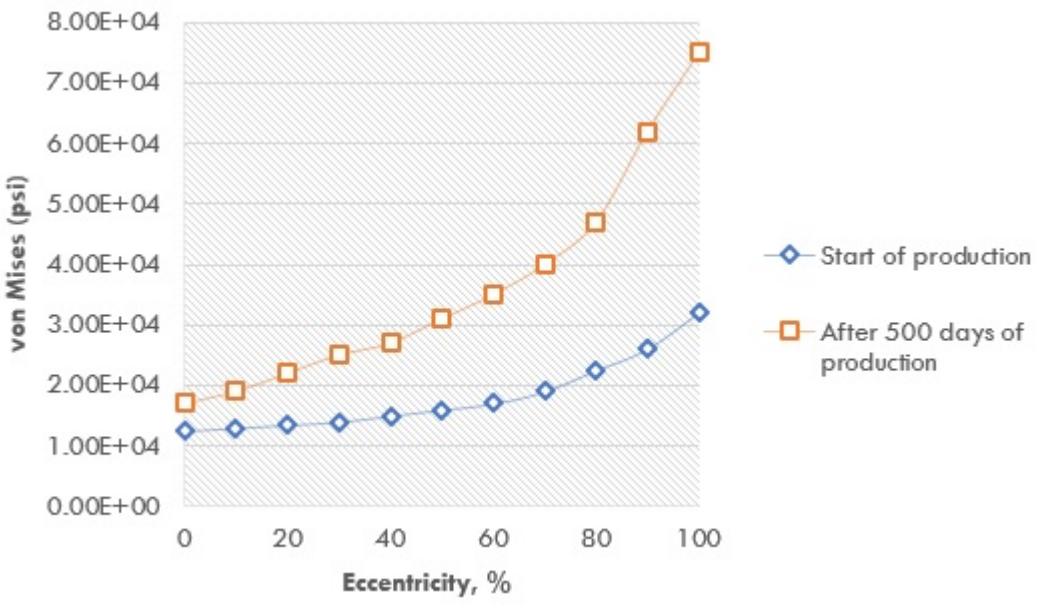


Figure 4.20: Plot showing effect of eccentricity on stress distribution at the start of production, and after 500 days of production.

### 4.3.5 Suggestion for Completion Design

To prevent casing collapse and subsequent cement failure, the well planning team must decide to increase the strength of the casings (by using thicker casings), or reduce the stress caused by gradual salt creep. The formation temperature is not within our control, so it is challenging to lower the effect of salt creep. As a result, this section presents a probable completion design solution that can reduce the differential stress caused by a salt formation, as presented in Figure 4.21. After the wellbore in a salt formation is cemented in place, it can be completed with a production string extending down to the bottom of the salt rock formation. The annular space between the tubing and casing can be filled with completion fluid that has high density in order to increase the pressure acting on the internal surface of the casing, and leave some space at the top of the annular space to account for changes in volume. Using this proposed completion design, the part of the wellbore below the packer can maintain pressure that is good enough to consistently produce at an acceptable rate. Furthermore, this proposed design will ensure that pressure in the annular space can be increased to reduce stress and lower the probability of salt creep.

## 4.4 Conclusions and Limitations

The following conclusions were drawn from the analysis presented in this chapter;

1. Assuming two-dimensional plane strain is not sufficient for investigating wellbore integrity issues in ductile formations because it neglects vertical strain imposed by overburden stress. A three-dimensional visco-plastic model is more realistic and provides better results for predicting well integrity.

2. It is achievable to reduce the stress exerted by salt creep during production-induced reservoir depletion using completion fluid that has high density. This increases the pressure acting on the casing and significantly reduces differential stress.

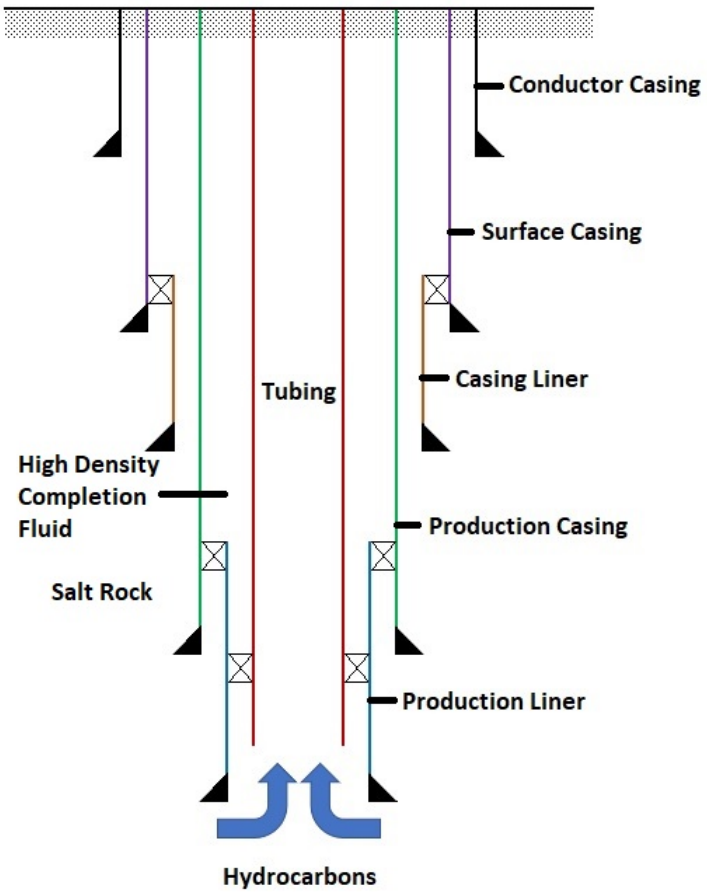


Figure 4.21: Schematic of suggested way to reduce the differential stress in a proposed completion design.

3. Casing eccentricity has a strong influence on integrity over time. It is pertinent to use a good cement mix and adequate centralisers to prevent eccentricity over the life cycle of the wellbore.

The LIMITATIONS of this analysis are enumerated as follows;

1. The stresses in this analysis were assumed to not vary with depth because a section of the wellbore was analysed, not the whole. In field applications, the stress profile is different across various depths and as the deep increases, the stress exponentially increases.

2. Given the abrupt changes that are sometimes unforeseen, it is important to understand the integrity of the wellbore at every certain time. This necessitates the application of real-time monitoring to avoid not being able to fix wellbore integrity issues.

# Chapter 5

# Real Time Monitoring of Wellbore Integrity

This chapter attempts to address one of the limitations outlined in the analysis of the previous chapter: monitoring the integrity of the oilwell cement in real time. Even though predictive models are useful for designing and engineering wellbore systems, there are some unforeseen technical issues that may arise during the life of the well – some of which could be catastrophic if not treated immediately. For this reason, it is important to regularly monitor the structural condition of the casing-cement-formation wellbore system, with particular emphasis on the oilwell cement sheath barrier.

To this end, a set of downhole tubing leak monitoring and diagnosis system has been proposed by combining fluid monitoring, acoustic wave detection, and tracer detection technology to monitor leakages in offshore platforms.

## 5.1 The composition and principle of the system.

### 5.1.1 The composition of the system.

The wellbore leakage and monitoring system is made up of fluid monitoring, liquid level detection, and tracer detection (see Figure 5.1).

- Fluid Monitoring: Pipelines are used to introduce air into the system and

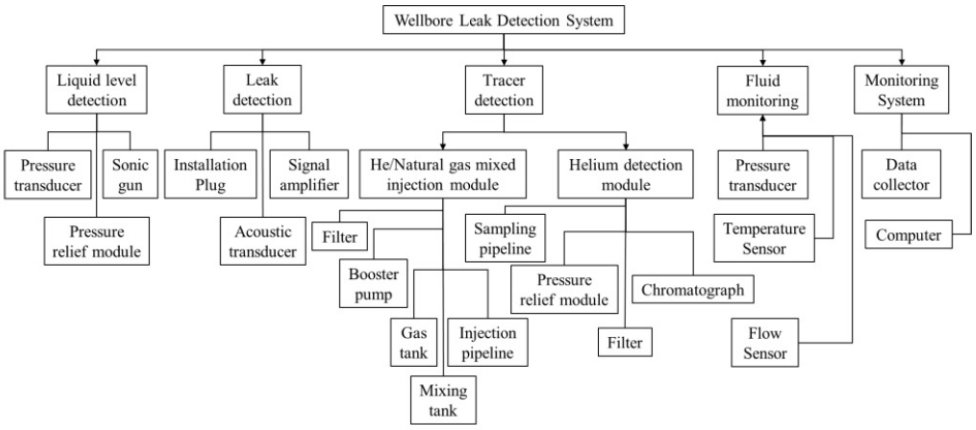


Figure 5.1: The composition of the proposed downhole leakage and monitoring system.

monitor the gas during the depressurisation process. The main parameters include, but are not limited to, the flow rate, pressure, and temperature in the pressure relief pipeline.

- Liquid Level Detection: Ascertaining the depth of the liquid level in the annular space by using the liquid level echo signal.
- Leak Point Detection: When the gate valve is opened, the acoustic wave in the annular space can receive signal.
- Tracer Detection: This is primarily made up of the tracer injection and detection. The tracer is injected from the annular space, and non-polluting helium gas is chosen as the tracer source.

### 5.1.2 Principle of the system.

The main causes of pressure in the annular space are thermal effects, pipe leakages, and production casing leakages. After ascertaining the existence, and extent, of a leakage, it is necessary to determine the specific leakage source (see Figure 5.2).

1. Principle of liquid level detection: The principle of liquid level detection is based on the acoustic wave method, and the mathematical formula is shown

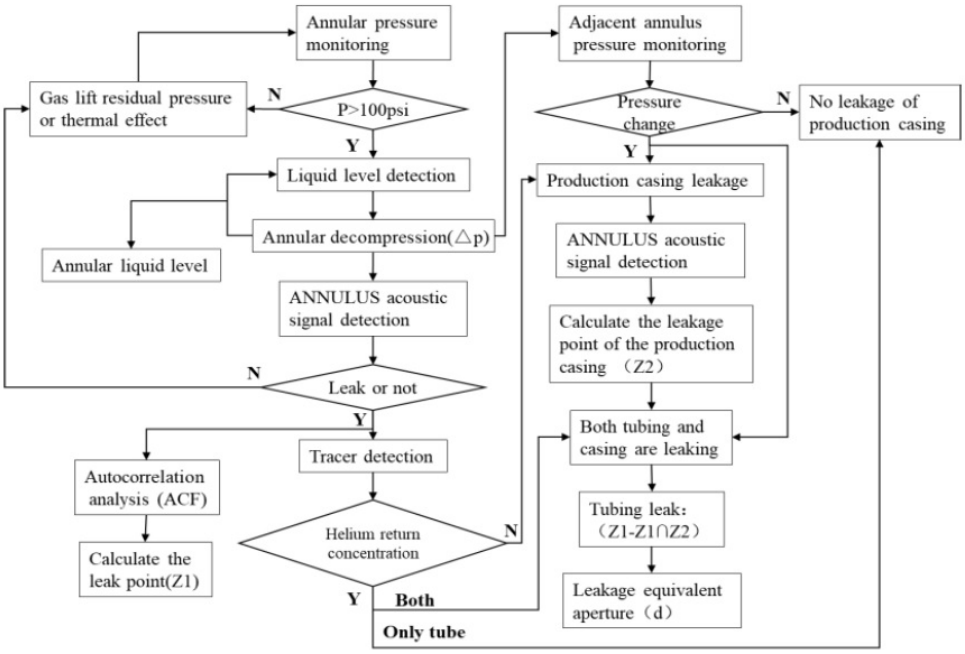


Figure 5.2: Detailed diagnosis process of oil casing leakages.

in equation (5.1.1). The speed of sound, $v$, can be calculated using equation (5.1.2)

$$H = vt \tag{5.1.1}$$

$$v = [(\frac{c_p}{c_v})(\frac{RT_g}{M_g})(Z_g + \rho(\frac{\partial Z_g}{\partial_\rho})_{T_g})] \tag{5.1.2}$$

where $c_p$ and $c_v$ are the heat capacities at constant pressure and volume ($J/mol \cdot K$), $R$ represents the general gas constant, $T_g$ represents temperature (in this case, gas), $Z_g$ is the factor of compressibility, $\rho$ is the mole density, and $M_g$ is the molar mass.

2. Principle of leak location: When the oil pipe or casing leaks, high-pressure natural gas will enter the production annulus through the leakage. A sensor (preferably a sound wave receiving type) can be installed at the exit of the Christmas tree tubing pipe to obtain a signal in the annular space. The mathematical relationship for the delay relative to the leakage in the annulus is represented in equation;

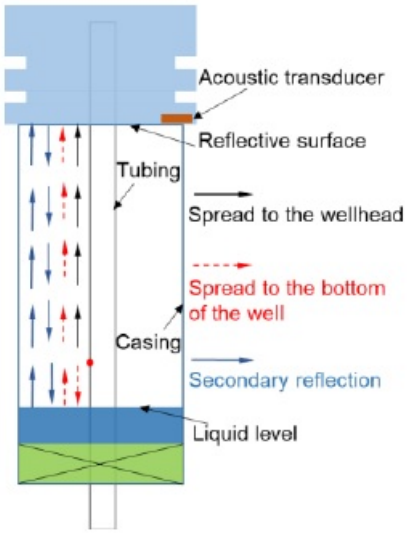


Figure 5.3: Schematic diagram of the position of the oil pipe leakage.

$$X = \frac{v(t_2 - t_1)}{2} \tag{5.1.3}$$

where $X$ represents the distance between the leakage point and the reflecting surface of the tubing hanger, $t_1$ represents the time of the return journey between the leaking sound wave from the point of leakage to the liquid surface in the annulus, and $t_2$ represents the return time of the sound wave.

### 5.1.3 System

A schematic of the proposed leakage monitoring system is shown in Figure 5.4

### 5.1.4 Results and conclusions

A number of lab experiments were carried out and the preliminary test results show that a single detection method is not sufficient to fully obtain downhole leakage information. This reinforces the need for an integrated leakage monitoring and diagnosis system that is suitable for field use. Also, the proposed leakage monitoring system does not need to adversely affect well production by moving the pipe string.

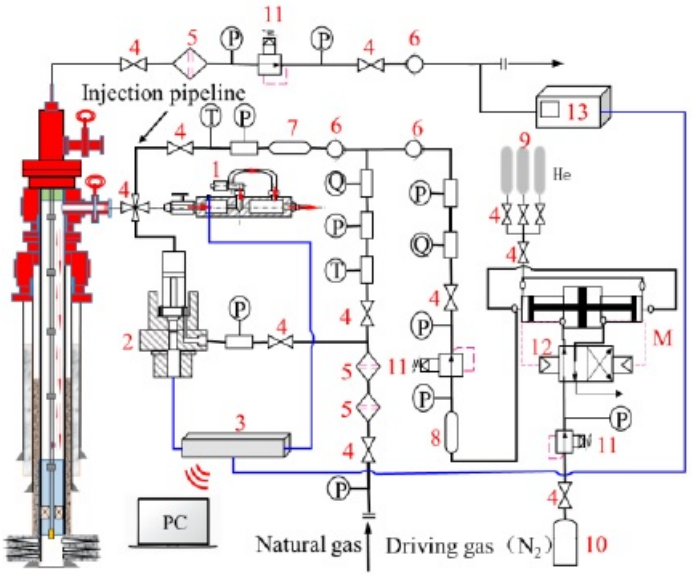


Figure 5.4: Working principle schematic of the propose leakage monitoring and diagnosis system.

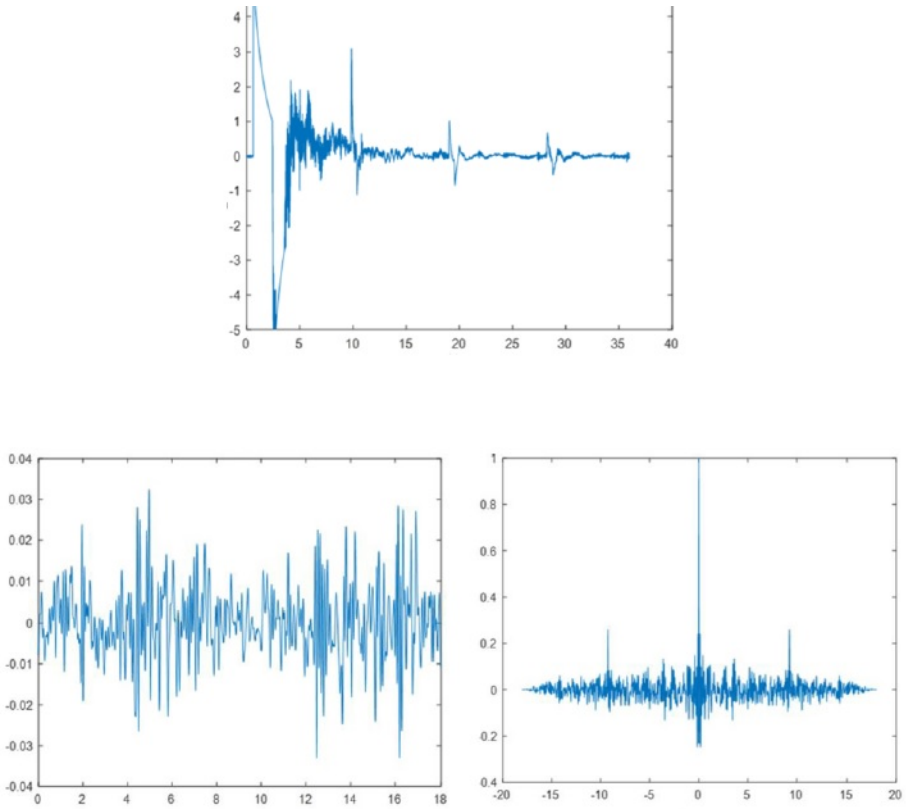

Figure 5.5: Time domain diagram of acoustic signals and their corresponding auto-correlation curve.

Table 5.1: Summary of components of the proposed downhole leakage monitoring system.

| No. | Name |
|---|---|
| 1 | Liquid level detection device |
| 2 | Leak point detection device |
| 3 | Surveillance system |
| 4 | Valve |
| 5 | Oil-gas separation device |
| 6 | Check valve |
| 7 | Mixing tank |
| 8 | Gas Tank |
| 9 | Helium cylinder |
| 10 | Driving gas (N2) |
| 11 | Pressure reducing valve |
| 12 | Supercharger |
| 13 | Chromatograph |
| P | Pressure transmitter |
| Q | Mass flow-meter |

### 5.1.5 Limitations

1. A field test needs to be conducted to show real time monitoring of the leakages within the wellbore. This needs to be extensive and thorough to fully ascertain the reliability of this method.

# Chapter 6

# Conclusion, Discussion, and Recommendation.

This chapter discusses the results and conclusions from the previous chapters, and presents potential areas for future research.

## 6.1 Conclusion and Discussion

### 6.1.1 Steady-State Analytical Model

This research project has shown that elastic models are useful for modelling wellbores under various downhole, operating conditions. The comprehensive analytical model is a good tool for obtaining the stress distribution within the casing-cement-formation wellbore without using numerical simulators. Moreover, this stress prediction model can be extended to general, concentric, inclined wellbores using a straightforward superposing principle. In summary, this analytical model has the following features:

- Uniqueness

1. This model utilises generalised plan strain.

2. It can incorporate fully coupled poroelasticity.

3. This model considers all drilling and well completion processes for a wellbore, including variation in tectonic stresses and temperature.

- Limitation

- This model does not consider plasticity.

- It does not use a full 3D solution.

- It ignores the coupling of temperature and fluid in the rock formation.

### 6.1.2 Cement Failure

The results of the cement failure analysis and investigation are enumerated below:

1. The numerical models are much more conservative than the analytical models because the numerical results are closer to the failure envelopes than the analytical results. This shows that the numerical models are preferable to the analytical models in order to make models for an inclined cased wellbore system. However, the analytical models are swifter and require less computing power than the numerical models.

2. This research produced a definitive guide, based on parametric analysis, of what factors affect tensile and shear failure the most.

### 6.1.3 Sand Production

- Uniqueness

1. The results quantitatively show that the critical drawdown increases at the cased wellbore rather than at the open-hole wellbore case. Previous sand production research has not shown this in detail. Furthermore, critical drawdown is significantly different in the near-wellbore region in cased and open-hole scenarios.

2. As time increases, the critical drawdown decreases.

3. The results show that if sand production near the wellbore occurs, perforating in the direction of the minimum horizontal stress is the best decision to increase critical drawdown.

- Limitations

1. Lots of sanding problems occur for ductile rock formations.

2. This research does not consider tensile failure of the rock formation but has considered shear failure.

### 6.1.4 3D Geomechanical Model

The results of the 3D geomechanical model are summarised below:

1. The 2D plane strain model is not readily applicable to deformation problems in ductile formations because it ignores the vertical strain imposed by the overburden stress, thereby underestimating the effect of rock mobility on the stress loading.

2. The differential stress acting on the internal surface of the casing determines the evolution of the von Mises stress in the casing.

3. Excessive casing stress can be mitigated by using high-density completion fluid to increase the internal pressure acting on the internal surface of casing and significantly reduce the differential stress.

4. The eccentricity of the casing has a large impact on the casing stress.

### 6.1.5 Proposed Leakage Monitoring System

The results of the lab tests for the propose leakage monitoring system are summarise as follows;

- Uniqueness

1. It is not possible to use a single detection method to obtain information about downhole, offshore leakages. This necessitates the development of an innovative leakage monitoring and diagnosis system, which is the direction of engineers and scientists alike in the industry.

2. Combining fluid monitoring, acoustic wave positioning, and liquid level detection is ideal for ascertaining downhole leakage.

3. This proposed monitoring system can perform leakage diagnosis without moving the pipe string and interrupting production. This is potentially valuable for the safe production of gas wells.

- Limitations

1. This system needs to be validated with field tests to fully ascertain its ability to monitor leakages in offshore platforms.

## 6.2 Recommendation for Future Research

Even though the developed analytical and numerical models in this thesis give useful and definitive results to better understand the mechanical behaviour of ductile reservoir formations, these models are primarily based on elastic approaches. The casing, oil-well cement, and rock formation are non-linear materials that exhibit elasticity and plasticity. Thus, further studies are needed to study the effect of plasticity in more detail to fully ascertain the behaviour of ductile formations and their concomitant effect on well integrity.

This research also ignores the important influence of well completion on cement failure. This influence may be critical and needs to be included in future research for a more realistic assessment.

Finally, the analytical models presented in this research ignore the coupling between temperature and fluid in the rock formation due to mathematical complexity. This could potentially cause unwanted discrepancies between the analytical and numerical results, so analytical models that consider this coupling should be developed in future research.

# Bibliography

[1] Lao, K., Bruno, M., and Seraijan, V. (2012), "Analysis of Salt Creep and Well Casing Damage in High Pressure and High Temperature Environments", Paper presented at the Offshore Technology Conference, Houston, TX, USA, 30 April–3 May.

[2] Hansen, F. (2011), "Salt Repository Geomechanics Research Agenda", Paper presented at the 45th US Rock Mechanics and Geomechanics Symposium, San Francisco, California, 26-29 June.

[3] Chatar, C. and Imler, M. (2010), "Overcoming A Difficult Salt Drilling Environment In The Gulf of Mexico: A Case Study", Paper SPE 128192 presented at the IADC/SPE Drilling Conference and Exhibition, New Orleans, Louisiana, 2-4 February.

[4] Mackay, F., Inoue, N., and Botelho, F. (2008), "Analysing Geomechanical Effects While Drilling Sub Salt Wells Through Numerical Modelling", Paper presented at the SPE Indian Oil and Gas Technical Conference and Exhibition, Mumbai, India, 4-6 March.

[5] Munson, D. (2004), "Constitutive Model Parameters Defined for Gulf Coast Salt Domes and Structures", Paper presented at the 6th North America Rock Mechanics Symposium, Houston, TX, 5-9 June.

[6] Costa, A., Poiate, E., Amaral, C., Goncalves, C., Falcao, J., and Pereira, A. (2010), "Geomechanics Applied To The Well Design Through Salt Layers In Brazil: A History of Success", Paper presented at the 44th US Rock Mechanics

Symposium and 5th US-Canada Rock Mechanics Symposium, Salt Lake City, Utah, 27-30 June.

[7] Carslaw, H. and Jaegar, J. (1959), "Conduction of Heat In Solids", 2nd Edition, Oxford University Press.

[8] Zienkiewicz, O. and Taylor, R. (2005), "The Finite Element Method", 5th Edition, London. Elsevier Ltd.

[9] Vipulanandan, C., Ramanathan, P., Ali, M., Basirat, B., and Pappas, J. (2015), "Real Time Monitoring of Oil Based Mud, Spacer Fluid and Piezoresistive Smart Cement to Verify the Oil Well Drilling and Cementing Operation Using Model Tests", Paper SPE 25851 presented at the Offshore Technology Conference, pp. 1-18.

[10] Wei, X., Lianzhen, X., and Li, Z. (2008), "Electrical Measurement To Assess The Hydration Process and The Porosity Formation", Journal of Wuhan University of Technology and Material Science, Edition, Volume 23, pp. 761-766

[11] Ridha, S., Irawan, S., and Ariwahjoedi, B. (2013), "Strength Prediction of Class G Oilwell Cement During Early Ages By Electrical Conductivity", Journal of Petroleum Exploration and Production Technology, Vol. 3, pp. 303-311

[12] Zuo, Y., Zi, J., and Wei, X. (2014), "Hydration of Cement With Retarder Characterised via Electrical Resistivity Measurements and Computer Simulation", Journal of Construction and Building Materials.

[13] Al-Saeedi, M., Munger, R., Tooms, P., Al-Mutairi, B., and Al-Quraini, K., Decaire, J., and Tuncer, T. (2001), "First High Pressure, High Angle Wells In Kuwait: Case Study of WMN-2", Paper IADC/SPE 72299 presented at the IADC/SPE Middle East Drilling Technology, Bahrain, 22-24 October.

[14] Bachu, S. and Watson, T. (2009), "Review of Failures for Wells Used for $CO_2$ and Acid Gas Injection In Alberta, Canada", Journal of Energy Procedia, **1** ISSN 1876-6102, pp. 3531-3537.

[15] Bennett, T. (2017), "Well Cement Integrity and Cementing Practices", University of Adelaide,

[16] Barlet-Gouedard, V., Rimmele, G., Goffe, B., and Porcherie, O. (2006), "Mitigation Strategies for the Risk of $CO_2$ Migration Through Wellbores", Paper SPE 98924 presented at the IADC/SPE Drilling Conference, Miami, Florida, 21-23 February

[17] Bosma, M., Ravi, K., van Driel, W., and Schreppers, G. (1999), "Design Approach To Sealant Selection for the Life of the Well", Paper SPE 56536 presented at the Annual Technical Conference and Exhibition, Houston, TX, 3-6 October.

[18] Boyd, D., Al-Kubti, S., Khedr, O., Khan, N., Al-Nayadi, K., Degouy, D., Elkadi, A., and Al-Kindi, Z. (2006), "Reliability of Cement Bond Log Interpretations Compared to Physical Communication Tests Between Formations", Paper SPE 101420 presented at the Abu Dhabi International Petroleum Exhibition and Conference, Abu Dhabi, UAE, 5-8 November.

[19] Al-Ajmi, A. (2006), "Wellbore Stability Analysis Based On A New True-Triaxial Failure Criterion", PhD Thesis, KTH Land and Water Resource Engineering.

[20] Calosa, W., Sadarta, B., and Ronaldi, R. (2010), "Well Integrity Issues In Malacca Strait Contact Area", Paper SPE 129083 presented at the SPE Oil and Gas India Conference and Exhibition, Mumbai, India, 20-22 January.

[21] Davies, R., Almond, S., Ward, R., Jackson, R., Adams, C., Worrall, F., Herringshaw, L., Gluyas, J., and Whitehead, M. (2014), "Oil and Gas Wells and their Integrity: Implications for Shale and Unconventional Resource Exploitation", Journal of Marine and Petroleum Geology, **45**, pp 511–526.

[22] di Lullo, G. and Rae, P. (2000), "Cements for Long Term Design Optimisation by Computer Modelling and Prediction", Paper IADC/SPE 62745 presented at the 2000 IADC/SPE Asia Pacific Drilling Technology Conference, Kuala Lumpur, September 11-13. **45**

[23] Duguid, A., Radonjic, M., and Scherer, G. (2011), "Degradation of Cement at the Reservoir/Cement Interface from Exposure to Carbonated Brine", International Journal of Greenhouse Gas Control, **5**, pp. 1413-1428.

[24] Crook, R., Kulakaofsky, D., and Griffith, J. (2003), "Tailor Lightweight Slurry Designs to Well Conditions and Productions Plans", World Oil. **224**.

[25] Dusseault, M., Maury, V., Sanfilippo, F., and Santarelli, F.. (2004), "Drilling Around Salt: Risks, Stresses, and Uncertainties", Paper ARMA 04-647 presented at the Gulf Rocks 2004, the 6th North American Rock Mechanics Symposium (NARMS): Rock Mechanics Across Borders and Disciplines, Houston, TX, June 5-9

[26] Lavrov, A. and Torsaeter, M. (2016), "Physics and Mechanics of Primary Well Cementing", SpringerBriefs in Petroleum Geoscience & Engineering, **01**.

[27] DHSG (2011), "Final Report on the Investigation of the Macondo Well Blowout", Deepwater Horizon Study Group, .

[28] De Andrade, J. and Sangesland, S. (2016), "Cement Sheath Failure Mechanisms: Numerical Estimates to Design for Long-Term Well Integrity", Journal of Petroleum Science and Engineering, **147**, pp. 682–698

[29] De Andrade, J., Sangesland, S., Todorovic, N., Vralstad, T. (2015), "Cement Sheath Integrity During Thermal Cycling: A Novel Approach for Experimental Tests of Cement Systems", Paper SPE 173871 presented at the SPE Bergen One Day Seminar, Bergen, Norway, 22 April

[30] Gray, K., Podnos, E., and Becker, E. (2007), "Finite-Element Studies of Near-Wellbore Region During Cementing Operations: Part I", Paper SPE 106998 presented at the Production and Operations Symposium, Oklahoma City, Oklahoma, 31 March-03 April.

[31] Jo, H. (2008), "Mechanical Behaviour of Concentric and Eccentric Casing, Cement, and Formation Using Analytical and Numerical Methods", PhD Thesis, The University of Texas at Austin.

[32] Kimura, K., Takase, K., Griffith, J., Gibson, R., Porter, D., and Becker, T. (1999), "Custom-Blending Foamed Cement for Multiple Challenges", Paper SPE/IADC 57585 presented at the SPE/IADC Middle East Drilling Technology Conference, Abu Dhabi, UAE, 8-10 November.

[33] Kutchko, B., Strazisar, B., Dzombak, D., Lowry, G., and Thaulow, N. (2007), "Degradation of Well Cement by $CO_2$ Under Geologic Sequestration Conditions", Journal of Environmental Science Technology **41**, pp 4787-4792.

[34] Kiran, R., Catalin, T., Dadmohammadi, Y., Nygaard, R., Wood, D., Mokhtari, M., and Salehi, S. (2017), "Identification and Evaluation of Well Integrity and Causes of Failure of Well Integrity Barriers (A Review)", Journal of Natural Gas Science and Engineering, **45**, pp 511–526

[35] Lecampion, B., Quesada, D., Loizzo, M., Bunger, A., Kaer, J., Deremble, L., and Desroches, L. (2011), "Interface Debonding as a Controlling Mechanism for Loss of Well Integrity: Importance for $CO_2$ Injector Wells", Journal of Energy Procedia, **4**, pp 5219-5226

[36] Mainguy, M., Longuemare, P., Audibert, A., and Lecolier, E. (2007), "Analysing the Risk of Well Plug Failure after Abandonment", Journal of Oil & Gas Science and Technology, **62**, No. 3, pp. 311-324.

[37] Goodwin, K. and Crook, R. (1990), "Cement Sheath Stress Failure", Paper SPE 20453 presented at the 65th Annual Technical Conference and Exhibition, New Orleans, USA, September 23-26.

[38] Carpenter, R., Brady, J., and Blount, C. (1992), "The Effects of Temperature and Cement Admixes on Bond Strength", Journal of Petroleum Technology, **44**, pp 880–941.

[39] Boukhelifa, L., Moroni, N., James, S., Roy-Delage, S., Thiercelin, M., and Lemaire, G. (2004), "Evaluation of Cement Systems for Oil and Gas-Well Zonal Isolation In A Full-Scale Annular Geometry", Paper SPE 87195 presented at the 2004 IADC/SPE Drilling Conference, Dallas, 2-4 March.

[40] Bois, A., Garnier, A., Rodot, F., Saint-Marc, J., and Aimard, N. (2009), "How To Prevent Loss of Zonal Isolation Through a Comprehensive Analysis of Microannulus Formation", Paper SPE 124719 presented at the SPE Annual Technical Conference and Exhibition, 4-7 October, New Orleans, Louisiana.

[41] Yuan, Z. (2012), "The Effect of Cement Mechanical Properties and Reservoir Compaction on HPHT Well Integrity", PhD Thesis, Texas A&M University.

[42] Robertson, C. and Krauss, C. (2010), "Gulf Spill Is The Largest of Its Kind, Scientists Say", The New York Times.

[43] Jervis, R. and Levin, A. (2010), "Obama, In Gulf, Pledges to Push on Stopping Leak", USA Today; Associated Press.

[44] Webber, H. (2010), "Blown-Out BP Well Finally Killed at Bottom of Gulf", Boston Globe; Associated Press.

[45] Wojtanowicz, A., Nishikawa, S., and Rong, X. (2001), "Diagnosis and Remediation of Sustained Casing Pressure In Wells", Technical Report, Louisiana State University.

[46] Nelson, E. and Guillot, D. (2006), "Well Cementing, $2^{nd}$ Ed.", Schlumberger, Sugar Land.

[47] Celia, M., Bachu, S., Nordbotten, J., Kavetski, D., and Gasda, S. (2005), "Modelling Critical Leakage Pathways In A Risk Assessment Framework: Representation of Abandoned Wells", Conference Proceedings, $4^{th}$ Annual Conference on Carbon Capture and Sequestration DOE/NETL, May 2-5.

[48] Torbergsen, H., Haga, H., Sangesland, S., Aadnoy, B., Saeby, J., Johnsen, S., Rausand, M., Lundeteigen, M. (2012), "An Introduction to Well Integrity", Norsk Olje & Gass.

[49] Xu, Y., Yang, Q., Li, Q., and Chen, B. (2006), "The Oil Well Casing's Anti-Corrosion and Control Technology of Changing Oilfield", Paper SPE 104445 presented at the International Oil & Gas Conference and Exhibition, China, 5-7 December.

[50] Dusseault, M., Gray, M., and Nawrocki, P. (2000), "Why Oilwells Leak: Cement Behaviour and Long-Term Consequences", Paper SPE 64733 presented at the SPE International Oil and Gas Conference and Exhibition, Beijing, China, 7-10 Nov.

[51] Backe, K., Lile, O., Lyomov, S., Elvebakk, H., and Skalle, P. (1999), "Characterising Curing-Cement Slurries by Permeability, Tensile Strength, and Shrinkage", Journal of SPE Drilling and Completion, **14**, pp 162–167

[52] Goboncan, V. and Dillenbeck, R. (2003), "Real-Time Cement Expansion/Shrinkage Testing Under Downhole Conditions for Enhanced Annular Isolation", Paper SPE/IADC 79911 presented at the SPE/IADC Drilling Conference, Amsterdam, The Netherlands, 19-21, Feb.

[53] Chenevert, M. and Shrestha, B. (1991), "Chemical Shrinkage Properties of Oilfield Cements", SPE Journal of Drilling Engineering,

[54] Bois, A., Garnier, A., Rodot, F., Saint-Marc, J., and Aimard, N. (2011), "How To Prevent Loss of Zonal Isolation Through A Comprehensive Analysis of Microannulus Formation", SPE Journal of Drilling and Completion, **26(1)**, pp. 13-31

[55] Liu, H., Bu, Y., and Guo, S. (2013), "Improvement of Aluminium Powder Application Measure Based On Influence of Gas Hole On Strength Properties of Oilwell Cement", Journal of Construction and Building Materials, **47**, pp. 480-488

[56] Opedal, N., Todorovic, J., Torsaeter, M., Vralstad, T., and Mushtaq, W. (2014), "Experimental Study On The Cement-Formation Bonding", Paper presented at the SPE International Symposium and Exhibition On Formation Damage Control, Lafayette, Louisiana, USA, 26-28 Feb

[57] King, G. and Valencia, R. (2014), "Environmental Risk and Well Integrity of Plugged and Abandoned Wells", Paper SPE 170949 presented at the SPE Annual Technical Conference and Exhibition, Amsterdam, The Netherlands, 27-29 October.

[58] Ladva, H., Craster, B., Jones, T., Goldsmith, G., and Scott, D. (2004), "The Cement-Formation Interface In Zonal Isolation", Paper IADC/SPE 88016 presented at the IADC/SPE Asia Pacific Drilling Technology Conference and Exhibition, Kuala Lumpur, Malaysia, 13-15 September

[59] Ceccarelli, T., Albino, E., Watson, G., and Deffieux, D. (2009), "Deepwater Completion Designs: A Review of Current Best Practices", Paper SPE 122518 presented at the Asia Pacific Oil and Gas Conference & Exhibition, 4-6 August

[60] McDaniel, J., Watters, L., and Shadravan, A. (2014), "Cement Sheath Durability: Increasing Cement Sheath Integrity To Reduce Gas Migration In The Marcellus Shale Play", Paper SPE 168650 presented at the SPE Hydraulic Fracturing Technology Conference, The Woodlands, Texas, USA, 4-6 February

[61] Nygaard, R., Salehi, S., Weideman, B., and Lavoie, R. (2014), "Effect of Dynamic Loading on Wellbore Leakage for the Wabamun Area $CO_2$ Sequestration Project", Journal of Canadian Petroleum Technology, **53 (01)** pp. 69-82.

[62] Schultz, R., Mutlu, U., and Bere, A. (2016), "Critical Issues In Subsurface Integrity", Paper ARMA 037 presented at the 50th US Rock Mechanics/Geomechanics Symposium, Houston, TX, 26-29 June.

[63] Saasen, A., Fjelde, K., Vralstad, T., Raksagati, S., and Moeinikia, F. (2013), "Plug and Abandonment of Offshore Exploration Wells", Paper OTC 23909 presented at the Offshore Technology Conference, Houston, TX, 6-9 May.

[64] Teodoriu, C., Kosinowski, C., Amani, M., Schubert, J., and Shadravan, A. (2012), "Wellbore Integrity and Cement Failure at HPHT Conditions", International Journal of Engineering and Applied Sciences, **2 (2)** ISSN 2305-8269, pp. 1-13.

[65] Nygaard, R., Salehi, S., and Lavoie, R. (2011), "Effect of Dynamic Loading on Wellbore Leakage for the Wabamum Area $CO_2$ Sequestration Project", Paper SPE 146640 presented at the Canadian Unconventional Resources Conference, Calgary, Canada, 15-17 November.

[66] Elshehabi, T. and Bilgesu, I. (2015), "Impact of Drilling With Oil Based Mud On Well Control In Horizontal Shale Gas Wells", Paper SPE 177294 presented at the SPE Eastern Regional Meeting, Morgantown, West Virginia, USA, 13-15 October

[67] Xie, J. and Liu, Y. (2008), "Analysis of Casing Deformations In Thermal Wells", Abaqus' Users Conference, Newport, Rhode Island, USA, pp. 542-553.

[68] Junior, R., Ribeiro, P., and Santos, O. (2009), "HPHT Drilling – New Frontiers for Well Safety", Paper SPE 177294 presented at the SPE/IADC Drilling Conference and Exhibition, Amsterdam, The Netherlands, 17-19 March.

[69] Yuan, Z., Schubert, J., Esteban, U., Chantose, P., and Teodoriu, C. (2013), "Casing Failure Mechanism and Characterisation Under HPHT Conditions In South Texas", Paper SPE/IPTC 16704 presented at the International Petroleum Technology Conference, Beijing, China, 26-28 March.

[70] Frittella, F., Babbo, M., and Muffo, A. (2009), "Best Practices and Lesson Learned from 15 Years of Experience of Cementing HPHT Wellbores In Italy", Paper SPE 125175 presented at the Middle East Drilling Technology Conference and Exhibition, Manama, Bahrain, 26-28 October.

[71] Heidarian, M., Jalalifar, H., Schaffie, M., and Jafari, S. (2014), "New Analytical Model for Predicting The Unstable Zone Around The Borehole", Original SPE manuscript received for review 16 August 2012. Revised manuscript received for review on 23 October 2013. Paper SPE 169899 peer approved 7 February 2014.

[72] Rimmele, G., Barlet-Gouedard, V., Porcherie, O., Goffe, B., and Brunet, F. (2008), Heterogeneous Porosity Distribution In Portland Cement Exposed to $CO_2$-Rich Fluids, Journal of Cement Concrete Research, **38** pp. 1038-1048.

[73] Ravi, K., Bosma, M., and Hunter, L. (2003), Optimizing The Cement Sheath Design In HPHT Shearwater Field, Paper SPE/IADC Drilling Conference, Amsterdam, Netherlands, 19-21 February

[74] Strazisar, B., Kutchko, B., and Huerta, N. (2009), Chemical Reactions of Wellbore Cement Under $CO_2$ Storage Conditions: Effects of Cement Additives, Journal of Energy Procedia, **I** pp. 3603-3607.

[75] Shadravan, A. and Amani, M. (2012), "HPHT 101: What Every Engineer or Geoscientist Should Know About High Pressure, High Temperature Wells", Paper SPE 163376 presented at the SPE Kuwait International Petroleum Conference and Exhibition, Kuwait, 10-12 December.

[76] Bybee, K. (2007), "Effects of Long-Term Exposure To Ultrahigh Temperature On The Mechanical Parameters of Cement", Journal of Petroleum Technology **59**

[77] NPC (2011), "Plugging and Abandonment of Oil and Gas Wells. Paper 25. Technology Subgroup of Operations and Environmental Task Group", National Petroleum Council **59**

[78] Posey, D. and Purvis, D. (2004), "Application of a Lightweight Cement Slurry for the Naturally Fractured Mesa Verde Formations", Paper SPE 90489 presented at the SPE Annual Technical Conference and Exhibition, Houston, TX, 26-29 September

[79] Ridha, S., Irawan, S., and Ariwahjoedi, B. (2013), "Strength Prediction of Class G Oilwell Cement During Early Ages By Electrical Conductivity", Journal of Petroleum Exploration and Production Technology, Vol. 3, pp. 303-311

[80] Shaughnessy, J. and Helweg, J. (2002), "Optimizing HPHT Cementing Operations", Paper IADC/SPE Drilling Conference, Dallas, TX, 26-28 February

[81] Salhebadi, M., Jin, M., Yang, J., Haghighi, H., Ahmed, R., and Tohidi, B. (2008), "Finite Element Modelling of Casing In Gas Hydrate Bearing Sediments", Paper SPE 113819 presented at the Europec/EAGE Conference and Exhibition, Rome, Italy, 9-12 June.

[82] Thiercelin, M., Dargaud, B., Baret, J., and Rodriquez, W. (1998), "Cement Design Based On Cement Mechanical Response", Journal of Drilling and Completion. Society of Petroleum Engineers. **13 (04)**

[83] Transocean (2011), "Macondo Well Incident", Transocean Investigation Report, Vol. I

[84] Um, W., Jung, H., Martin, P., McGrail, B. (2011), "Effective Permeability Change In Wellbore Cement With Carbon Dioxide Reaction", PNNL-20843. Pacific Northwest National Laboratory, Richland, WA.

[85] Ichim, A. and Teodoriu, C. (2016), "Revisiting Thermal Well Integrity Through A Closer Look at Casing-Cement-Formation Interaction", Paper SPE 182525 presented at the SPE Thermal Well Integrity and Design Symposium, Banff, Canada, 28 Nov-01 December

[86] Ugwu, I. (2008), "Cement Fatigue and HPHT Well Integrity with Application to Life of Well Prediction", MSc Thesis, Texas A&M University.

[87] Vignes, B. and Aadnoy, B. (2008), "Well Integrity Issues Offshore Norway", Paper SPE 112535 presented at the IADC/SPE Drilling Conference at Orlando, FL, 4-6 March.

[88] Wang, W. and Taleghani, A. (2014), "Three Dimensional Analysis of Cement Sheath Integrity ", Paper SPE 112535 presented at the IADC/SPE Drilling Conference at Orlando, FL, 4-6 March.

[89] Wilcox, B., Oyeneyin, B., and Islam, S. (2016), "HPHT Well Integrity and Cement Failure", Paper SPE 184254 presented at the SPE Nigeria Annual International Conference and Exhibition, Lagos, Nigeria, 2-4 August.

[90] Watson, T. (2013), "Alberta Regulations: Wellbore Integrity Issues Driving Regulatory Changes", North America Wellbore Integrity Workshop, Denver, CO, USA.

[91] Williams, R., Khatri, D., Keese, R., Roy-Delage, S., Roye, J., Leach, D., Porcherie, O., Rottler, P., and Rodriguez, J. (2011), "Flexible, Expanding Cement System (FECS) Successfully Provides Zonal Isolation Across Marcellus Shale Gas Trends", Paper SPE 149440 presented at the Canadian Unconventional Resources Conference, Calgary, Canada, 15-17 November.

[92] Yuan, Z., Schubert, J., Teodoriu, C., and Gardoni, P. (2012), "HPHT Gas Well Cementing Complications and its Effect on Casing Collapse Resistance", Paper SPE 153986 presented at the SPE Oil and Gas India Conference and Exhibition, 28-30 March, Mumbai, India

[93] Zhang, M. and Talman, S. (2014), "Experimental Study of Well Cement Carbonation Under Geological Storage Conditions", Journal of Energy Procedia, **63** pp. 5813-5821, ISSN 1876-6102.

[94] Zhou, D. and Wojtanowicz, A. (2000), "New Model of Pressure Reduction to Annulus During Primary Cementing", Paper SPE 59137 presented at the IADC/SPE Drilling Conference, New Orleans, Louisiana, February 23-25.

[95] Liu, K., Gao, D., and Taleghani, A. (2018), "Analysis On Integrity of Cement Sheath In The Vertical Section of Wells During Hydraulic Fracturing", Journal of Petroleum Science and Engineering, doi: 10.1016/j.petrol.2018.05.016.

[96] Shahri, M., Schubert, J., and Amani, M. (2005), "Detecting and Modelling Cement Failure in High-Pressure/High-Temperature (HPHT) wells, Using Finite Element Method (FEM)", Presented at the International Petroleum Technology Conference, Doha, Qatar, 21-23 November.

[97] Zoback, M. (2007), "Reservoir Geomechanics", Cambridge University Press.

[98] Pinto, H. and Braga, A. (2013), Well Integrity Monitoring: Challenges and Perspectives, Offshore Technology Conference.

[99] Sutton, I. (2013), Summarising the Deepwater Horizon/Macondo Reports, Offshore Technology Conference, 6-9 May, Houston, Texas, USA

[100] Donnelly, J. (2015), Comments: Macondo 5 Years Later, Journal of Petroleum Technology, Vol. 67(4)

[101] Bellabarba, M., Bulte-Loyer, H., Froelich, B., Le Roy-Delage, S., van Kuijk, R., Zeroug, S., Guillot, D., Moroni, N., Pastor, s., and Zanchi, A. (2008), Ensuring Zonal Isolation Beyond the Life of the Well, Oilfield Review Spring, pp. 18-31

[102] Ramos, R. and Camus, A. (2017), Borehole Cement Sheath Integrity – Numerical Simulation Under Reservoir Conditions, Mecanica Computacional Vol. XXXV, pp. 193-225, 7-10 November.

[103] Celia, M., Bachu, S., Nordbotten, J., Kavetski, D., and Gasda, S. (2005), Modelling Critical Leakage Pathways In A Risk Assessment Framework: Representation of Abandoned Wells, Fourth Annual Conference on Carbon Capture and Sequestration DOE/NETL.

[104] Bustgaard, M. and Nesheim, M. (2016), Model for Prediction of Cement Sheath Failure, MSc Thesis in Petroleum Geoscience and Engineering, Department of Petroleum Engineering and Applied Geophysics, Norwegian University of Science and Technology.

[105] Cui, L., Abousleiman, Y., Cheng, A., and Roegiers, J. (1999), Time Dependent Failure Analysis of Inclined Boreholes In Fluid Saturated Formations, Journal of Energy Resources Technology, American Society of Mechanical Engineers. **121(1):31-39**

[106] Cui, L., Cheng, A., and Abousleiman, Y. (1997), Poroelastic Solution for an Inclined Borehole, Journal of Applied Mechanics, ASME. **64(1):32-38**

[107] Himmelberg, N. (2014), Numerical Simulations for Wellbore Stability and Integrity for Drilling and Completions, MSc Thesis, Missouri Science and Technology, USA.

[108] Jo, H. (2008), Mechanical Behaviour of Concentric and Eccentric Casing, Cement, and Formation Using Analytical and Numerical Methods, PhD Thesis, The University of Texas at Austin, USA.

[109] Handin, J. (1965), Strength of Oilwell Cements at Downhole Pressure-Temperature Conditions, SPE 1300

[110] Fjaer, E., Holt, R., Horsrud, P., Raaen, A., and Risnes, R. (2008), Petroleum Related Rock Mechanics, Vol. 53, Elsevier, $2^{nd}$ Edition.

[111] Zoback, M. (2007), Reservoir Geomechanics, Cambridge University Press

[112] Restrepo, M., Ichim, A., and Teodoriu, C. (2018), The Effect of Wellbore Centralisation in Geothermal Wells, Proceedings at the $43^{rd}$ Workshop on Geothermal Reservoir Engineering, Stanford University, California, USA, February 12-14.

[113] Wang, H. and Samuel, R. (2016), 3D Geomechanical Modelling of Salt Creep Behaviour on Wellbore Casing for Presalt Reservoirs. SPE Drilling and Completion, Society of Petroleum Engineers, 31 (04), pp. 261-272. **¡10.2118/166144-PA¿ . ¡hal-01626417¿**

[114] Saint-Marc, J., Garnier, A., and Bois, A. (2008), Initial State of Stress: The Key to Achieving Long-Term Cement Sheath Integrity. SPE Paper 116651 presented at the Annual Technical Conference, Denver, Colorado, USA.

[115] Ramanathan, P. (2014), Mechanical, Piezoresistive and Fracture Behaviour of Various Types of Smart Cements. MSc Thesis, University of Houston, USA.

[116] Ramsey, M. and Garrett, R. (2010), Drilling Fluids Module. Texas Drilling Associates

[117] Vipulanandan, C. and Mohammed, A. (2015), Smart Cement Rheological and Piezoresistive Behaviour for Oil Well Applications. Journal of Petroleum Science and Engineering, Vol. 135, pp. 50-58.

[118] Vipulanandan, C. and Mohammed, A. (2015), Smart Cement Modified with Iron Oxide Nanoparticles to Enhance the Piezoresistive Behaviour and Compressive Strength for Oil Well Applications. Journal of Smart Materials and Structures, Vol. 24, No. 12, pp. 1-11.

[119] Vipulanandan, C., Krishnamoorti, R., and Mohammed, A., Narvaez, G., Head, B., and Pappas, J. (2015), Iron Nanoparticle Modified Smart Cement for Real Time Monitoring of Ultra Deepwater Oil Well Cementing Applications. Offshore Technology Conference (OTC), OTC-25842-MS, pp. 1-20

[120] Wei, X., Lianzhen, X., and Li, Z. (2008), Electrical Measurement to Assess Hydration Process and the Porosity Formation. Journal of Wuhan University of Technology Material Science, Vol. 23, pp. 761-766

[121] Zuo, Y., Zi, J., and Wei, X. (2014), Hydration of Cement With Retarder Characterized via Electrical Resistivity Measurements and Computer Simulation. Journal of Construction and Building Materials.

[122] Philippacoupoulos, A. and Berndt, M. (2001), Mechanical Property Issues for Geothermal Well Cements. Geothermal Reservoirs, Vol. 25, pp. 119-224

[123] Reddy, B., Santra, A., David, M., Gray, D., Chad, B., and Rick, D. (2005), Cement Mechanical Property Measurements Under Wellbore Conditions. Paper SPE 95921 presented at the SPE Annual Technical Conference and Exhibition, 9-12 October, Dallas, TX.

[124] Stiles, D. (2006), Effects of Long-Term Exposure to Ultrahigh Temperature on the Mechanical Parameters of Cement. Paper IADC/SPE 98896 presented at the IADC/SPE Drilling Conference, 21-23 February, Miami, Florida.

# Appendix A

# Appendices

## A.1 Appendix A

### A.1.1 Steady-State Analytical Model for Casing-Cement-Formation System

For the casing-cement-formation wellbore model under consideration (see Figure $A.5$), the internal wellbore pressure, $p_i$, acting on the inner surface of the steel casing, combined with significant temperature increase, will expand the casing radially while the oilwell cement sheath will resist the expansion. As a result, an interfacial pressure $P_{c1}$ will develop at the contact between the steel casing and oilwell cement (see Figure $A.6$).

The hoop strain can be calculated using the following mathematical equation;

$$\varepsilon_h = \frac{1}{E}[\sigma_h - \nu(\sigma_z + \sigma_r)] + \alpha\Delta T \tag{A.1.1}$$

The axial/longitudinal strain can be calculated using the following equation;

$$\varepsilon_z = \frac{1}{E}[\sigma_z - \nu(\sigma_h + \sigma_r)] + \alpha\Delta T \tag{A.1.2}$$

Considering large wellbore depths, the axial strain ($\varepsilon_z$) is assumed to be negligible (i.e. plane strain assumption);

$$\varepsilon_z = 0 \tag{A.1.3}$$

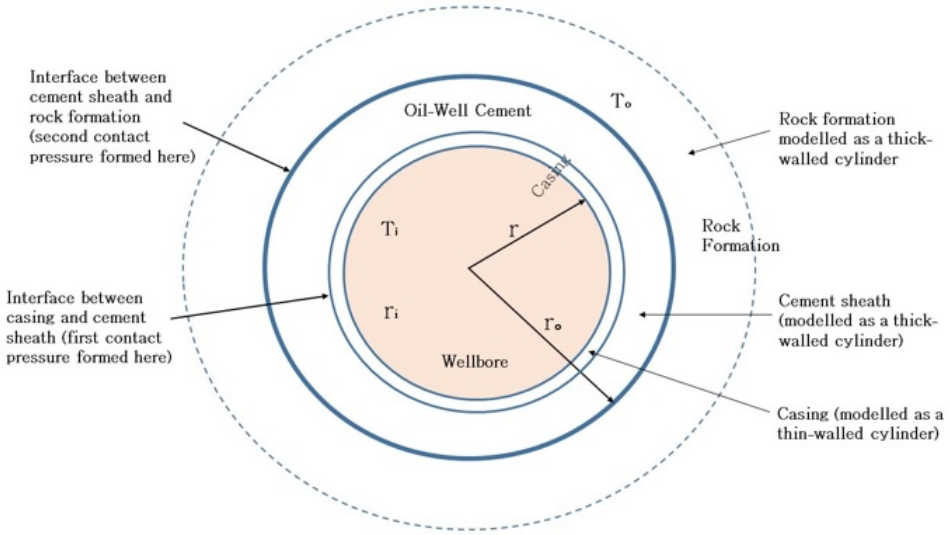


Figure A.1: Schematic for concentric casing-cement-formation system.

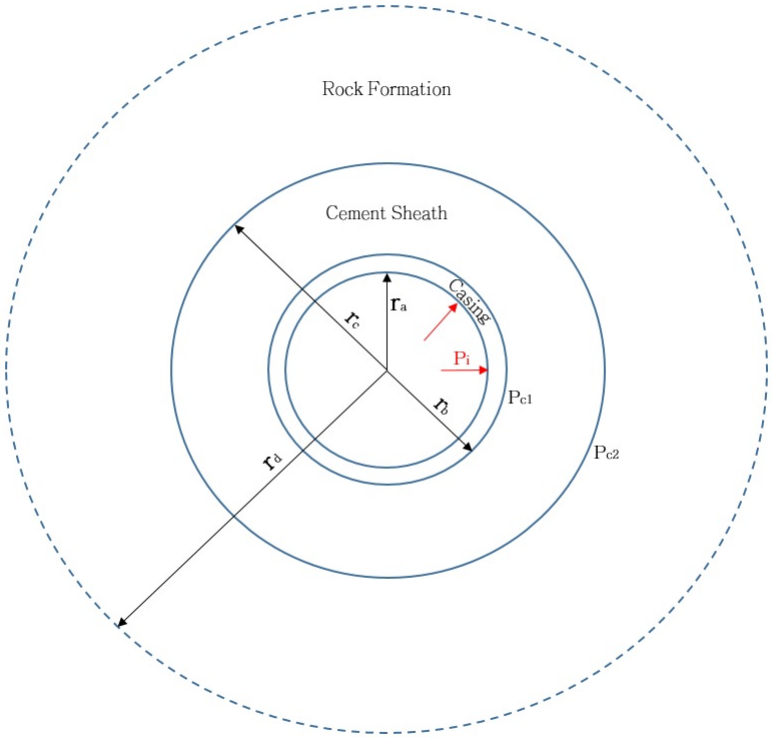


Figure A.2: Schematic for Casing-Cement-Formation system including contact pressures and radii.

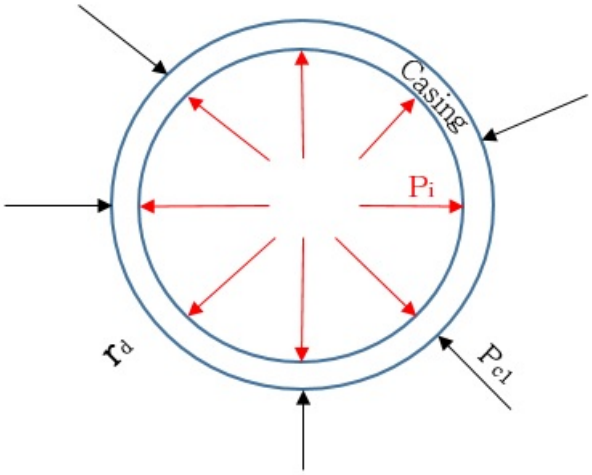


Figure A.3: Schematic showing the internal wellbore pressure acting on the inner walls of the steel casing and the interfacial pressure acting at the interface between the steel casing and the oilwell cement sheath.

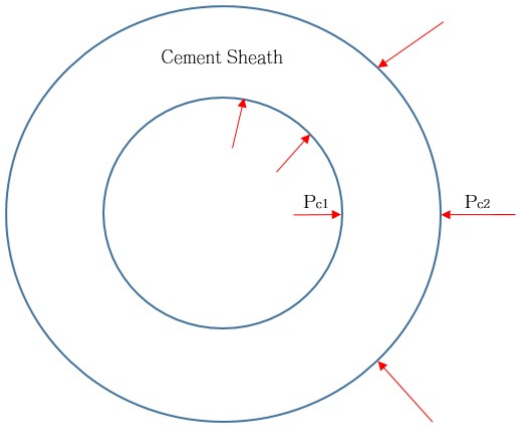


Figure A.4: Schematic showing the oilwell cement sheath and the pressures acting on it, i.e. the contact pressures at the casing/cement and cement/formation interfaces acting as the internal and external pressures.

Substituting Equation (A.2.25) into Equation (A.2.24), it follows that;

$$\sigma_z = \nu(\sigma_h + \sigma_r) - \alpha \Delta T E \tag{A.1.4}$$

Substituting Equation (A.2.26) into Equation (A.2.23);

$$\varepsilon_h = \frac{1}{E}[\sigma_h \cdot (1 - \nu^2) - (\nu + \nu^2) \cdot \sigma_r + (1 + \nu) \cdot \alpha E \Delta T] \tag{A.1.5}$$

The next step is to derive the contact pressures at the casing/cement interface and the cement/formation interface. Expressing Equation (A.2.27) in terms of strain in the steel casing and the oilwell cement sheath as presented in Equations (A.2.28) and (A.2.29) respectively;

$$\varepsilon_{cas} = \frac{1}{E_{cas}}[\sigma_{cas} \cdot (1 - \nu_{cas}^2) - (\nu_{cas} + \nu_{cas}^2) \cdot \sigma_r + (1 + \nu_{cas}) \cdot \alpha_{cas} E_{cas} \Delta T] \tag{A.1.6}$$

$$\varepsilon_{cem} = \frac{1}{E_{cem}}[\sigma_{cem} \cdot (1 - \nu_{cem}^2) - (\nu_{cem} + \nu_{cem}^2) \cdot \sigma_r + (1 + \nu_{cem}) \cdot \alpha_{cem} E_{cem} \Delta T] \tag{A.1.7}$$

Expressing Equation (A.2.27) in terms of the radial displacement, $\delta_r$;

$$\delta_r = \frac{r}{E}[\sigma_\theta \cdot (1 - \nu^2) - (\nu + \nu^2) \cdot \sigma_r + (1 + \nu) \cdot \alpha E \Delta T] \tag{A.1.8}$$

As shown in Figure A.6, the internal radius of the casing is represented by $r_a$, the outer radius of the casing (casing/cement interface) is represented by $r_b$, and the outer radius of the rock formation is represented by $r_d$. At the casing/cement interface, the radial and hoop stresses can be represented by $-p$ and $\frac{Pr_m}{t_s}$ respectively (where $p = P_i - P_{C1}$, $r_m$ represents the mean radius of the casing, and $t_s$ represents the thickness of the steel casing). Substituting these into Equation (A.2.30);

$$\delta_{r-cas} = \frac{r_a(P_i - P_{c1})}{E_{cas}}[\frac{r_m}{t_{cas}}(1 - \nu_{cas}^2) + (\nu_{cas} + \nu_{cas}^2)] + [(1 + \nu_{cas}) r_a \alpha_{cas} \Delta T] \tag{A.1.9}$$

Considering the oilwell cement sheath to be a thick-walled cylinder and assuming that $\frac{\partial(\Delta T)}{\partial r} = 0$, the tangential and radial stresses are mathematically represented by the following equations;

$$\sigma_r = \frac{P_{c1} \cdot r_b^2}{r_c^2 - r_b^2}[1 - \frac{r_c^2}{r^2}] - \frac{P_{c2} \cdot r_c^2}{r_c^2 - r_b^2}[1 - \frac{r_b^2}{r^2}] \tag{A.1.10}$$

$$\sigma_\theta = \frac{P_{c1} \cdot r_b^2}{r_c^2 - r_b^2}[1 + \frac{r_c^2}{r^2}] - \frac{P_{c2} \cdot r_c^2}{r_c^2 - r_b^2}[1 + \frac{r_b^2}{r^2}] \tag{A.1.11}$$

At $r = r_b$, Equations (A.2.32) and (A.2.33) respectively reduce to;

$$\sigma_r = -P_{c1} \tag{A.1.12}$$

$$\sigma_\theta = P_{c1}[\frac{r_c^2 + r_b^2}{r_c^2 - r_b^2}] - P_{c2}[\frac{2r_c^2}{r_c^2 - r_b^2}] \tag{A.1.13}$$

Substituting Equations (A.2.34) and (A.2.35) into Equation (A.2.30) gives;

$$\delta_{r-cem} = \frac{r_b}{E_{cem}}(1 - \nu_{cem}^2)[P_{c1}(\frac{r_b^2 + r_c^2}{r_c^2 - r_b^2}) - P_{c2}(\frac{2r_c^2}{r_c^2 - r_b^2})] + P_{c1}(\nu_{cem} + \nu_{cem}^2)] + (1+ \nu_{cem})r_b\alpha_{cem}\Delta T \tag{A.1.14}$$

Given that both radial expressions are equal [i.e. Equations (A.2.31) and (A.2.36)], it follows that;

$$P_{c1}[\frac{r_b}{E_{cem}}[(1 - \nu_{cem}^2)[\frac{r_b^2 + r_c^2}{r_c^2 - r_b^2}] + (\nu_{cem} + \nu_{cem}^2)] + \frac{r_a}{E_{cas}}[\frac{r_m}{t_{cas}}(1 - \nu_{cas}^2) + (\nu_{cas} + \nu_{cas}^2)]]$$
$$-P_{c2}[\frac{r_b}{E_{cem}}(\frac{2r_c^2}{r_c^2 - r_b^2})(1-\nu_{cem}^2) = \frac{P_i r_a}{E_{cas}}[\frac{r_m}{t_{cas}}(1-\nu_s^2)+(\nu_{cas}+\nu_{cas}^2)]+[(1+\nu_{cas})r_a\alpha_{cas}\Delta T]-$$
$$[(1 - \nu_{cem})r_b\alpha_{cem}\Delta T] \tag{A.1.15}$$

Equation (A.2.37) can instead be represented in the form of;

$$A \cdot P_{c1} + B \cdot P_{c2} = C \tag{A.1.16}$$

Where;

$$A = [\frac{r_b}{E_{cem}}[(1 - \nu_{cem}^2)[\frac{r_b^2 + r_c^2}{r_c^2 - r_b^2}] + (\nu_{cem} + \nu_{cem}^2)] + \frac{r_a}{E_{cas}}[\frac{r_m}{t_{cas}}(1 - \nu_{cas}^2) + (\nu_{cas} + \nu_{cas}^2)]] \tag{A.1.17}$$

$$B = -[\frac{r_b}{E_{cem}}(\frac{2r_c^2}{r_c^2 - r_b^2})(1 - \nu_{cem}^2) \tag{A.1.18}$$

$$C = \frac{P_i r_a}{E_{cas}}[\frac{r_m}{t_{cas}}(1 - \nu_s^2) + (\nu_{cas} + \nu_{cas}^2)] + [(1 + \nu_{cas})r_a\alpha_{cas}\Delta T] - [(1 - \nu_{cem})r_b\alpha_{cem}\Delta T] \tag{A.1.19}$$

Considering the cement/formation interface in Figure A.6, $P_{c2}$ is the contact pressure formed at the cement/formation contact as a result of the pressure from the rock formation pressure, $P_f$. At $r = r_c$;

$$\sigma_r = -P_{c2} \tag{A.1.20}$$

$$\sigma_\theta = P_{c1}[\frac{2 \cdot r_b^2}{r_c^2 - r_b^2}] - P_{c2}[\frac{r_c^2 + r_b^2}{r_c^2 - r_b^2}] \tag{A.1.21}$$

To determine the radial expansion in the oilwell cement sheath, at the cement/formation interface (at $r = r_c$), when Equations (A.2.42) and (A.2.43) are substituted into Equation (A.2.30) as;

$$\delta_{r-cem} = \frac{r_c}{E_{cem}}(1 - \nu_{cem}^2)[P_{c1}(\frac{2r_b^2}{r_c^2 - r_b^2}) - P_{c2}(\frac{r_c^2 + r_b^2}{r_c^2 - r_b^2}] + P_{c2}(\nu_{cem} + \nu_{cem}^2)] + (1+ \nu_{cem})r_c\alpha_{cem}\Delta T \tag{A.1.22}$$

Analysing the rock formation as a thick walled pressure vessel with radius $r_d$;

$$\sigma_r = -P_{c2} \tag{A.1.23}$$

$$\sigma_\theta = P_{c2}(\frac{r_c^2 + r_d^2}{r_d^2 - r_c^2}) - P_f(\frac{2r_d^2}{r_d^2 - r_c^2}) \tag{A.1.24}$$

Substituting Equations (A.2.44) and (A.2.45) into Equation (A.2.30);

$$\delta_{r-for} = \frac{r_c}{E_{for}}[(1-\nu_{for}^2)[P_{c2}(\frac{r_c^2 + r_d^2}{r_d^2 - r_c^2}) - P_f(\frac{2r_d^2}{r_d^2 - r_c^2})] + P_{c2}(\nu_{for} + \nu_{for}^2)] + [(1+\nu_{for})r_c\alpha_f\Delta T] \tag{A.1.25}$$

Given that both radial displacements are equal, it follows from Equation (A.2.44) and Equation (A.2.47);

$$\mathrm{P}_{c2}\frac{r_c}{E_f}[(1-\nu_f^2)[\frac{r_d^2+r_c^2}{r_d^2-r_c^2}]+(\nu_f+\nu_f^2)]+\frac{r_c}{E_{cem}}[1-\nu_{cem}^2](\frac{r_b^2+r_c^2}{r_c^2-r_b^2})-(\nu_{cem}+\nu_{cem}^2)-P_{c1}[\frac{r_c}{E_{cem}}(\frac{2r_b^2}{r_c^2-r_b^2})(1-\nu_{cem}^2)]=P_f[\frac{r_c}{E_f}(\frac{2r_d^2}{r_d^2-r_c^2})(1-\nu_f^2)]-[(1+\nu_f)r_c\alpha_f\Delta T]+[(1+\nu_{cem})r_c\alpha_{cem}\Delta T] \quad \text{(A.1.26)}$$

For simplicity, Equation (A.2.48) can be presented in the following form;

$$D\cdot P_{c1}+K\cdot P_{c2}=F \quad \text{(A.1.27)}$$

Where;

$$D=[\frac{r_c}{E_{cem}}(\frac{2r_b^2}{r_c^2-r_b^2})(1-\nu_{cem}^2)] \quad \text{(A.1.28)}$$

$$K=\frac{r_c}{E_f}[(1-\nu_f^2)[\frac{r_d^2+r_c^2}{r_d^2-r_c^2}]+(\nu_f+\nu_f^2)]+\frac{r_c}{E_{cem}}[1-\nu_{cem}^2](\frac{r_b^2+r_c^2}{r_c^2-r_b^2})-(\nu_{cem}+\nu_{cem}^2) \quad \text{(A.1.29)}$$

$$F=P_f[\frac{r_c}{E_f}(\frac{2r_d^2}{r_d^2-r_c^2})(1-\nu_f^2)]-[(1+\nu_f)r_c\alpha_f\Delta T]+[(1+\nu_{cem})r_c\alpha_{cem}\Delta T] \quad \text{(A.1.30)}$$

Solving the equations simultaneously, the mathematical equations for the contact pressures are given as;

$$P_{c1}=\frac{FB-KC}{DB-AK} \quad \text{(A.1.31)}$$

$$P_{c2}=\frac{C-(P_{c1})A}{B} \quad \text{(A.1.32)}$$

Based on the analytical model presented, the stresses in the cement sheath (radial, axial, and circumferential) can be calculated using Equations (A.2.55), (A.2.56), and (A.2.57);

$$\sigma_{r-cem} = P_{c1}\frac{r_b^2}{r_c^2 - r_b^2}[1 - \frac{r_c^2}{r^2}] - P_{c2}\frac{r_c^2}{r_c^2 - r_b^2}[1 - \frac{r_b^2}{r^2}] \tag{A.1.33}$$

$$\sigma_{\theta-cem} = P_{c1}\frac{r_b^2}{r_c^2 - r_b^2}[1 + \frac{r_c^2}{r^2}] - P_{c2}\frac{r_c^2}{r_c^2 - r_b^2}[1 + \frac{r_b^2}{r^2}] \tag{A.1.34}$$

$$\sigma_{z-cem} = \nu[\sigma_r + \sigma_\theta] - \alpha E \Delta T \tag{A.1.35}$$

## A.2 3D Geomechanical Model

### A.2.1 Mathematical Model

The equations and descriptions of the mechanisms considered in this research are presented in the following equations.

$$\rho C\frac{\partial T}{\partial t} + \nabla \cdot (-\lambda \nabla T) = q \tag{A.2.36}$$

where $\rho$ represents the density of the rock formation, $C$ is the heat capacity of the rock formation, $\lambda$ is the thermal conductivity, $T$ represents the temperature, and $q$ is the heat source. For steady-state problems, the terms $\rho C\frac{\partial T}{\partial t}$ and $q$ are both zero.

The stress equilibrium is defined by writing the principle of work for the volume that is under consideration is its current configuration;

$$\int_v \sigma : \delta\epsilon dV = \int_s \gamma \cdot \delta v dS + \int_v f \cdot \delta v dV \tag{A.2.37}$$

where $\delta v$ represents the virual velocity field, $\delta\epsilon$ represents the rate of deformation, $\gamma$ represents the surface traction per unit area, and $f$ represents the body force. This equation is further discretized using a Lagrangian formation with displacements. The equation for the solid is expressed as;

$$d \cdot \sigma = E \cdot d \cdot \epsilon + \int_0^t (t - \tau)\frac{d\epsilon}{d\tau}d\tau \tag{A.2.38}$$

where $\sigma$ represents stress, $\epsilon$ is the strain, $E$ represents the material stiffness, and $\tau$ represents the relaxation time. The constitutive equation of the behaviour of a ductile rock formation can be solved using the following iteration method:

1. After initial equilibrium, the displacement field $[\delta_i]$ and stress field $[\sigma_i]$ are solved – which are used by the production process as initial values.

$$[K][\delta_i] = [F] \tag{A.2.39}$$

$$[\sigma_i] = [D][B][\sigma_i] \tag{A.2.40}$$

where $[K]$ represents the stiffness matrix of the entire system, $[F]$ represents the equivalent nodal force, $[D]$ represents the elasticity matrix, and $[B]$ represents the geometric stiffness matrix.

2. An assumption is made that the stress field remains unchanged during each and every increment. Within the interval from $t$ to $t + \Delta t$, the stress is $[\sigma_t]$. Calculate the strain increment (creep) during the time interval, $\Delta t$:

$$[\Delta\epsilon_t^c]_{\Delta t} = \Delta t[\epsilon_t] \tag{A.2.41}$$

where $[\epsilon_t]$ represents the creep rate, and its components can be expressed as follows;

$$\epsilon_1 = \frac{\epsilon}{\sigma_{eff}}[\sigma_1 - \frac{1}{2}(\sigma_2 + \sigma_3)] \tag{A.2.42}$$

$$\epsilon_2 = \frac{\epsilon}{\sigma_{eff}}[\sigma_2 - \frac{1}{2}(\sigma_1 + \sigma_3)] \tag{A.2.43}$$

$$\epsilon_3 = \frac{\epsilon}{\sigma_{eff}}[\sigma_3 - \frac{1}{2}(\sigma_1 + \sigma_2)] \tag{A.2.44}$$

3. The incremental changes in nodal force for each time interval can be expressed using the following equation;

$$[\Delta F_c(t)] = \int_{\Omega} [B][D][\Delta \cdot \epsilon_t^c] d\Omega \tag{A.2.45}$$

Equation (A.3.67) is applied to the entire ductile rock formation. The coupled system of equations is solved using the Newton-Raphson technique, and a Jacobian matrix is generated. Incremental corrections are found by using a linear solver that updates the variables at the end of each time increment.